Dynamic Effects on Migration of Light Non-Aqueous Phase Liquids in Subsurface

Muhd Harris Bin Ramli

ABSTRACT

This is an environmental geotechnical study on the migration behavior of light non-aqueous phase liquids (LNAPLs) due to precipitation in subsurface. The aim of this research is to evaluate LNAPL migration behavior in the subsurface due to precipitation. Since water and LNAPL are immiscible, it is believed that precipitation infiltrated water will bring mobile LNAPL deeper into the saturated layers and thus extend the degree of groundwater contamination.

Groundwater contamination by LNAPL is known to increase environmental and health risks due to their toxicity and carcinogenic compounds such as benzene, toluene, ethylbenzene and xylene (BTEX) and methyl tertiary-butyl ether (MTBE). Although LNAPL is lighter than water, many studies have shown that it can contaminate groundwater. Once LNAPL is introduced into the subsurface, the remediation work should start before it contaminates the groundwater. Therefore, researches have been focusing on making the remediation work more efficient and cost-effective; but the lack of understanding in LNAPL migration behavior has impeded this aim. Recent study found that groundwater fluctuation can cause LNAPL migration into the saturated zone. As precipitation indirectly affects the groundwater fluctuation, direct effects of precipitation on LNAPL migration have not yet been studied.

Considering this issue, the effect of LNAPL spill volume as well as the effect of intensity and volume of precipitation had been studied in a one-dimensional column test to understand the LNAPL migration mechanism due to precipitation. Further, the saturation-capillary pressure analysis also had been done in one-dimensional and two-dimensional studies to identify the controlling parameter that initiates LNAPL migration in the subsurface due to precipitation.

After LNAPL was spilled, it migrated downward reaching a stable condition. It no longer migrated deeper once the two immiscible liquids had reached interfacial tension equilibrium. This condition changes as soon as precipitation infiltrates the contaminated sand layer, and helps LNAPL migrated into saturated zone. Considering the effect of spill volume, the more LNAPL contaminated the sand, the more LNAPL migrated deeper due to precipitation. Comparing the low and high LNAPL spilled volume when subjected to

precipitation, more mobile LNAPL was spread through the contamination plume in low-LNAPL infiltration cases. In high-LNAPL infiltration cases, LNAPL migrated downward and concentrated near the LNAPL wetting front region. Consequently, deeper high-LNAPL saturation regions were created due to precipitation.

In considering the precipitation intensity effect, the higher the precipitation intensity, the deeper LNAPL will migrate into saturated zone due to precipitation. This is because the high amount of infiltrating water provided a high wetting front propagation force that pushed down any LNAPL within its flow path. This mechanism helped LNAPL migrate easily into the saturated zone. When precipitation intensity is as low as 2.4 mm/hr, it was only able to wet the soil, but not able to initiate the migration of LNAPL into saturated zone. In considering precipitation total volume, it was found that the total precipitation volume plays an important role in determining the depth of migrated LNAPL. Whether the contaminated sand is subjected to either low or high precipitation intensity, if the precipitation total is the same, then the total depth of LNAPL migration will also be the same. The infiltrating water is the main mechanisms pushing the LNAPL deeper into the saturated zone. If subjected to high precipitation, the high wetting front force will help LNAPL migrate at a faster rate.

In this study, it also has been demonstrated that the LNAPL migration in the subsurface due to precipitation can be described using the saturation-capillary pressure relations (*S-p* relations) with the help of a van Genuchten (1980) model. From the *S-p* relations, it can be said that capillary pressure plays an important role, or is the controlling parameter, that causes the migration of LNAPL due to precipitation. If we consider the physical meaning of capillary pressure in the soil system, it is the pressure that holds the LNAPL or serves as a barrier that stops the LNAPL from migrating deeper into the saturated capillary zone. Therefore, as the capillary pressure drops to a low value due to precipitation water infiltration, it is now considered a normal fluid flow, as is the water infiltrating downward. Consequently, since LNAPL and water are immiscible, the infiltrated water will push the LNAPL down until the migrated LNAPL becomes entrapped in deeper soil pores, or stops due to capillarity, and thus, increases the contamination degree of the groundwater. Based on the findings from this study, *S-p* relations can be used to monitor possible spills of LNAPL and its migration as affected by precipitation.

ACKNOWLEDGEMENTS

I am grateful to several people for helping, in one way or other, with the writing of this thesis. I would like to express my gratitude to all of them, realizing that those whom I owe the most I cannot thank enough, and that the things for which I am most grateful, I cannot put into words.

This study was possible thanks to the SLAB Scholarship granted by Ministry of Higher Education, Malaysia. I am very grateful to Universiti Sains Malaysia for the support and great opportunity to study in Japan.

I would like to expresses my deep and sincere gratitude to my supervisor, Dr. Takeshi Katsumi, Professor of the Graduate School of Global Environmental Studies at Kyoto University, main advisor of this research, for his patience, motivation, enthusiasm, detailed and constructive comments, and for his important guidance and his inestimable support throughout this work at the Environmental Infrastructure Engineering Laboratory.

I would like to extend my gratitude to Dr. Giancarlo Flores, Associate Professor of the Graduate School of Engineering at Kyoto University, for his invaluable guidance, encouragement, advice and supervision throughout the research.

I would also like to extend my gratitude to Dr. Toru Inui, Associate Professor of the Graduate School of Global Environmental Studies at Kyoto University, for continues help, encouragements, constructive comments and suggestions about research.

Special thanks to Dr. Shuhei Tanaka, Associate Professor of the Graduate School of Global Environmental Studies at Kyoto University, for his valuable suggestions and comments on the content of this thesis.

My sincere thanks also go to Takai-sensei, Assistant Professor of the Graduate School of Global Environmental Studies at Kyoto University, for his invaluable support on the experimental work as well as his warmheartedly assistance in the aspects of Japanese culture, traditional and custom.

My special thanks go to Yasumoto-san, the laboratory Assistant, and my laboratory friends of the Environmental Infrastructure Engineering Laboratory at Kyoto University for all the fun we have had in theses three years of PhD and for making me enjoy the laboratory life. Special thanks to Mogami-san, Morita-san, Oshima-san, Yano-chan, Sano-chan, Kihara-san and Kimura-san for their kind support and help with Japanese translation not only related to research but also extracurricular activities. I also grateful to all laboratory member, Dr. Abedin, Katayama-san, Kodama-san, Tua-san, Suwa-san, Giang-san, Sado-chan, Ikeda-kun, Goto-san, Angelica-san, Lan-san, Uddin-san, Wang-san, Bobea-san, Mae-san, Sumoto-san, Ogawa-san, Mo-san, Tamura-san, Kaori-san, Miura-san, Yamane-san.

Lastly, I would like to thank my wife, Mastura Azmi, and my kids, Aiman and Aidan, for their support and encouragement for my studying in Japan.

TABLE OF CONTENTS

LIST OF FIGURES

LIST OF TABLES

CHAPTER 1: INTRODUCTION

1.1 General Remarks

Water is the most essential element to life on earth, composed of two hydrogens and one oxygen atom. Water is available everywhere, in oceans, inland, underground, and even in the air, as water vapor. All of this water is circulating in the environment by a process called the hydrological cycle. It is a natural and continuous process which produces a fresh water supply to earth through precipitation. It does not matter if the evaporated water comes from ocean or contaminated soil, precipitation water will always be fresh water. Precipitation water is also the main source for groundwater recharge, considering that groundwater volume constantly fluctuates due to seepage into surface water or directly evaporates from soil surface, affected by the hydrological cycle. Even though the volume of groundwater constantly fluctuates due to natural processes, this fluctuation becomes greater due to anthropological effects such as the use of groundwater as a water supply.

Groundwater has been used for centuries as major resource for water supply either for domestic, industrial or agriculture uses. As civilization grew rapidly and population increased constantly, dependence on this resource increased tremendously. Thus, it became the world's most extracted raw material with current withdrawal rates around 982 km^3 per year (US NGWA 2013). Table 1.1 shows 15 nations that have the largest estimated annual groundwater abstractions in 2010 (Margat and Van Der Gun 2013). As water is essential to all known forms of life, it can be seen in the same table that groundwater has been extensively used in the domestic and agriculture sectors.

Under most conditions, groundwater is safer and more reliable for use than surface water. One reason for this is that surface water is exposed to numerous pollutants than groundwater (Arafat et al. 2013). This does not mean that groundwater is not vulnerable to contamination. Groundwater contamination is even more dangerous because the degree of contamination cannot be easily detected. Therefore, the quality of the groundwater needs to be properly managed to ensure a safe water supply.

Table 1.1 Nations with the largest estimated annual groundwater abstractions in 2010 (Margat and Van Der Gun 2013).

Country	Estimated groundwater abstraction (km^3/yr)	Irrigation use (%)	Domestic use (%)	Industry (%)
India	251.00	89	9	2
China	111.95	54	20	26
United States	111.70	71	23	6
Pakistan	64.82	94	6	0
Iran	63.40	87	11	2
Bangladesh	30.21	86	13	1
Mexico	29.45	72	22	6
Saudi Arabia	24.24	92	5	3
Indonesia	14.93	2	93	5
Turkey	13.22	60	32	8
Russia	11.62	3	79	18
Syria	11.29	90	5	5
Japan	10.94	23	29	48
Thailand	10.74	14	60	26
Italy	10.40	67	23	10

Groundwater can be contaminated by several pollutants from different types of human activities. There is a wide variety of contaminants, from organic to inorganic, pathogens to radionuclides that can reach the groundwater and negatively impact human health and the environment. Contaminants such as *Non-Aqueous Phase Liquids* (NAPLs) are hazardous organic contaminants due to its toxicity. NAPLs can be divided into two types based on their density. NAPLs with densities lower than water density is called *Light Non-Aqueous Phase Liquids* (LNAPLs). Common LNAPLs are diesel and fuel oil. On the other hand, NAPLs with densities higher than water density are called *Dense Non-Aqueous Phase Liquids* (DNAPLs). Examples of DNAPLS are chlorinated solvents and halogenated hydrocarbons.

Due to difference in densities, migration behavior of both LNAPL and DNAPL are also different. LNAPLs tend to float on top of water table, whereas, DNAPLs deposit on the bottom of the aquifers, following the slopes of the confining layers (Figure 1.1). This condition also causes LNAPL to migrate further from the spill point source, following the groundwater flow direction. Consequently, the environmental impact of LNAPLS will be greater considering that the affected area is usually bigger than the source radius.

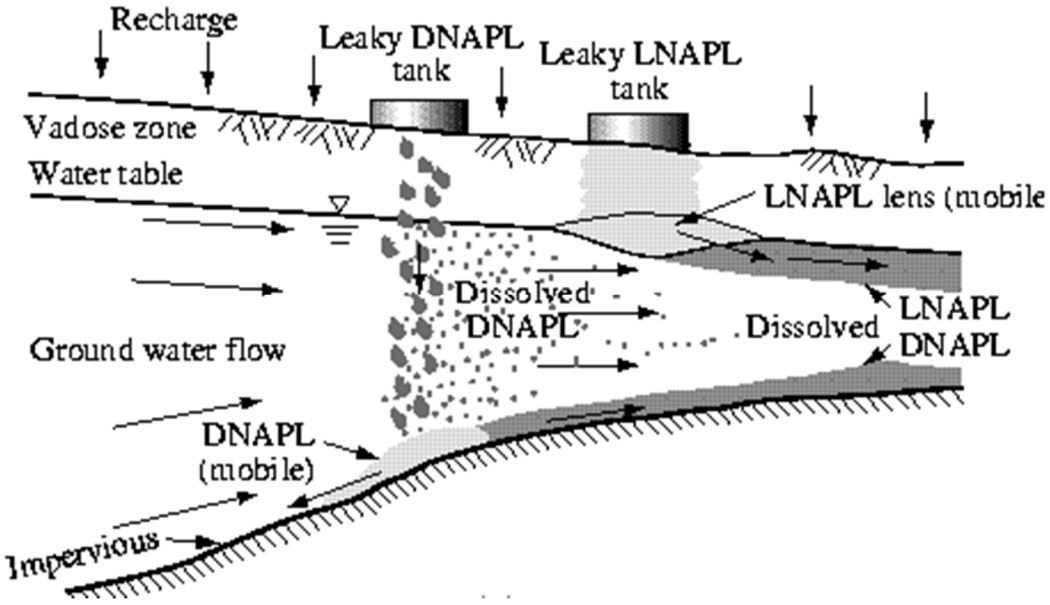

Figure 1.1 Typical LNAPL and DNAPL spill plumes (Bear 2000).

After the release of LNAPL into the subsurface, it can move through the pores within the soil due to gravitational and capillary forces. During this migration, the liquid leaves behind ganglia trapped and immobilized in the pores as non-drainable residual LNAPL (Wipfler and van der Zee 2001). High leaking volume may lead to downward migration and accumulation in the groundwater table. As the groundwater table is subjected to fluctuations due to precipitations, LNAPL migration is also affected by this phenomenon. Groundwater fluctuations can cause vertical displacement and redistribution of LNAPL within the saturated and unsaturated zones (Flores et al. 2011).

Although it is known that rainfall indirectly affects vertical displacement of LNAPL through the groundwater fluctuation level, the direct effects of precipitation on LNAPL migration need to be evaluated. The study of these effects is necessary in order to assess the LNAPL contamination plume when subjected to precipitation. Currently, the behavior of LNAPL migration into the saturated zone due to drainage and imbibition, which can be related to groundwater fluctuation conditions, have been discussed up to the pore level (Helland and Skjæveland 2007; Porter et al. 2009; Raeesi and Piri 2009). A good understanding of migration behavior at the pore level, such as the relationship between saturation and capillary pressure and the mechanisms involved, is important for further research development, especially in predicting LNAPL migration behavior. However, the effect of precipitation on LNAPL migration has not been studied either in general behavior or at pore level. A clear understanding of LNAPL migration mechanism due to precipitation at pore level is necessary in order to accurately evaluate LNAPL migration behavior at spill sites. When precipitation infiltrates unsaturated zones, the wetting front propagation will increase the soil saturation, affecting the capillarity behavior and LNAPL migration behavior. The precipitation can directly affect the infiltration behavior and wetting front propagation as well. Although LNAPL is lighter than water, it is believed that precipitation infiltrated water will bring mobile LNAPL deeper into saturated layers and thus extend the degree of groundwater contamination.

1.2 Objectives and Scopes of this Study

The aim of this research is to evaluate LNAPL migration behavior in the subsurface due to precipitation. To cope with this, LNAPL migration behaviors at different precipitation conditions were experimentally studied by designing laboratory one-dimensional columns and two-dimensional tank tests. The goals of the experimental tests were (a) to investigate LNAPL migration behavior affected by LNAPL spill volume, precipitation intensity, and equal precipitation volume in one-dimensional column test and (b) to investigate LNAPL migration behavior in a two-dimensional tank test, and evaluate the saturation-pressure relation for both one-dimensional column and two-dimensional tank tests.

1.3 Dissertation Outline

This dissertation is composed of six chapters. The structure and content of this dissertation is shown in Figure 1.2. In chapter one presents the objectives of this research and outlines of this dissertation. In chapter two reviews the literature on NAPL migration in porous media, image analysis method and precipitation. In chapter three discusses the effects of LNAPL spill volume on LNAPL migration behavior due to precipitation. This chapter discusses the redistribution of LNAPL saturation in contamination plume of different spill volume condition when subjected to precipitation. In chapter four discusses the effects of intensity and equal volume of precipitation on LNAPL migration behavior due to precipitation. Based on migration behavior pattern obtained from previous chapter three, the investigation was extended to various intensity and volume of precipitation. The mechanism of LNAPL migration due to precipitation is proposed based on the results and discussion. In chapter five describes LNAPL migration behavior due to precipitation in two-dimensional condition. Also, it discusses the saturation-capillary pressure relation for one-dimensional and two-dimensional conditions. Based on saturation-capillary pressure relationship results and discussions, the controlling parameter that causes LNAPL migration due to precipitation was identified. Finally, in chapter six summarizes the results of this study and presents further research.

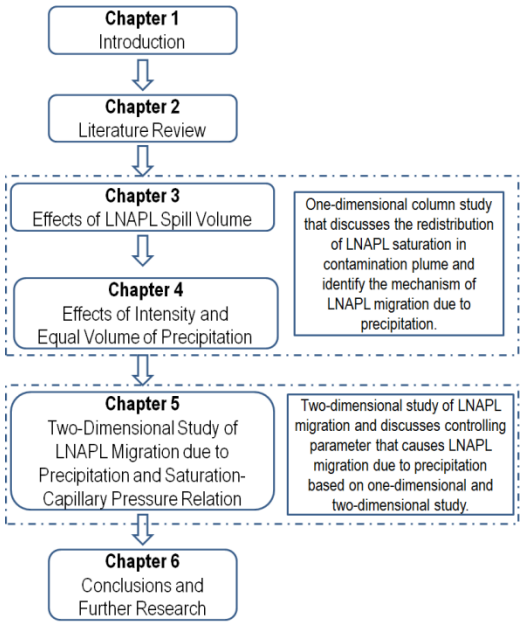

Figure 1.2 Outline of this dissertation.

CHAPTER 2: LITERATURE REVIEW

2.1 General Remarks

In Japan, the Soil Environmental Standard was established based on the Pollution Control Basic Act (which was revised to Environmental Basic Act in 1993) as an administrative target in order to prevent human health impact caused by agricultural land and groundwater (MOE Japan 1993). In England, the legal definition of contaminated land as land where substances could cause either significant harm to people or protected species, or significant pollution of surface water or groundwater (DEFRA 2012). Everywhere in the world, regulatory agencies try to protect the health of humans and other living creatures by limiting or preventing exposure to groundwater pollution.

The contaminant can be introduce in the groundwater by naturally occurring activities, such as natural leaching of the soil and mixing other groundwater sources having different chemistry. They also introduced by planning human activities such as waste disposal, mining, and agricultural operation. The contamination from naturally occurring activities is usually small, whereas human activities are the leading cause of groundwater contamination and the focus of most regulatory agencies (David and Bela 2000).

The purpose of this chapter is to briefly introduce the LNAPL contamination in the subsurface as well as the basic concept of multiphase flow in porous media. The experimental technique to measure water and LNAPL saturation on soil samples was also introduced. This technique is unique as it is able to measure soil saturation in dynamic conditions. Since this research is regarding the LNAPL migration due to precipitation, a basic hydrology cycle concept is also introduced in this chapter.

2.2 LNAPL Contamination in Subsurface

In today's industrial society, the utilization of non-aqueous phase liquid (NAPL) is very prevalent. From solvent to fuel oil, this organic hydrocarbon has served industrial evolution very well. Despite NAPL's good deeds for society, mismanagement of this chemical may have a negative impact on human health and the environment due to its

toxicity. NAPL can be introduced into the unsaturated zone as a result of spill, leaks from faulty storage tank or pipes, leakages from corroded drums, and burst of pipelines.

When its quantity is small, the NAPL will move and spread out in the unsaturated zone, occupying part of the void space within a certain domains, jointly water and air. If the quantity of NAPL is sufficiently large, this soil domain will continue to expand, primarily downward, until reaching an underlying water table. In the subsurface, certain species of an organic liquid may dissolve in the water moving in the void space due to precipitation water infiltration. In this way, these species will reach and contaminate an underlying aquifer.

NAPL are nonpolar compounds which if introduced into a natural environment will remain as a separate liquid phase. NAPL is subdivided into those which have density lower than water as *Light Non-aqueous Phase Liquid* (LNAPL) and those which are denser than water as *Dense Non-aqueous Phase Liquid* (DNAPL). Common example of LNAPL is diesel, gasoline, and kerosene, while DNAPL such as Tetrachloroethylene (PCE) and Polycyclic Aromatic Hydrocarbons (PAH). LNAPL may be pure organic compounds, or like diesel and gasoline, complex mixture of a large number of compounds. The various LNAPL components may dissolve in the aqueous phase in small quantities, each according to its own water solubility. Unfortunately, some chemical species in drinking water may have deleterious effects on human being, even at concentrations as low as few parts per billion (ppb) (Bear and Cheng 2010). According to US EPA guideline, the *Benzene, Toluene, Ethylbenzene, Xylenes* (BTEX) limits in the discharges resulting from the cleanup of gasoline released from underground storage tanks must be less than 0.1 mg/L (United States Environmental Protection Agency 2005). The BTEX concentration in the contaminated groundwater could reach up to 15,000 mg/L (Schubert et al. 2007). Therefore, the groundwater contamination due to LNAPL is a very serious problem.

If a small quantity of LNAPL is spilled on ground surface, it will percolate through the vadose zone, primary downward. As the NAPL travels downward, it leaves behind isolated blobs and ganglia of NAPL. When the quantity of spilled LNAPL is larger, the downward moving LNAPL may reach the capillary fringe and form a lens floating and moving according to the prevailing hydraulic gradient (Figure 2.1). The moving lens leaves behind a trail of ganglia at residual LNAPL saturation. Eventually the floating LNAPL lens

may become immobile at residual LNAPL saturation. Water passing through this domain of immobile water will be contaminated (Bear and Cheng 2010).

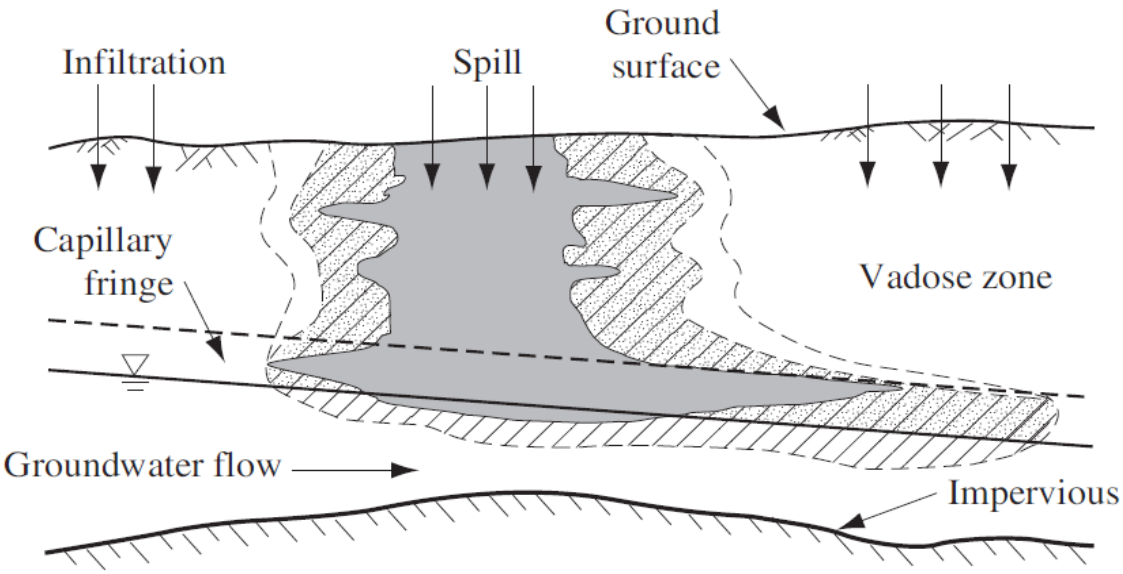

Figure 2.1 LNAPL spill in subsurface (Bear and Cheng 2010).

2.3 Multiphase Flow in Porous Media

2.3.1 Fluid Density

The fluid density (ρ) is its mass per unit volume. Density is defined as mass (m) divided by volume (v):

$$\rho = \frac{m}{v} \tag{2.1}$$

The relative density (RD), or specific gravity (SG), is the dimensionless ratio of the density (mass of a unit volume) of a substance to the density of a given reference material. The reference material can be indicated using subscripts: $RD_{\text{substance/reference}}$, which means "the relative density of substance with respect to reference." Specific gravity usually means relative density with respect to water at 4°C, which is the temperature at which water reaches its maximum density. In SI units, the density of water is approximately 1000 kg/m^3 or 1 g/cm^3, which makes relative density calculations particularly convenient. The density of the substance only needs to be divided by 1000 or 1, depending on the units.

2.3.2 Viscosity and Relation to Hydraulic Conductivity

The viscosity is the fluid resistance to shear or flow and is a measure of the frictional fluid property. The resistance is caused by intermolecular friction exerted when layers of fluids attempt to slide by one another. Viscosity is temperature-dependent, and viscosity reduces as temperature increases for most liquids. For NAPL, the variation of viscosity is significant between different types, especially in low temperature, as shown in Figure 2.2 (Franco and Nguyen 2011).

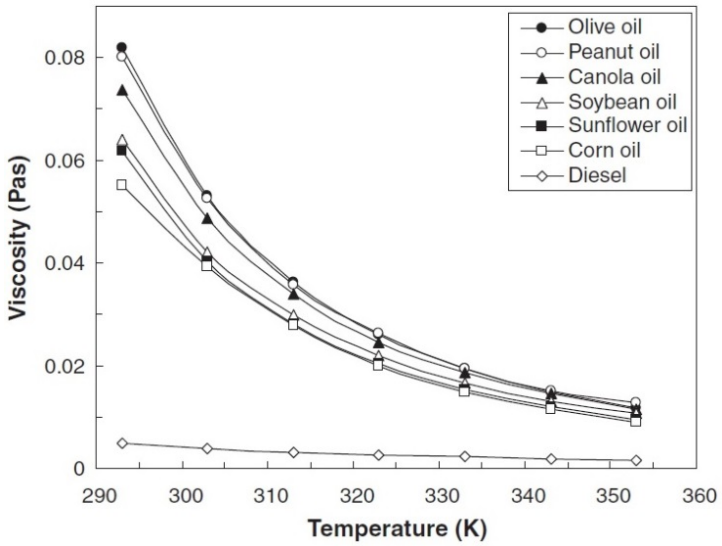

Figure 2.2 Variation of various oil viscosities in temperature (Franco and Nguyen 2011).

Fluid viscosity is usually described in two terms: kinematic viscosity and dynamic viscosity. Kinematic viscosity (v) is the ratio of dynamic viscosity (μ) to density (ρ), a quantity in which no force is involved:

$$v = \frac{\mu}{\rho} \tag{2.2}$$

As dynamic viscosity (μ) represents force required for a liquid to flow in a porous medium, the hydraulic conductivity increases as the liquid viscosity decreases. The effect of dynamic viscosity (μ) on hydraulic conductivity (κ) with the given permeability (K) can be seen in hydraulic conductivity (K) expression as:

$$\kappa = \frac{K\rho g}{\mu} \tag{2.3}$$

where κ is the hydraulic conductivity in unit m/s, which represents the flow of water through a porous media over a period of time, and K is the permeability of a porous medium in unit m^2, which represents the ability of a porous material to allow fluids to pass through it.

2.3.3 Interfacial Tension

When two different liquid or gases phases are in contact with each other, the molecules at the interface experience an imbalance of forces. This will lead to an accumulation of free energy at the interface. The excess energy is called surface free energy and can be quantified as a measurement of energy per area, which means energy required to increase the surface area of the interface by a unit amount. It is also possible to describe this situation as having a line tension or interfacial tension, which is quantified as a force per length measurement. If an interface arising from one of the phases is the gas phase, it is normally referred to as surface tension.

When two immiscible fluids coexist on a porous media, an interface which divides these immiscible fluids is formed. This interface is actually a very thin zone of transition between the two phases. In order to maintain the force equilibrium, the interface is pulled by the fluid whose molecules are bound by greater attractive forces. Thus, either a convex or a concave meniscus is formed. The stretched interface behaves much like an elastic membrane subjected to tension. The tension existing at the interface, known as interfacial tension, is a result of the internal pressure difference of the two adjoining phases, as shown in Figure 2.3.

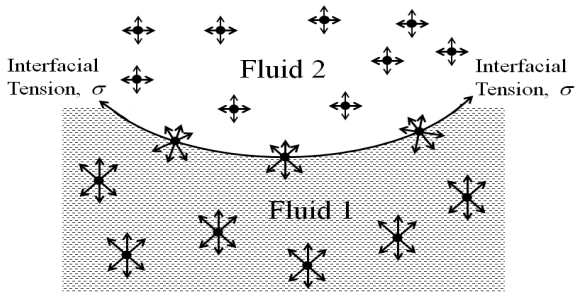

Figure 2.3 Molecular attraction forces in the individual phases and at the interface of two phases.

2.3.4 Wetting Angle

When two immiscible fluids are in contact with a plane solid surface, the interfaces between the solid and the fluid phases control the phase configuration. The interfaces between the solid and the fluids can be shown in Figure 2.4. In this figure, three interface boundaries can be delineated in the three configurations. The first configuration is the interface between solid (*s*) and fluid 1 (*n*), the second configuration is the interface between solid (*s*) and fluid 2 (*w*), and the third configuration is the interface between fluid 1 (*n*) and fluid 2 (*w*). The stable configuration will be one where the tensions associated with these three interfaces are in equilibrium. At equilibrium,

$$\sigma_{sn} = \sigma_{sw} + \sigma_{nw} \cos \lambda_{nw} \qquad \text{or} \qquad \lambda_{nw} = \cos^{-1}\left[\frac{\sigma_{sn} - \sigma_{sw}}{\sigma_{nw}}\right] \tag{2.4}$$

Equation (2.4) is called Young's or Dupré equation, which states that cos λ_{nw} is the ratio of the work required to change a unit area of the *s*-*n*-interface into a unit area of the *s*-*w*-interface to the work required to form a unit area between the *w*-phase and the *n*-phase.

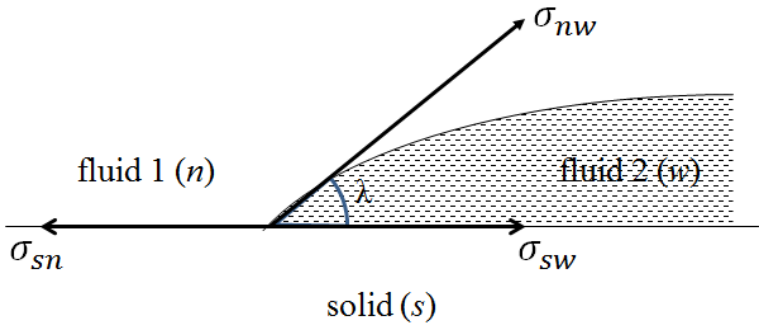

Figure 2.4 Forces acting along interfaces between the three phases at equilibrium.

The angle λ_{nw}, which is the angle between the surface of the solid phase (*s*) and the fluid-fluid interface (fluid 1 (*n*) – fluid 2 (*w*)), is called the contact angle or wetting angle. The fluid-fluid interface angle is measured through the denser fluid. The angle λ_{nw} is a measure of wettability of the solid surface with respect to fluid 2 (*w*).

There are three possibilities for the magnitude of the contact angle between fluids and solid surfaces, as shown in Figure 2.5. Figure 2.5.a refers to complete wetting of the solid surface by fluid 2 when $\lambda = 0$. If fluid 2 is water, the solid surface is hydrophilic. A partial wetting of the solid surface occurs in the range, $0° < \lambda < 90°$, as shown in Figure 2.5.b. Figure 2.5.c indicates that the surface is relatively non-wetting with respect to fluid 2 when λ is more than 90°. If fluid 2 is water, the solid surface in this case will be hydrophobic. With regard to a soil mass whose pores are filled with two fluids (1 and 2), the angle λ therefore dictates which fluid coats the solid particles.

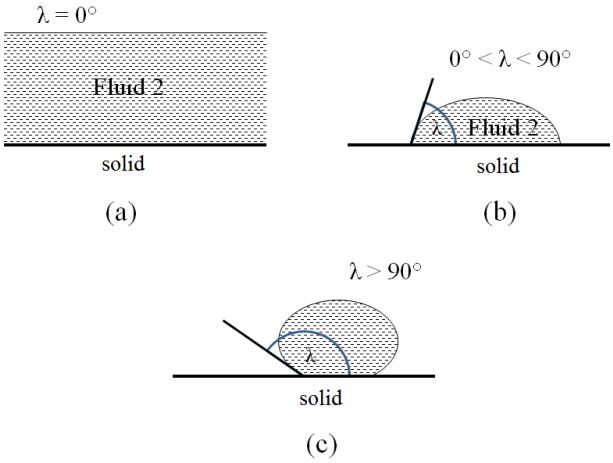

Figure 2.5 Possible contact angles between fluids and solid surfaces, with: (a) complete wetting, (b) partial wetting, and (c) surface being relatively non-wetting.

When a porous medium is in contact with NAPL and water, it is considered to be water-wet if λ (between water and the solids) < 70°, NAPL-wet if $\lambda > 110°$, and neutral if λ is between 70° and 110° (Anderson 1986). In most cases with NAPL and water, the porous medium is commonly treated as water-wet. In an unsaturated medium where NAPL and air are present, the medium is treated as NAPL-wet.

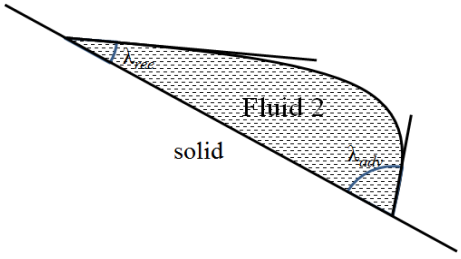

Figure 2.6 Nonuniqueness of contact angle for a moving liquid phase.

When considering the movement of the fluid phase wetting the surface, the contact angle may not be unique. The contact angle λ_{rec} at the receding end is generally less than the contact angle λ_{adv} at the advancing end of the drop, as shown in Figure 2.6. This is the primary reason for hysteresis behavior in soil-water retention. The λ_{rec} is called the receding contact angle and λ_{adv} is called the advancing contact angle.

2.3.5 Saturation of Soils

When the void space of the porous medium is filled by two or more immiscible fluids (liquids or gases), the saturation (or degree of saturation) at a point, with respect to a particular fluid, is defined as the fraction of the void volume of the porous medium occupied by the particular fluid within a Representative Elementary Volume (REV) around the considered point (Bear 1972). The total of the saturation for all the fluids present, including air, adds up to 1.0.

$$S_\alpha = \frac{V_\alpha}{V_t}; \qquad \sum_\alpha S_\alpha = 1 \tag{2.5}$$

where S_α represents the saturation of fluid α, V_α is the volume of the fluid α within an REV, and V_t the volume of voids within the REV.

2.3.6 Capillary Pressure

Capillary pressure is the difference between the internal pressures across the interface of the two immiscible fluids. It is the pore pressure difference between the non-wetting phase, P_n, and wetting phase, P_w. Capillary pressure is considered the negative pressure due to its direct relation with interfacial tension. The capillary pressure, P_c, may be defined as:

$$P_c = P_n - P_w \tag{2.6}$$

where P_n is the pore pressure of the non-wetting phase and P_w is the pore pressure of the wetting phase. It is assumed that the water phase is the most preferential wetting phase, followed by the NAPL phase, and the least preferential wetting air phase (Lenhard and Parker 1987). In an NAPL-water system, water is typically the wetting phase, while for an air-NAPL

system, NAPL is typically the wetting phase. In an air-water system, a natural uncontaminated subsurface, capillary pressure is normally referred to matric suction or matric pressure. This pressure exists in the vadose zone (above ground water level).

In the vadose zone, the negative pressure system that represents capillary pressure can be easily explained in a capillary tube analogy, as shown in Figure 2.7. In this figure, the negative pressure value at point A and point B is the capillary pressure at interfacial tension equilibrium. Capillary pressure is directly proportional to the interfacial tension, contact angle, but inversely proportional to the radius of the curvature (radius of the tube), r, as follows:

$$P_c = \frac{2\sigma_{nw}\cos\lambda}{r} \tag{2.7}$$

where σ_{nw} represents the interfacial tension between non-wetting and wetting phases and λ represents the contact angle of the wetting phases with the surface of the tube.

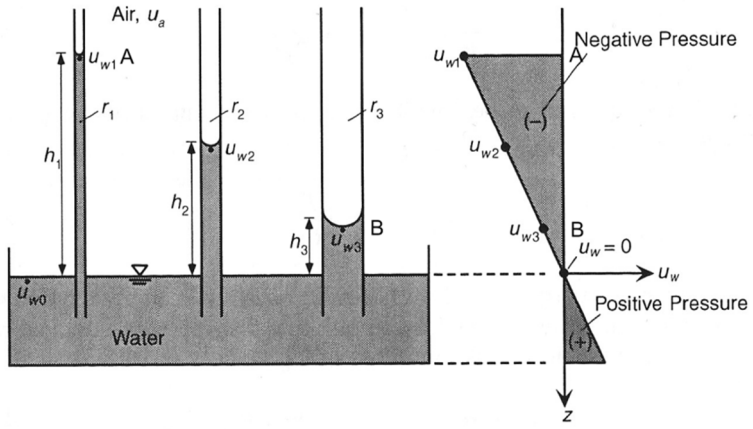

Figure 2.7 Analogy of capillary pressure at various sizes of the capillary tube (Lu and Likos 2004).

In a porous medium, the narrow passage in the pore throat may visualize as a capillary tube, with *r* in Equation (2.7) representing some equivalent radius of such a passage or a pore size. This condition can be illustrated in Figure 2.8. As capillary pressure is inversely proportional to the radius of the curvature, it can be seen that as the pore throat became small, the capillary pressure would increase.

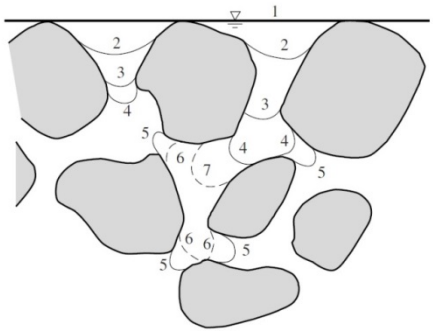

Figure 2.8 Various pore radii of the pore throat in the soil pores (Bear and Cheng 2010).

2.3.7 Relative Permeability

In a porous medium with multiphase flow, Darcy's Law is extended as follows (Dullien 1992):

$$v_i = -\frac{k_{ei}}{\mu_i}(\nabla P_i - \rho_i g) \tag{2.8}$$

where v_i is defined as the average velocity of the fluid i, and P_i, μ_i, ρ_i, and k_{ei} are the hydrostatic pressure, the viscosity, the density, and the effective permeability of the ith fluid, respectively.

The effective permeability, k_{ei}, is generally expressed as a function of the intrinsic permeability k of the medium, which is defined as follows:

$$k_{ei} = kk_{ri} \tag{2.9}$$

where k_{ri} is called the relative permeability of the fluid i.

2.3.8 Saturation-Capillary Pressure Relation (*S-p* Relations)

A Saturation-capillary pressure relation (*S-p* relations) describes the amount of water retained in a soil expressed as saturation, at a given capillary pressure. The general features of an *S-p* relation can be seen in Figure 2.9, in which there can be either the drainage curves, which reflect the reduction of wetting fluid saturation, or the wetting curves, which reflect the increases of the wetting fluid saturation.

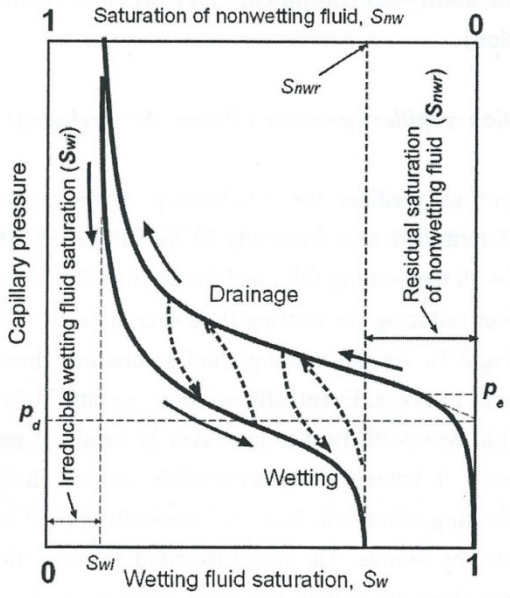

Figure 2.9 *S-p* relations during drainage and wetting (Corey 1994).

The drainage or drying curve projected the reduction of wetting fluid saturation, S_w, from high to low. If the porous medium starts off saturated with the wetting fluid and this wetting fluid is slowly displaced by a non-wetting fluid, it thus reduces the wetting fluid saturation, as shown in the drainage curve. As the wetting fluid saturation drops, the corresponding capillary pressure will increase. Eventually, no more wetting fluid will be displaced by the non-wetting fluid, even with further increases in capillary pressure. The value at this point is known as the irreducible, or residual, wetting fluid saturation, S_{wi}. If from this point the non-wetting fluid is displaced by forcing the wetting fluid into the sample, we obtain a wetting or imbibition curve. When the imbibition curve reaches zero capillary pressure, some of the non-wetting fluid will remain in the porous medium. The value of saturation at this point is known as the irreducible, or residual, non-wetting fluid saturation, S_{nwr}.

When porous medium is subjected to rewetting, the capillary pressures, P_c, of the rewetting *S-p* curve may differ from the one obtained during initial wetting for the same saturation value. This phenomenon, the dependence of the capillary pressure curve on the direction and history of drainage and wetting of a sample, is called hysteresis. Hysteresis is attributed to several factors which can be grouped into two main categories: saturation hysteresis and fluid entrapment. Figure 2.10 shows the effects of saturation hysteresis and fluid entrapment.

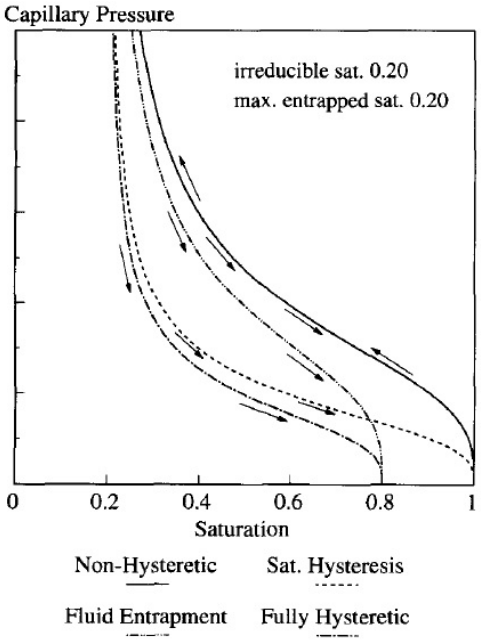

Figure 2.10 Saturation hysteresis and fluid entrapment (Van Geel and Sykes 1997).

Saturation hysteresis is a result of the pore space geometry, with interchanging narrow and wide passages in the pore throats. The second contributing factor, fluid entrapment, occurs as a wetting fluid displaces a non-wetting fluid in its path. A fraction of the non-wetting fluid becomes entrapped in the wetting fluid.

The analytical expressions of the general shape of *S-p* relation curves have been proposed by few authors, such as Brooks and Corey (1966), Brutsaert (1966), Vauclin et al. (1979), and van Genuchten (1980). These expressions involve coefficients that must be determined by solving the inverse problem by means of fitting the analytical expression to measured experimental data. All of these expressions are proposed based on unsaturated soil study where the interaction between the non-wetting phase and wetting phase is basically the interaction of air and water in soil. These expressions are derived by considering the effective wetting saturation, S_{we}, and the capillary pressure head, P. The effective saturation is considering the difference between the wetting phase saturation, S_w, and irreducible wetting saturation, S_{wr}, which is defined as:

$$S_{we} = \frac{S_w - S_{wr}}{1 - S_{wr}} \tag{2.10}$$

Among those expressions for *S-p* relations, the relation proposed by van Genuchten (1980) is frequently used, and it is widely known as the VG model. The expression derived by van Genuchten:

$$S_{we} = \begin{cases} \left[\frac{1}{1+(\alpha P)^n}\right]^m, & h > 0 \\ 1 & , \ h \leq 0 \end{cases} \tag{2.11}$$

Where P is the capillary pressure head, α and n are the curve shape parameter with $m = 1 - 1/n$.

2.3.9 Scaling Factor Methods for Predicting *S-p* Relationship

The prediction of immiscible phase movement requires consideration of simultaneous convection of all concurrently existing continuous fluid phases, generally water, NAPL and air. Due to the difficulty and time required to directly measure three-phase *S-p* relations, researchers start to propose the scaling factor to approximate the three-phase relationships from the more easily measured two-phase relationships (Stone 1970; Parker et al. 1987). In most of this research, the three-phase behavior is predicted using the scaling factor based on assumptions first proposed by Leverett (1941). In Leverett's work, the magnitude of the capillary pressure between any two immiscible fluid phases is proportional to the interfacial tension between those phases, given as:

$$\frac{P_{ow}}{\sigma_{ow}} = \frac{P_{ao}}{\sigma_{ao}} = \frac{P_{aw}}{\sigma_{aw}} \tag{2.12}$$

where σ_{ow}, σ_{ao}, and σ_{aw} are the interfacial tensions along the interfaces between the NAPL and water phases, the gas and NAPL phases, and the gas and water phases, respectively. P_{ow}, P_{ao}, and P_{aw} are the capillary pressure between the NAPL and water phases, the gas and NAPL phases, and the gas and water phases, respectively.

The scaling factor is beneficial for multiphase flow study in a porous medium, as it is only necessary to measure one set of *S-p* relations to obtain the other set of *S-p* relations in the system. Therefore, the *S-p* relations for the third system may then be predicted (Parker et

al. 1987). Based on Leverett's work, Parker et al. (1987) proposed a scaling factor, which is frequently used nowadays, that is able to extend the two-phase data to the three-phase systems using the following expression:

$$\beta_{aw}P_{aw} = \beta_{ow}P_{ow} = \beta_{ao}P_{ao} \tag{2.13}$$

where according to Lenhard and Parker (1987):

$$\beta_{aw} = 1 \tag{2.14}$$

$$\beta_{ow} = \frac{\sigma_{aw}}{\sigma_{ow}} \tag{2.15}$$

$$\beta_{ao} = \frac{\sigma_{aw}}{\sigma_{ao}} \tag{2.16}$$

where β_{ij} is a fluid pair-dependent scaling factor. In this scaling factor, *S*-*p* relations of two-phase air-water, air-organic and organic-water systems are adjusted so as to obtain a unique function for a given porous medium after applying a linear transformation to capillary heads, such that:

$$S_{we}(\beta_{aw}P_{aw}) = S^*(P^*) \tag{2.17}$$

$$S_{we}(\beta_{ow}P_{ow}) = S^*(P^*) \tag{2.18}$$

$$S_{we}(\beta_{ao}P_{ao}) = S^*(P^*) \tag{2.19}$$

where $S^*(P^*)$ is a scaled saturation-capillary head function. For a rigid porous medium, scaling coefficients are related by (Lenhard and Parker 1987):

$$\frac{1}{\beta_{ow}} + \frac{1}{\beta_{ao}} = \frac{1}{\beta_{aw}} \tag{2.20}$$

Accordingly, if β_{ao} is known, at a given wetting phase saturation, P_{ao} can be obtained depending on Equation (2.13) and the S-p relations in an air-NAPL system can be obtained. The procedure for predicting S-p relations in an air-NAPL system can be described as follows: (1) taking an air-water system as a reference fluid pair system and setting β_{aw} = 1, (2) fitting S-p relation data in an air-water system to obtain $S^*(P^*)$, (3) obtaining β_{ow} depending on Equation (2.18) and β_{ao} depending on Equation (2.20), and (4) calculating S_{oe} and P_{ao} depending on Equation (2.19). Here, $S_{oe} = (S_o - S_{or}) / (1 - S_{or})$, and S_{or} is the wetting phase residual saturation in an air-NAPL system. Compared to air, NAPL is a wetting phase fluid in an air-NAPL system. S_{wr} is assumed to be constant for all two-phase systems (Lenhard and Parker 1987).

2.4 Saturation Measurement in Dynamic Conditions

Saturation-capillary pressure relation (*S-p* relation) is often used in LNAPL contamination and migration studies due to its ability to describe the amount of fluid retained in soil, expressed as saturation at a given capillary pressure. There are two parameter requirements for *S-p* relations, which are saturation and capillary pressure. Soil capillary pressure can be measured using a tensiometer in either static or dynamic conditions. There are several methods to measure soil saturation, such as gravimetric soil sampling (ASTM 1987), gamma ray attenuation (Oostrom et al. 1998), X-ray attenuation (Hill Iii et al. 2002), electrical conductivity probe (Kamon et al. 2003) and image analysis method (Kechavarzi et al. 2000). These saturation measurement procedures can be divided approximately into two categories, ex-situ and in-situ methods.

The gravimetric soil sampling method involves extraction of the sample, weighing and heating to obtain soil saturation. Since this method requires extraction of a soil sample, it is considered an ex-situ method. Therefore, it is not suitable for soil saturation measurement in cases when the soil is subjected to saturation changes, such as in dynamic conditions. Gamma ray attenuation and X-ray attenuation methods are both considered in-situ saturation measurement tests. However, the ability of the testing apparatus in these radiation techniques has some limitation in obtaining continuous measurements, thus, this method is also not suitable for soil saturation measurement in dynamic conditions. Electrical conductivity probe and image analysis methods are both methods that are non-destructive, in-situ and able to

measure soil saturation continuously. Thus, these methods are suitable for soil saturation measurement in dynamic conditions. For LNAPL study in a laboratory setup, the image analysis method proves more advantageous in taking soil saturation measurements because of the utilization of a camera. Since saturation measurement with the image analysis method is based on analysis of the image taken from the camera, the soil saturation of the entire domain can be obtained as the picture of the whole domain can be taken in a split second using a camera. In this section, the electrical conductivity probe and image analysis methods are discussed further.

2.4.1 Electrical Conductivity Probe

The water content in a porous medium can be measured by the changes in electrical resistivity of this medium as described by Archie (1942, 1947). Soil systems with higher water content are endowed with lower electrical resistivity values. Endo (2002) and Kamon et al. (2003) describe a three-electrode probe (Figure 2.11) that can be used to estimate water saturation via the measurement of the electrical conductivity of a soil system under immiscible two-phase flow conditions. A one-probe schematic circuit of the water saturation measurement system is shown in Figure 2.12. Low-voltage AC is preferred so that the probes do not interfere with each other and electrolytic reactions in the vicinity of the electrodes do not occur. A data logger records the potential difference on a resistance attached to the probe. To estimate the water content of a sand sample, a regression curve relating both output signal and water content is needed. This calibration curve needs to be prepared for every soil sample (Li 2005).

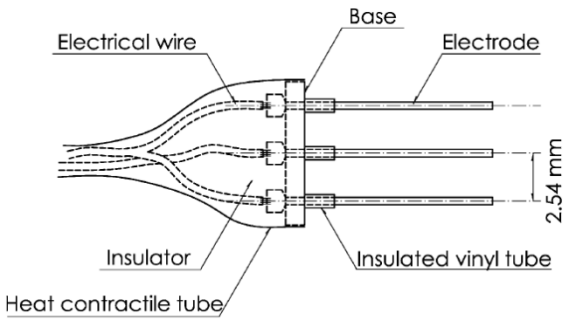

Figure 2.11 Three-electrode conductivity probe (Kamon et al. 2003).

In accordance with Ohm's Law, if the resistance across the sample has a good relation with its water content, the voltage across the same sample must have a good relation with its water content. Thus the output voltage across the resistance attached to the probe can be used as a parameter to estimate the water content. The cosine function describing the output voltage is:

$$f(t) = A_0 + C_1 cos(w_0 t + \theta) \tag{2.18}$$

where, *f(t)* is the voltage received by the data logger from the electrical conductivity probe, A_0 is the average height above the abscissa, C_1 is the amplitude or height of the oscillation, w_0 is the angular frequency ($w_0 = 2\pi f, f = 0.1$) and is the phase angle.

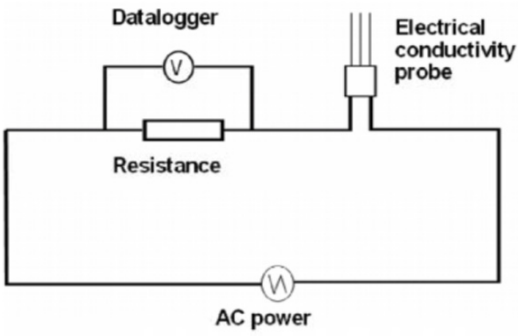

Figure 2.12 Water saturation measurement system circuit (Endo 2002).

Based on the fitting method by Canale and Chapra (1998) the parameters A_0, C_1 and w_0 can be calculated from:

$$\theta = \arctan\left(-\frac{B_1}{A_1}\right) \tag{2.19}$$

$$C_1 = \sqrt{A_1^2 + B_1^2} \tag{2.20}$$

$$A_0 = \frac{\sum y}{N} \tag{2.21}$$

where:

$$A_1 = \frac{2}{N}\sum y \cos(w_0 t) \tag{2.22}$$

$$B_1 = \frac{2}{N}\sum y \sin(w_0 t) \tag{2.23}$$

Saturation follows the empirical equation:

$$S_w = A\left(1 - e^{B \cdot R/R_0}\right) \tag{2.24}$$

Where S_w is water saturation, R is the corresponding output voltage, R_0 is a reference output voltage, and A and B are fitted parameters.

2.4.2 Image Analysis Method

Lambert's Law was discovered by Pierre Bouguer before 1729, and states that for a parallel beam of monochromatic radiation passing through homogenous solutions of equal concentration, the absorbance is proportional to the path length. Much later, August Beer extended the exponential absorption law in 1852 to include the concentration of solutions in the absorption coefficient. This finding, which is called Beer's Law, states that for a parallel beam of monochromatic radiation passing through homogenous solutions of equal path length, the absorbance is proportional to the concentration. This comes to their relation which states that for a parallel beam of monochromatic radiation passing through a homogenous solution, the absorbance is proportional to the product of the concentration and path length depending on the substance, the solvent, the wavelength, and the units for concentration and path length. The laws can be mathematically combined (Lohman 1955) and called Beer-Lambert Law with the equation:

$$-\log_{10}\frac{I}{I_o} = alc \tag{2.21}$$

where a is absorptivity, l is length of the distance the light travels through material, c is concentration of the absorbing species, and I and I_o are the intensity of the transmitted light and incident light, respectively. This law is most frequently used in an image analysis method either in the chemistry, biology or physics field.

The saturation-pressure relation (*S-p* relations) is one of the important analysis tools in evaluating contamination migration in the soil. Measurement of pore pressure proves to be simple, with some of these researchers relying on mechanical set-ups that manually increase suction values (Høst-Madsen and Høgh Jensen 1992; Sharma and Mohamed 2003) and others

on pressure transducers (Van Geel and Sykes 1994; Rimmer et al. 1998; Kamon et al. 2003). Measurement of saturation, on the other hand, doesn't have a prevalent technique and can be divided roughly into two categories: ex situ and in situ. An ex situ technique involves drying-oven heating, which destroys the sample. An in situ technique is a non-intrusive and non-destructive method, and can be used to acquire dynamic fluid saturations. Of the latter technique, gamma ray attenuation and x-ray synchrotron techniques do not allow the acquisition of dynamic fluid saturation distribution in the entire domain at one time; therefore, an image analysis method has been developed as an alternative tool in measuring transient phenomena in the entire domain at one time (Kechavarzi et al. 2000).

2.4.3 Multispectral Image Analysis Method

Kechavarzi et al. (2000) presented a Multispectral Image Analysis Method (MIAM) to determine dynamic fluid saturation distributions of water, NAPL and air in two-dimensional intermediate-scale laboratory experiments. This technique provides a non-destructive and non-intrusive tool for multiphase fluid flow imaging for systems with rapid changes. Optical density (D) can be defined in terms of reflectance:

$$D = \log_{10}(\rho) \tag{2.22}$$

Reflectance is defined as:

$$\rho = \frac{I^r}{I^o} \tag{2.23}$$

where I^r and I^o are the intensity of the reflected light and the light that would be reflected by an ideal white surface, respectively. Differences in reflectance of water and the LNAPL within the narrow spectral bands, measured with a spectrometer, formed the basis of the saturation determinations. Digital images were obtained within these spectral bands by placing band-pass interference filters in front of the camera lens. A gray scale was placed next to each sample to allow for correction of spatial and temporal lighting condition variations between images. The light intensity was divided into 4096 gray levels. Each sample contained a fixed area (fixed number of pixels on the image) of interest (AOI) for which the average optical density for the water phase and LNAPL was determined from the

following:

$$D_i = \frac{1}{N}\sum_{j=i}^{N} d_{ji} = \frac{1}{N}\sum_{j=i}^{N}\left[-\log_{10}\left(\frac{I_{ji}^{r}}{I_{ji}^{o}}\right)\right] \tag{2.24}$$

where N is the number of pixels contained in the AOI for a given spectral band i (i = 500, 760 or 970), and d_{ji} is the optical density of the individual pixels. Plotting D values versus aqueous phase saturation, S_1, in the air-water systems, and versus saturation of the LNAPL saturation, S_n, in the air-LNAPL systems, resulted in the linear relationships.

$$\begin{aligned} D_i^w &= \lambda_i^w S_w + \beta_i^w \\ D_i^o &= \lambda_i^w S_w + \beta_i^o \end{aligned} \tag{2.25}$$

where w and o refer to the water and LNAPL, respectively, i refers to the centered wavelength of the three spectral bands (i = 500, 760 or 970), and λ and β are regression coefficients. The fluid saturation is obtained by solving the equation.

2.4.4 Simplified Image Analysis Method

Flores et al. (2011) presented a Simplified Image Analysis Method (SIAM); similar to the Multispectral Image Analysis Method, it employs the extension of the Beer-Lambert Law of transmittance that a linear relationship exists between average optical density (D_i) and water and LNAPL saturation values (S_w and S_o). It is used to calculate both water and LNAPL saturation distributions for porous subsurface domains subject to contamination by an LNAPL and to fluctuating groundwater conditions, under laboratory-controlled environmental conditions. The SIAM accounts for the effects of the variable angle of incidence of the reflected light and eliminates the need to prepare the dozens of samples required for calibrating the regression linear plane, while at the same time improving its accuracy for points far from the center.

The development of the Simplified Image Analysis Method was brought about by the simplification of the complex calibration process of MIAM. Table 2.1 gives a summary of the difference between the two Image Analysis Methods. In simplifying the calibration process, the Simplified Image Analysis Method (SIAM) increases the mathematical complexity of the

computational analysis by providing not one set of regression equations for the whole domain, but one set of equations for each mesh element of the whole domain. This increase in complexity improves the accuracy of the method by providing each mesh element with its own set of non-related equations (from the images taken by two different spectral bands) that account for both spatial variations of light and other surface imperfections.

Table 2.1 Difference between MIAM and SIAM.

	Multispectral Image Analysis Method (MIAM)	**Simplified Image Analysis Method (SIAM)**
Average Optical Density Calculations	Image Subtraction	Each mesh element (matrix) have its own set of AOD equations
Cameras	1	2
Filters	3 Filters (500nm, 760nm, 970nm)*	2 Filters (450nm & 640nm)
Calibrated Sample	Sample container	Experimental Domain (column)
Experiment Calibration	>40 samples with different degrees of LNAPL saturation and water saturation (the more samples, the higher accuracy level)	3 Non-linear points to recreate linear regression plane taken from these pictures (S_w= 0% S_o = 0% Dry Sand S_w=100% S_o = 0% Sand fully saturated with water S_w= 0% S_o = 100% Sand fully saturated with LNAPL)

*only two are used for the calculations of S_o and S_w equations

SIAM obtains the saturation distribution matrices ([S_w] and [S_o]) by comparing average optical densities between the matrix element (D_i) and three calibration pictures (D_i^w, D_i^o, and D_i^d), for the same domain. The average optical density values for each mesh element of the studied domain can be calculated and compared to the corresponding ones for all three calibration pictures, and a matrix of correlation equation sets can also be obtained, with each one corresponding to each mesh element (Equation 2.26):

$$\begin{bmatrix} D_i \\ D_j \end{bmatrix}_{mn} = \begin{bmatrix} (D_i^w - D_i^d)S_w + (D_i^o - D_i^d)S_o + D_i^d \\ (D_j^w - D_j^d)S_w + (D_j^o - D_j^d)S_o + D_j^d \end{bmatrix}_{mn} \quad (2.26)$$

where m and n are the dimensions of the matrix, $[D_i]_{mn}$ and $\left[D_j\right]_{mn}$ are the values of average optical density of each mesh element for wavelengths i and j; $\left[D_i^d\right]_{mn}$and $\left[D_j^d\right]_{mn}$ are the average optical density of each mesh element for dry sand; $[D_i^w]_{mn}$ and $\left[D_j^w\right]_{mn}$ are for water saturated sand; and $[D_i^o]_{mn}$ and $\left[D_j^o\right]_{mn}$ are for NAPL saturated sand.

2.5 Groundwater Recharge from Hydrologic Cycle

2.5.1 Hydrologic Cycle

The hydrologic cycle begins when the water (in a form of water vapor) evaporates from the surface water and then rises up to form a cloud. Surface water is water on the surface of the planet, e.g., river, lake or ocean. Evaporation of water occurs when the surface of the liquid is exposed, allowing molecules to escape and form water vapor. Rising air currents take the vapor up into the atmosphere where cooler temperatures cause it to condense into clouds. Air currents move water vapors around the globe; cloud particles collide, grow, and fall out of the upper atmospheric layers as precipitation. Once the water reaches the ground, the water may penetrate the surface (infiltration) and become groundwater. Groundwater either seeps its way into the oceans, rivers and lakes or is released back into the atmosphere through transpiration, where the cycle begins again (Figure 2.13).

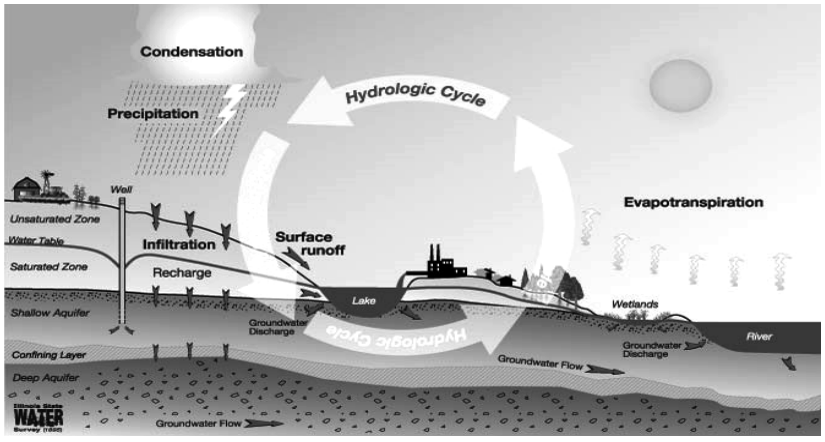

Figure 2.13 Hydrologic Cycle (ISWS 2014).

2.5.2 Precipitation Characteristic

Precipitation is the primary mechanism for transporting water from the atmosphere (in the clouds) to the surface of the earth. The clouds floating overhead contain water vapor and cloud droplets, which are small drops of condensed water. These droplets are way too small to fall as precipitation, but they are large enough to form visible clouds. Water is continually evaporating and condensing in the sky. Most of the condensed water in clouds does not fall as precipitation because its fall speed is not large enough to overcome updrafts which support the clouds. For precipitation to happen, tiny water droplets must first condense on even tinier dust, or smoke particles, which act as a nucleus. Water droplets may grow as a result of additional condensation of water vapor when the particles collide. If enough collisions occur to produce a droplet with a fall velocity which exceeds the cloud updraft speed, then it will fall out of the cloud as precipitation.

As a raindrop increases in size, its shape becomes more oblate, with its largest cross-section facing the oncoming airflow. The small drops' shape is normally spherical. The water droplets can continue to grow by combining with other drops during collision as they fall. Some drops undergo more collisions than others; thus, a distribution of drop sizes develops. Figure 2.14 shows a microphotograph of raindrops collected in a dish of oil showing the range of drop sizes as large as 5 mm in diameter (Pruppacher and Klett 1978).

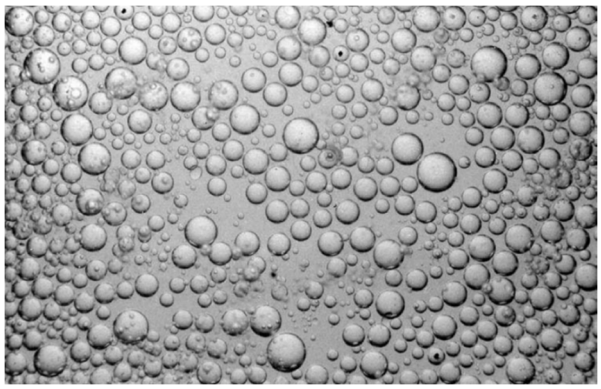

Figure 2.14 Wide range of drop sizes in the course of one rain event (Pruppacher and Klett 1978).

Precipitation has sizes ranging from 0.1 mm to 8 mm in mean diameter. Normally, raindrops can be up to 6 mm in diameter, but anything less than 0.5 mm in diameter is classed as drizzle (UK National Weather Service). Drizzle consists of very small droplets of water falling from low-level stratus clouds. Drops larger than about 10 mm in diameter are hydrodynamically unstable and break up, even in a laminar air stream (Pruppacher and Klett 1978). The largest drops recorded had a diameter as large as 8 mm (Illingworth 1988). Large drops (more than 3 mm in diameter) are found to be very rare in precipitation with intensity less than 50 mm/hr (Mason and Andrews 1960; Blanchard and Spencer 1970; Waldvogel 1974; Zawadzki and Antonio 1988; Willis and Hallett 1991). Typically, a raindrop diameter is limited to less than 2 to 3 mm due to the collisional break-up of drops that destroy large drops in natural clouds (McTaggart-Cowan and List 1975; Takahashi 1978; Low and List 1982).

CHAPTER 3: EFFECTS OF LNAPL SPILL VOLUME

3.1 General Remarks

Rupture of pipelines (Farias et al. 2008), storage tank leakages (Chang and Lin 2006) and fuel truck accidents (McCleneghan et al. 2002) are the common causes of LNAPL spills that normally discharge varied amounts into the soil and surrounding areas. When LNAPL infiltrates the ground, it is normally concentrated in the small radius of the released point at the top, and spreads to a larger cross-section area as it goes deeper; creating a contamination plume like a cone shape. Therefore, when a spill occurs, the LNAPL saturation near the released point area would be high and gradually reduce further from source. This also means that the volume of LNAPL in the soil pores in the area near the released point is higher. When contaminated sand was subjected to precipitation, most probably a one-dimensional flow condition would occur around the released point area, as the soil pores filled with more LNAPL. A two-dimensional condition would probably occur around the boundary of the contamination plume where saturation is not so high, thus, water have preferential to flow vertically or incline as it infiltrated downward. In the study by Schubert et al. (2007), it was shown that the BTEX concentration obtained from groundwater was reduced as the sample point moved further from the spill source in this case a petrol station storage tank. Therefore, the effect of precipitation on LNAPL migration needed to be assessed for both one-dimensional and two-dimensional conditions.

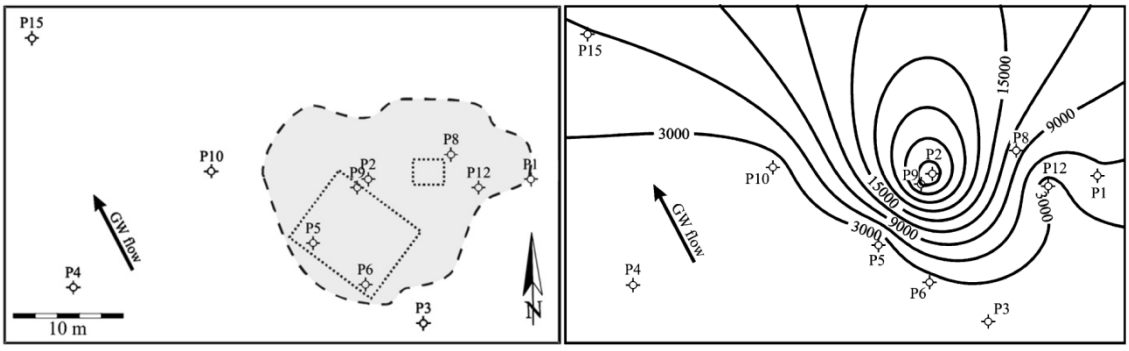

Figure 3.1 (a) Layout of petrol station facilities (dotted lines). (b) BTEX distribution pattern in groundwater (mg/L) (Schubert et al. 2007).

As a first step, the experimental program in this study focused on a one-dimensional condition to obtain a clear understanding on the LNAPL migration mechanism before a more complex condition of two-dimensional condition could be conducted and discussed in Chapter 5. In this chapter, a basic understanding of the LNAPL migration mechanism was obtained through one-dimensional experimental program consisting experiment of different LNAPL spill volume and precipitation intensity.

3.2 LNAPL and Water Saturation Measurement Using Simplified Image Analysis Method (SIAM)

The *Simplified Image Analysis Method* (SIAM) (Flores et al. 2011) is capable of measuring the saturation distribution values for water and NAPL in granular soils for a whole range of large domains instantaneously. Using the Beer-Lambert Law of Transmissivity, the average optical densities of each matrix element (D_i) are compared with those of the same domain fully saturated with water (D_i^w), LNAPL (D_i^o), and completely dry (D_i^d) to obtain the saturation distribution matrices for water ([S_w]) and LNAPL ([S_o]).

Optical density data is obtained from pictures taken with two consumer-grade digital cameras attached to two different band-pass filters. Thus, this method is considered as a non-intrusive and non-destructive technique to measure temporal and spatial distribution of fluid saturations in the whole domain. For each digital image, the average optical density (D_i) is defined for the reflected light intensity as shown in Equation (3.1), where N is the number of pixels in the area of interest and, for a given spectral band i, $d_{ji,}$ the optical density of individual pixels, I_{ji}^r, the intensity of the reflected light given by individual pixel values, and I_{ji}^o, the intensity of light reflected by an ideal white surface (Kechavarzi et al. 2000):

$$D_i = \frac{1}{N}\sum_{j=i}^{N} d_{ji} = \frac{1}{N}\sum_{j=i}^{N}\left[-\log_{10}\left(\frac{I_{ji}^r}{I_{ji}^o}\right)\right] \tag{3.1}$$

SIAM obtains the saturation distribution matrices ([S_w] and [S_o]) by comparing average optical densities between matrix element (D_i) and three calibration pictures (D_i^w, D_i^o, and D_i^d) for the same domain. The first calibration pictures are taken on the model filled with dry sand (S_w = 0%, S_o = 0%), the second ones with water-saturated sand (S_w = 100%, S_o = 0%), and the third ones with LNAPL-saturated sand (S_w = 0%, S_o = 100%).

To compare the average optical densities, each camera uses a different band-pass filter with wavelength, λ (equal to i and j), similar to the predominant color wavelengths in the dyes for water and LNAPL. Thus, two different sets of linear equations can be obtained and solved for S_w and S_o. The average optical density values for each mesh element of the studied domain can then be calculated and compared to the corresponding ones for all three cases, and a matrix of correlation equation sets can also be obtained, each one corresponding to each mesh element:

$$\begin{bmatrix} D_i \\ D_j \end{bmatrix}_{mn} = \begin{bmatrix} (D_i^w - D_i^d)S_w + (D_i^o - D_i^d)S_o + D_i^d \\ (D_j^w - D_j^d)S_w + (D_j^o - D_j^d)S_o + D_j^d \end{bmatrix}_{mn} \tag{3.2}$$

where m and n are the dimensions of the matrix, $[D_i]_{mn}$ and $\left[D_j\right]_{mn}$ are the values of average optical density of each mesh element for wavelengths i and j; $\left[D_i^d\right]_{mn}$ and $\left[D_j^d\right]_{mn}$ are the average optical density of each mesh element for dry sand; $[D_i^w]_{mn}$ and $\left[D_j^w\right]_{mn}$ for water-saturated sand; $[D_i^o]_{mn}$ and $\left[D_j^o\right]_{mn}$ for LNAPL-saturated sand.

In this research, the studied domains were photographed using two consumer-grade digital cameras, each one attached to either one of the two different bandpass filters, 450 and 656 nm wavelengths. All pictures were exported from NEF format (Nikon proprietary RAW version files) to TIFF (Tagged Image File Format) using Nikon ViewNX 2.7. The TIFF images were analyzed with an in-house program written in MATLAB.

Red Sudan III dye was used for LNAPL and Brilliant Blue FCF dye for water to enhance visual observation and increase their light absorbance properties. Both dyes were used at concentrations of 1:10,000 by weight, without any noticeable change in the physical properties of water and LNAPL. The dyes are not absorbed or filtered by soil particles.

3.3 Capillary Pressure Measurement

Capillary pressure is an important parameter in analyzing the migration of NAPL in subsurface. Capillary pressure was obtained by measuring the pore liquid pressure in each phase. To measure the pore liquid pressure, tensiometer (SWT5, Delta-T Devices Ltd) was used in this research. The pore liquid pressure was recorded by the data logger (DL2e, Delta-T Devices Ltd). Generally, normal tensiometer is hydrophilic only for measuring pore water pressure, and hydrophobic tensiometer for measuring NAPL pressure is not commercially available. However, hydrophilic tensiometer can be modified to hydrophobic tensiometer to measure NAPL pressure.

The tensiometer can be modified from hydrophilic to hydrophobic by changing the characteristic element contact point which is the porous ceramic cup from hydrophilic to hydrophobic. The porous ceramic cup is a semi-permeable barrier that transfers the soil water tension as a negative pressure into the tensiometer. To render the porous cups suitable for wetting to LNAPL (hydrophobic), they were soaked in water-proofing material. The hydrophobic modification by chemicals such as Glassclad 18 (Busby et al. 1995), chlorotrimethylsilane (Lenhard and Parker 1988; Van Geel and Sykes 1994b; Van Geel and Roy 2002; Kechavarzi et al. 2005), and trichloromethylsilane (Kamon et al. 2003) has made measurement of NAPL pressure possible. In this study, the modified tensiometer, similar to Kamon et al. (2003), was used (Figure 3.2).

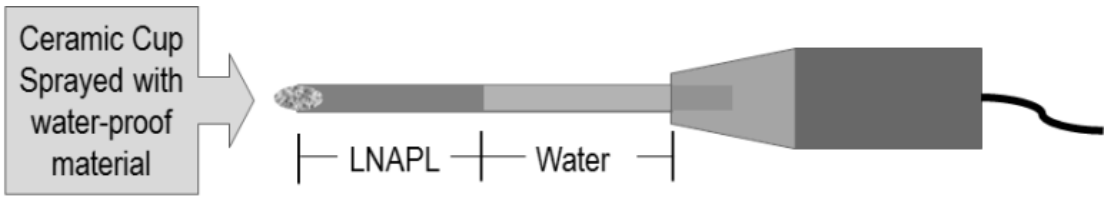

Figure 3.2 Schematic of modified hydrophobic tensiometer.

The measuring range capability is between -85 kPa (852 hPa) and 0 kPa (0 hPa) for tensiometer (water tension) and 0 kPa and 100 kPa (1003 hPa) for piezometer (water level). The pressure output signal for water tension is 1 mV equal to -1 kPa and -1 mV equal to 1 kPa of water level. As the signal calibration value of both water tension and water level is similar (only difference is the sign of the number), the tensiometer can be calibrated easily as

piezometer procedure. The liquid is filled in the column without sand at different liquid levels. Then the hydrostatic or LNAPL-static pressure and its corresponding output voltage from hydrophilic or hydrophobic tensiometer was measured. The calibration result of tensiometer is shown in Figure 3.3. The tensiometer calibration value is then used to offset the pore liquid pressure value.

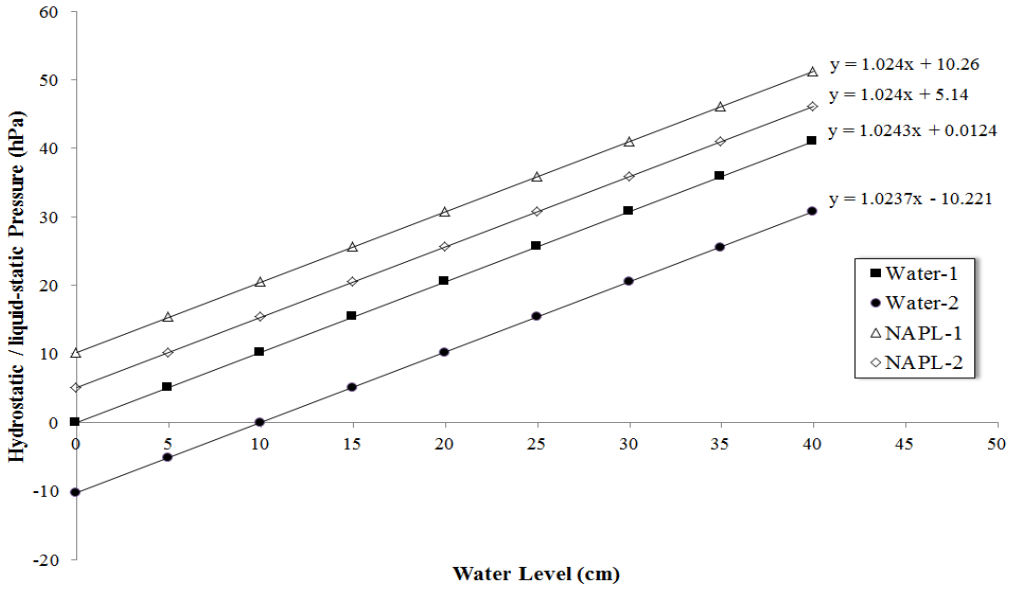

Figure 3.3 Calibration results.

3.4 Materials and Methods

3.4.1 Materials

To understand the complexity of LNAPL migration in the subsurface, simple materials were used in our study. Basically, we have used only three materials here; sand as porous medium, de-aired water as wetting liquid and diesel as non-wetting liquid (as LNAPL is a contaminant).

Toyoura sand was used as a porous medium and is a Japanese standard sand. Toyoura sand is widely used as porous media in geotechnical engineering laboratories all over Japan. It can be classified as SP according to Unified Soil Classification System. Its particle density, ρ, is 2.65 g/cm^3, equivalent grain size, D_{50}, is 0.18 mm and void ratio, e, is 0.65. The grain size distribution of Toyoura sand is shown in Figure 3.4.

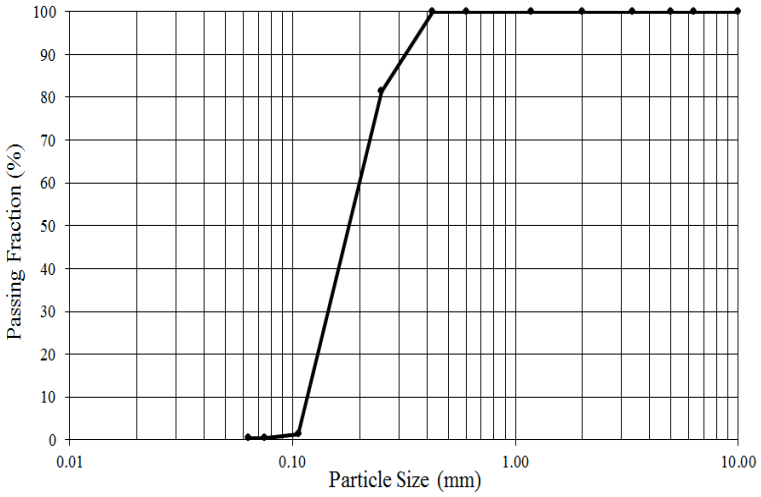

Figure 3.4 Grain size distribution of Toyoura sand.

The LNAPL used in this research is diesel and is widely available in the world as it is a consumer fuel product, in general as a liquid fuel. Its density used in this research is 0.865 g/cm^3, with viscosity of 7 mm^2/s, surface tension of 0.2675 N/m, and vapor pressure of 0.40 mm-Hg.

3.4.2 Experimental Apparatus

A 35 × 35 × 500 mm one-dimensional column with a front transparent glasswall was designed to study the LNAPL migration behavior in Toyoura sand due to precipitation. A transparent glass wall was used as it provides a clear view of the liquid movement inside the sand column. SIAM was used to obtain the soil saturation reading.

Two consumer-grade digital cameras (Nikon D7000 and Nikon D90) with two different bandpass filters (λ = 450 nm and 656 nm) are placed in front of the sand column to capture images through the test. Figure 3.5 show the one-dimensional column test set-up used in this study. Two LED floodlights were installed in the dark room as sole lighting sources and a Gretagmacbeth white balance card was located next to the column for a constant white reference.

To obtain capillary pressure value changes due to precipitation, a pair of tensiometers (hydrophobic and hydrophilic) was placed in vadose zone. The tensiometers were placed at an elevation of 450 mm. While the tensiometers would ideally be placed at the center of its

elevation (Figure 3.6), this one-dimensional column test allows it to be placed at any side of the column, as long as it is not covering the front panel and therefore obstructing the collection of saturation data from the image. The LNAPL pressure and water pressure measurement is taken for every minute throughout the experiment and stored by a data logger connected to the computer. The capillary pressure value is the non-wetting pressure minus the wetting pressure, thus, LNAPL pressure minus water pressure.

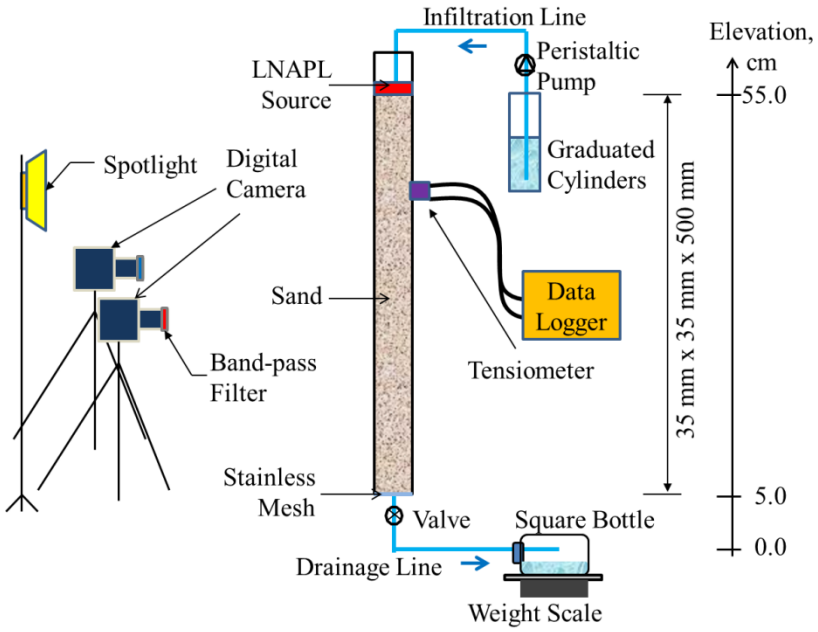

Figure 3.5 One-dimensional column test set-up.

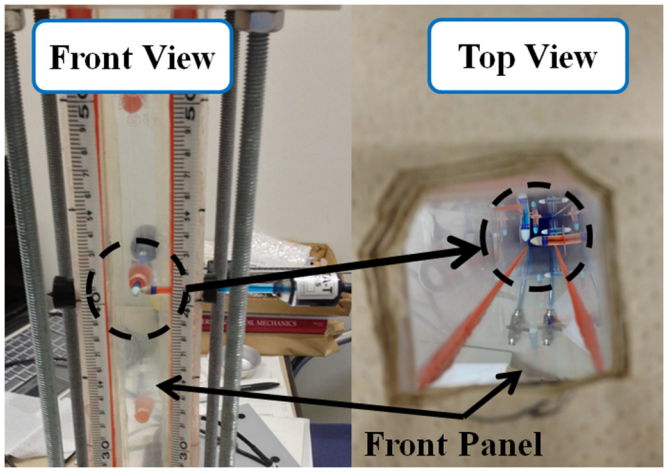

Figure 3.6 Tensiometer layout.

A digital controlled peristaltic pump supplies precipitation water from above. This pump controls the rate of precipitation and a graduated cylinder confirms the precipitation volume supplied during the precipitation stage. The outflow water is collected inside a square bottle where the mass of outflow is monitored for mass-balance check. Two 6-mm diameter holes were made in the bottle cap to receive a 4-mm diameter glass tube that connects to the drainage line. By having the small holes on the side of the bottle, evaporation from the collected outflow can be minimized. The elevation of the outflow was 50 mm below the bottom of the column.

3.4.3 Experimental Program

The spill of LNAPL will not only contaminate the soil and the surrounding area, but also affects the groundwater quality. The more LNAPL contaminates the aquifer, the greater is the difficulty in remediation work and the higher is the possibility of risk to human health and to other living organisms. The LNAPL spill takes place normally due to accidents or mismanagement. Rupture of pipelines, storage tank leakages or fuel truck accidents are the common causes of LNAPL spill that normally discharge varied amounts into the soil and surrounding areas. If the spill is not noticeable, such as in the case of underground leakage of storage tank, or uncontrollable spill such as system malfunction during pipeline rupture it could result in higher volume of LNAPL infiltration into the soil. Once LNAPL infiltrates the soil, it will occupy the soil pores and release toxic compounds while degrading slowly.

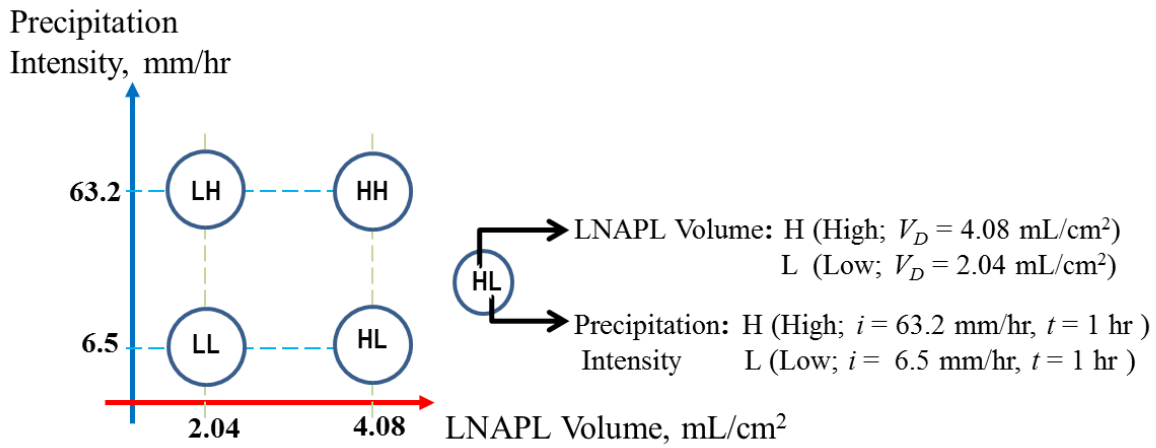

Figure 3.7 The experiment conducted to study LNAPL infiltration volume.

When LNAPL occupy the soil pores, it will alter the level of saturation of the soil. As the flow and migration of LNAPL is closely related to soil saturation, and its condition inside the soil pores, the variation in LNAPL spill volume was studied. In this study, the two values of LNAPL volume were used to represent a high and low spill volume condition. Figure 3.7 shows the experiment conducted in this study to understand the LNAPL flow and migration behavior due to precipitation in relation to the effect of LNAPL spill volume.

Four experiments were conducted during the study to cover the minimum and maximum range of LNAPL infiltration volume, V_D, and precipitation intensity, i. The low LNAPL infiltration volume condition used in this study was 25 mL (2.04 mL/cm^2), whereas the high was 50 mL (4.08 mL/cm^2). The low precipitation intensity used in this study was 6.5 mm/hr, whereas the high precipitation intensity was 63.2 mm/hr.

The rate of precipitation intensity varies among climates in the world, and so does its classification in each country. According to World Metrological Organization, if the precipitation is more than 50 mm in 24 hours it is classified as heavy rain. There is, however, no specific precipitation intensity for other classes. In tropical countries such as Malaysia, there are however specific classes for different precipitation intensities. In this study, 6.5 mm/hr was considered light rain and 63.2 mm/hr as very heavy rain (> 60 mm/hr) according to the Malaysia Drainage and Irrigation Department Standard.

3.4.4 Experimental Procedure

In one-dimensional study, Toyoura sand was packed into a test column to simulate the LNAPL migration behavior due to precipitation. Prior to starting the experiments, the sand was fully saturated with blue-dyed water. The sand was previously saturated with blue-dyed water and left for 24 hours in a vacuum chamber to remove air from it and ensure complete saturation. Then, the saturated sand was slowly poured with the help of a spoon into the column filled with de-aired water. Throughout the pouring process, the column was put on the top of a vibrator to ensure uniform compaction until the final elevation is reached. The vibration rate in the vibrator must be the same for all column samples to ensure a similar sample void ratio of 0.65 is obtained. In this research, 50 hertz of vibration ensures uniform compaction of Toyoura sand.

The experiment started as soon as the drainage valve was opened, and the soil-saturated water was drained out of the column. The flow chart for the one-dimensional column test procedure is shown in Figure 3.8. The drained-out liquids were collected in a square bottle. Two 6-mm diameter holes were made in the bottle cap to receive a 4-mm diameter glass tube that connected to the drainage line. The rate of liquid lost inside the bottle due to evaporation was about 1 g per 10 days. The elevation of the outflow was 50 mm below the bottom of the column. The outflow was automatically measured by an electronic scale and recorded every 15 seconds. Throughout the experimental period, the drainage valve was never closed, and the outflow elevation was never changed. The room temperature was kept at 20°C and the humidity was maintained at 70%.

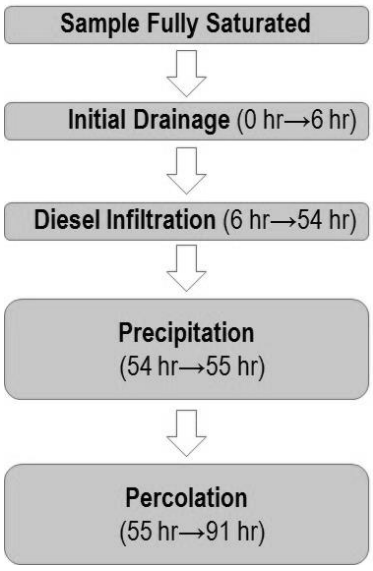

Figure 3.8 One-dimensional column test procedure.

When the bottom drainage valve was opened, the fully water-saturated Toyoura sand was drained for 6 hours. Then, designated volumes of LNAPL were released using a pipette from the top of the column. The LNAPL was allowed to migrate downward for 48 hours. Then, in the precipitation stage, the blue dye water was poured from the top of the column according to designated precipitation intensity. The precipitation intensity and supply volume were controlled using a digital peristaltic pump. The precipitation water supplies were taken from a graduated cylinder to check if the precipitation volume is similar to the designed level. Finally, during the percolation stage, the LNAPL contaminants and precipitation water were allowed to drain for 36 hours.

Digital pictures were taken every 5 minutes during the first hour of each stage and every 30 minutes after that until the end of the stage. The cameras were set in manual mode, and the aperture, shutter speed, and white balance were defined and maintained constant throughout the experiment. The cameras were remotely controlled using Nikon Camera Control Pro 2 software to avoid vibrations and camera displacement. The two LED floodlights were turned on 30 seconds prior to taking picture and turned off 30 seconds afterwards.

3.5 Determination of Stages Experimental Duration

3.5.1 Initial Drainage and LNAPL Infiltration

Whenever LNAPL spills, it will migrate deeper into the subsurface due to gravitational force. The LNAPL will migrate deeper until it reaches capillary fringe. However, due to capillarity and low density of LNAPL, migration becomes difficult and it will cease at the stable migration depth.

In simulating the migration of LNAPL in subsurface due to precipitation, the study should ideally start at the stable migration depth. To obtain this depth, an LNAPL infiltration test has been conducted to obtain the time duration needed for the studied LNAPL to reach this state. The test was conducted in the same column apparatus that was used for the one-dimensional experiment in this study. The sample preparation and the experimental procedure are also similar up to the LNAPL infiltration stage to all one-dimensional experiments in this research. The main different in this test is the time duration for this test is much longer. The time for the studied LNAPL to reach it stable migration depth from this experiment will be used as the standard for LNAPL infiltration stage for the rest of the one-dimensional experiments.

Prior to LNAPL migration stage, the time taken for the soil to reach the stable water content in the vadose zone and the capillary fringe also has been tested. This time duration will be used as the standard time for the initial drainage stage for the rest of one-dimensional experiments. Figure 3.9 show the soil water saturation and Figure 3.10 the soil LNAPL saturation test result for both initial drainage and LNAPL migration stages.

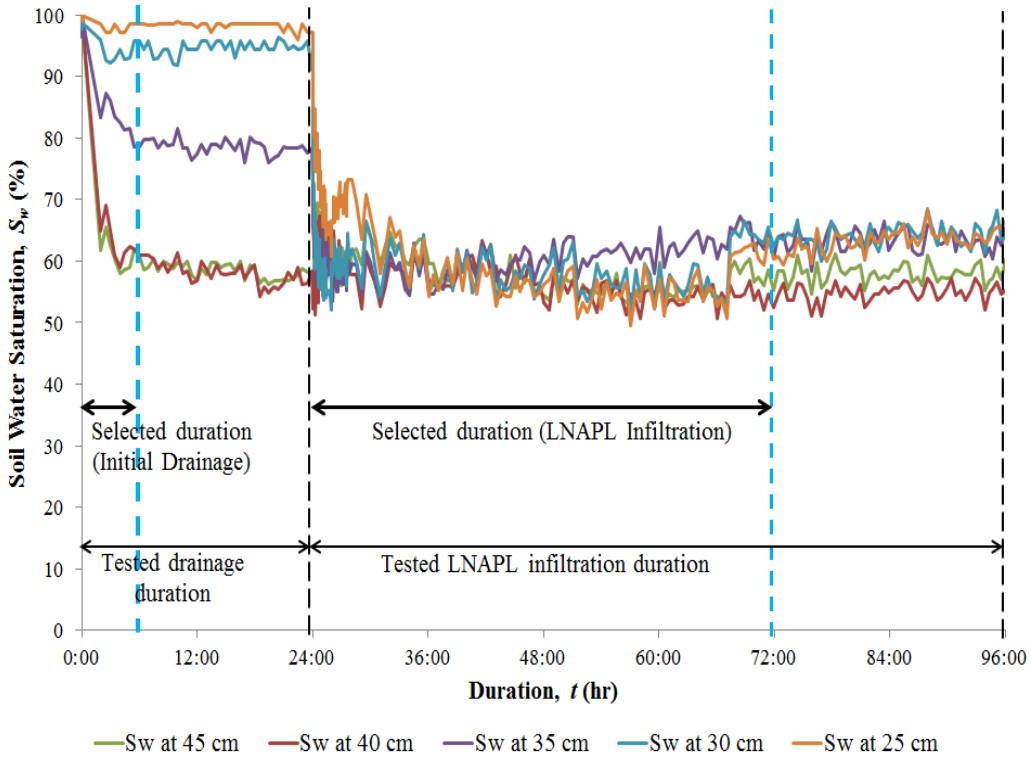

Figure 3.9 Soil–water saturation to determine the duration for stable condition.

The test is conducted over four days, with one day dedicated for water drainage (initial drainage), and three days for LNAPL migration. Due to fast water drainage because of high permeability of Toyoura sand, water saturation reduces very fast in vadose zone (Figure 3.9) as soon as the sand column starts draining. The saturation of sand column water reaches its stable level in less than six hours. Therefore, the duration for the initial drainage for one-dimensional experiment in this research is set at six hours. This will represent a stable saturated capillary zone and vadose zone, as in natural state.

In the test to determine the time required for LNAPL to reach its stable migration depth, it could be seen that as the time increases, water (Figure 3.9) and LNAPL (Figure 3.10) saturation changed in the soil. The LNAPL saturation in upper layer changes from high to low saturation, and near capillary fringe from low to high saturation with increase in time. The changes in LNAPL saturation show that LNAPL migrated deeper from the released point in the vadose zone to the capillary fringe. Once LNAPL reaches the capillary fringe, it requires some time for it to reach its stable migration depth and ceases further migration. It took about 43 hours for the studied LNAPL and water saturation to reach stable level.

Therefore, we chose 48 hours as the duration for the LNAPL infiltration for one-dimensional experiment in this study. This condition will represent a stable LNAPL contamination plume in the subsurface when spill occurs.

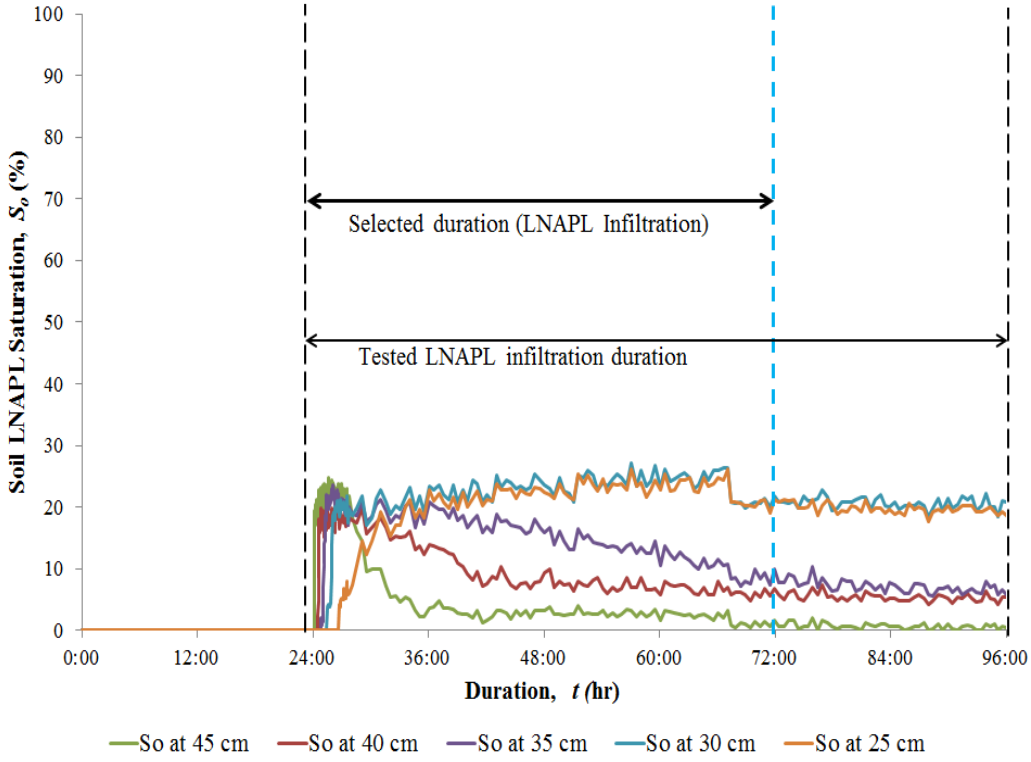

Figure 3.10 Soil–LNAPL saturation to determine the duration for stable condition.

3.5.2 Precipitation and Percolation

Similar to the precipitation intensity, the precipitation duration varies among climates in the world. It could be as long as a day or two and as little as less than an hour. The duration is also dependent on intensity. Normally, if the precipitation lasts a very long time, its intensity would be low. If the intensity is high, the duration will be short. Figure 3.11 shows the example of rainfall data for 9 days in one metrological station at Kuala Lumpur, Malaysia (DID Malaysia 2013). To better appreciate the LNAPL migration due to precipitation, a simple approach was followed to determine the duration. The duration chosen was one hour, similar to the time unit of intensity which is also per hour.

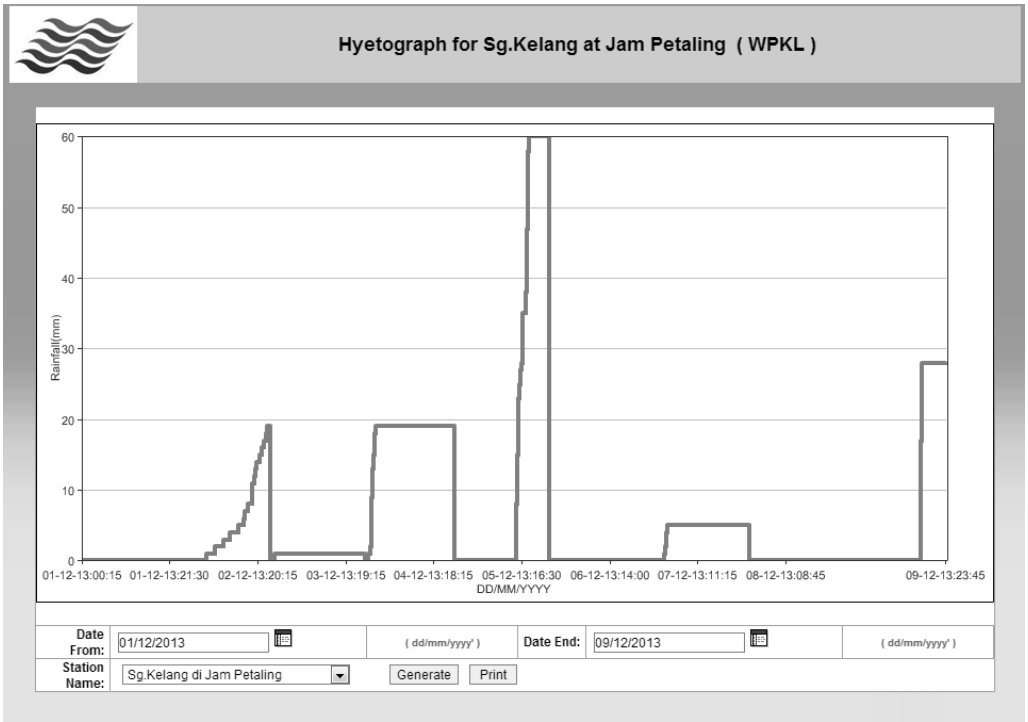

Figure 3.11 Rainfall data for 9 days at Kuala Lumpur, Malaysia (DID Malaysia 2013).

3.6 One-Dimensional Column Test Result

3.6.1 SIAM Output

In SIAM, the migration behavior of LNAPL was studied with images taken from two cameras fitted with different bandpass filters. These images record the changes in the color of the soil inside the column. Then, using in-house computer codes, these changes are converted to either water or LNAPL saturation value. The output of saturation value is based on average saturation of analyzed mesh in every 0.5 cm height and 0.5 cm width.

The saturation value ranges from 0%, which means there is no specified liquid (either water or LNAPL) present in the soil void, to 100% of saturation which means the soil void is fully saturated with the specified liquid. Figure 3.12 shows the image taken during the end of initial drainage stage and the SIAM analyzed output. At this stage, LNAPL has not yet spilled on the sand column, and therefore its saturation level is 0%, whereas in Figure 3.13 it has already infiltrated the sand column, and its presence is shown in the LNAPL saturation value.

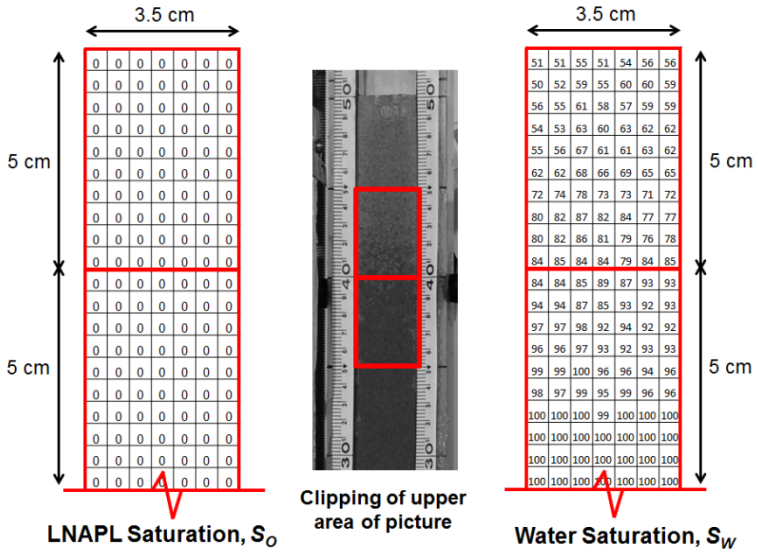

Figure 3.12 Image taken after the initial drainage and SIAM analyzed output.

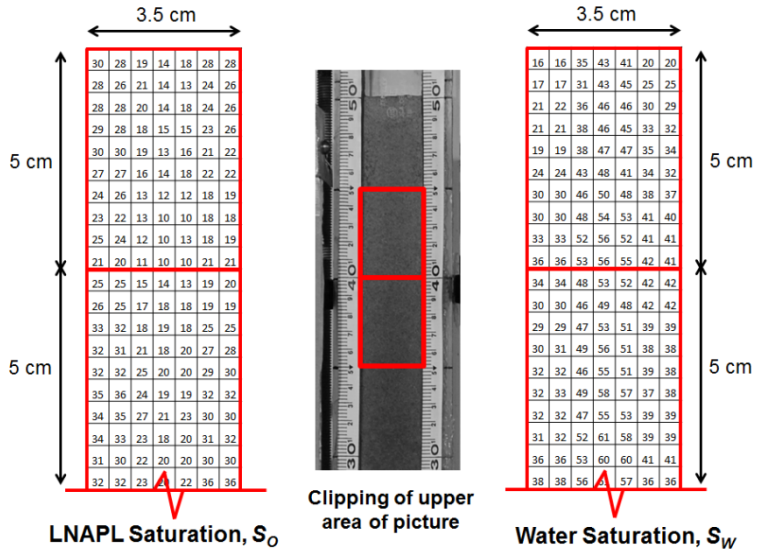

Figure 3.13 Image taken after LNAPL migration and SIAM analyzed output.

3.6.2 LNAPL and Water Saturation Profile

Throughout the experiment, images were captured at least every 30-minute interval. This means for a single 91-hour experiment, more than 180 images were taken which will provide 180 sets of saturation output data. Each set comprises LNAPL and water saturation output, with each output containing 672 saturation values in a matrix meaning that for a single 91-hour experiment, around 250,000 saturation data have to be studied to understand the behavior of LNAPL migration.

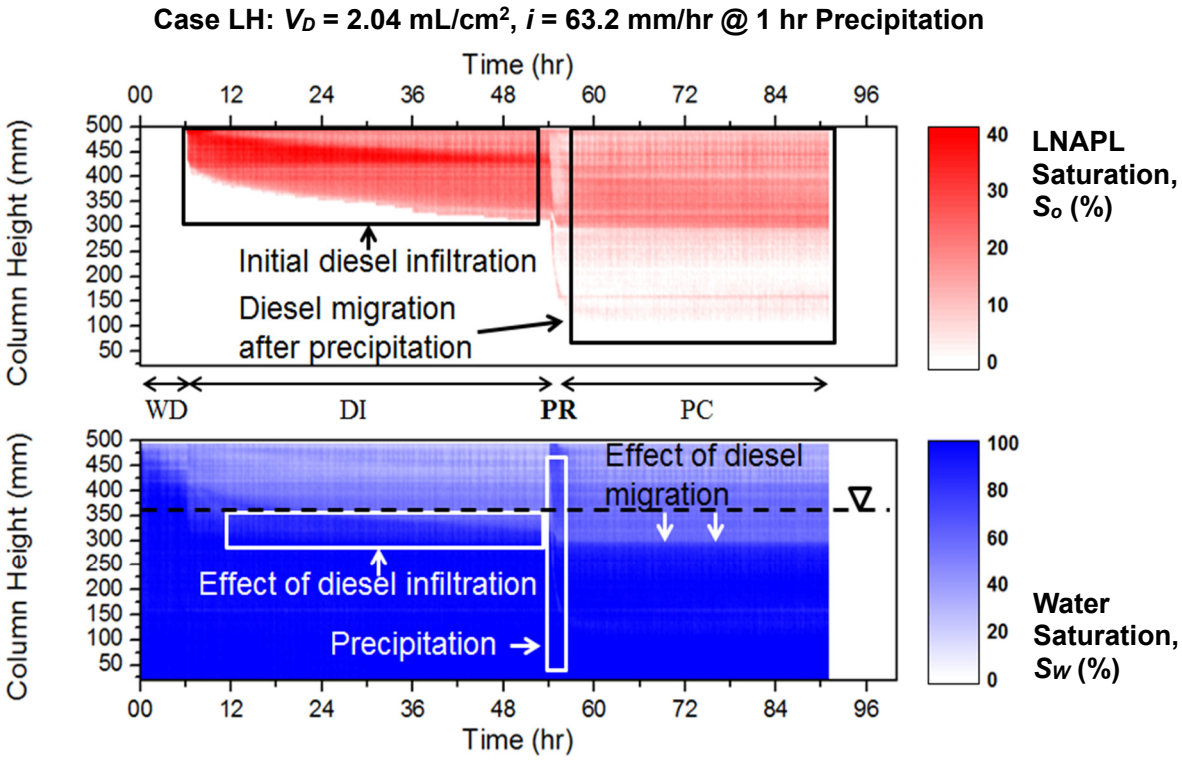

Figure 3.14 LNAPL and water saturation profile.

The huge amount of saturation data need to be studied carefully to fully understand the LNAPL migration behavior. Therefore the value is rearranged in a saturation profile based on the height of the column and time. The saturation profile can be presented as in Figure 3.14, where a set of LNAPL (percentage of S_o) and water saturation (percentage of S_w) distribution is presented for each case.

Since the experiments were conducted using a one-dimensional column, the results show the LNAPL and water saturation distribution in vertical direction. The horizontal axis shows the elapsed time during experiment. By using the saturation profile, the changes in LNAPL behavior can be studied more accurately according to the elapsed time during experiment. The result of one-dimensional test of LNAPL spill volume effect is shown in Figure 3.15 to Figure 3.18.

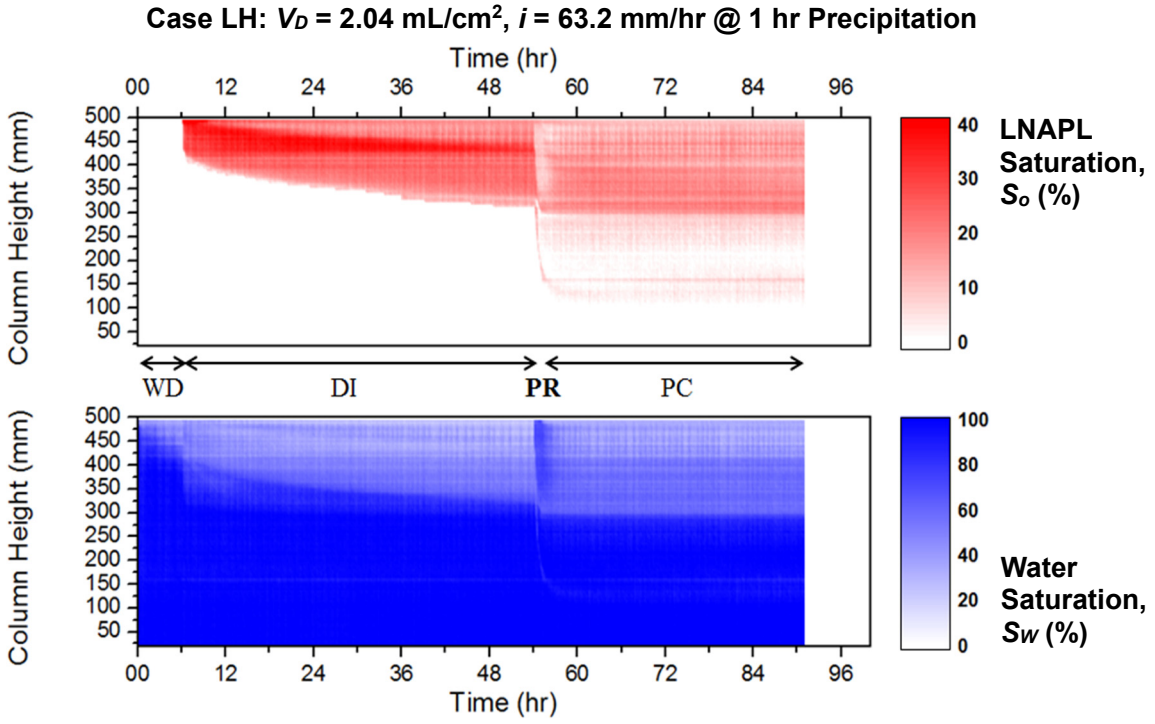

Figure 3.15 LNAPL and water saturation profile for case LH.

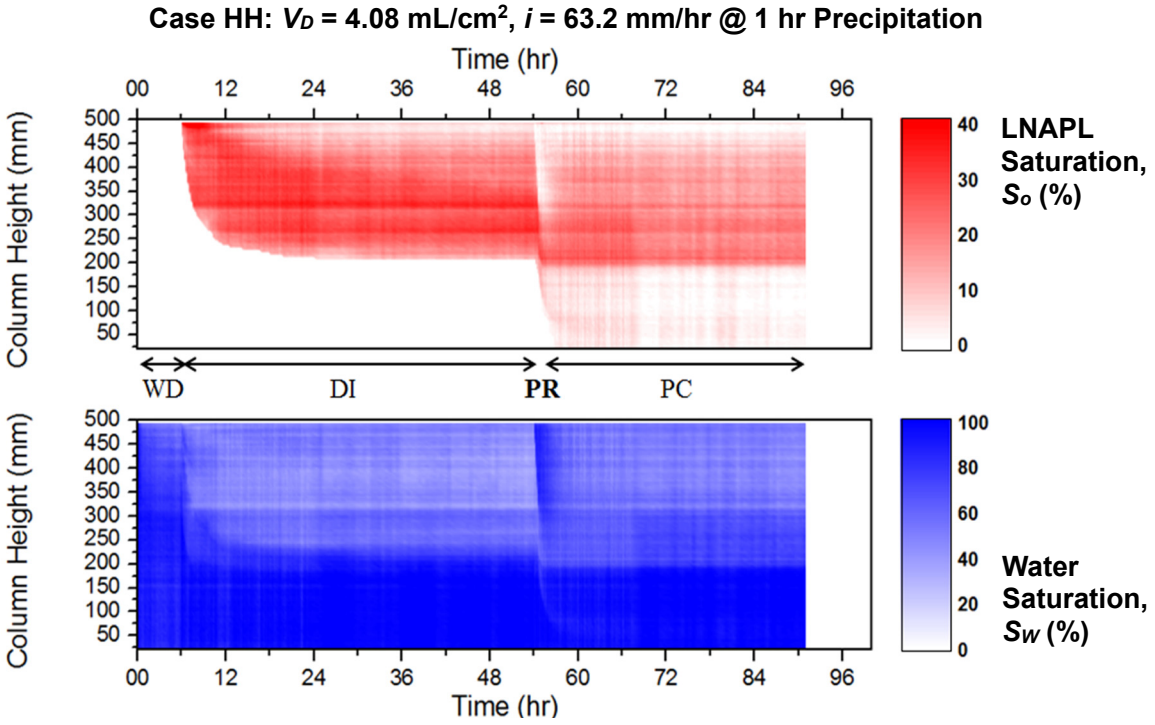

Figure 3.16 LNAPL and water saturation profile for case HH.

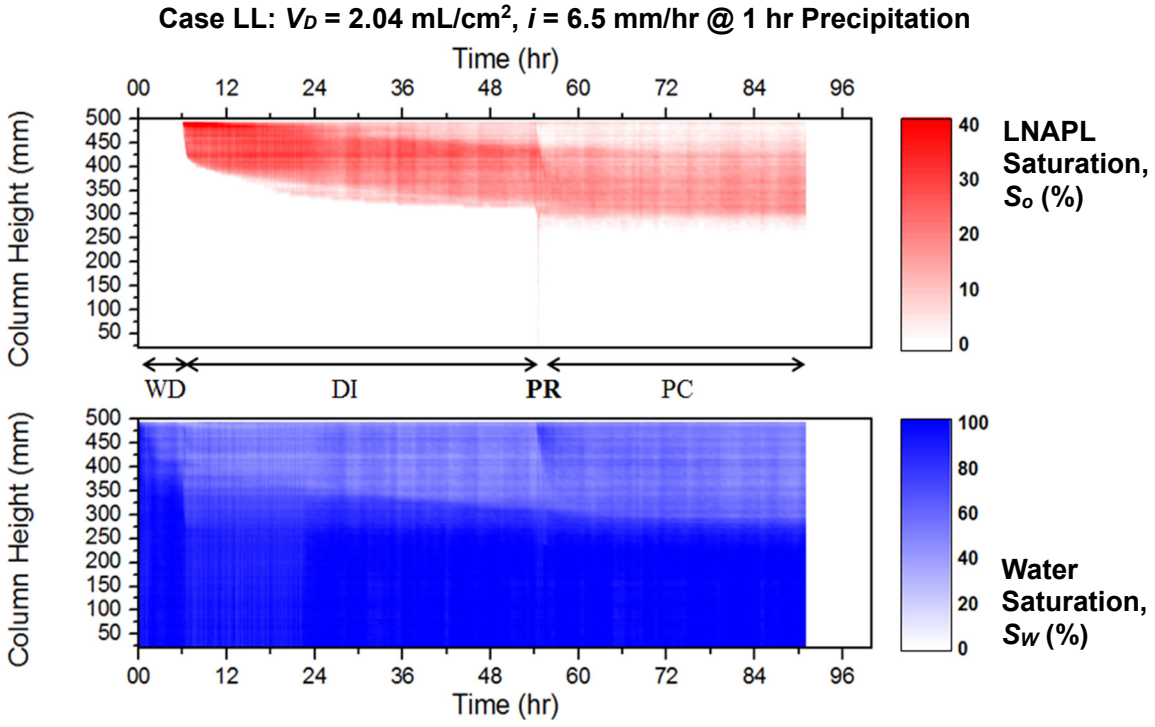

Figure 3.17 LNAPL and water saturation profile for case LL.

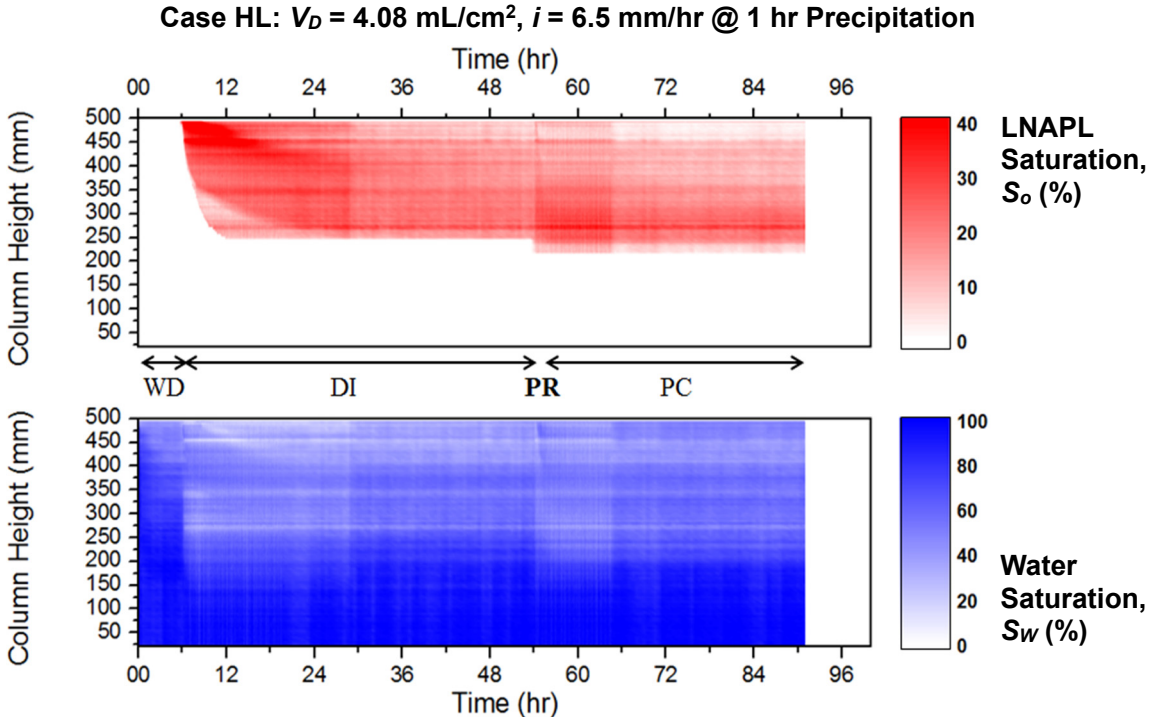

Figure 3.18 LNAPL and water saturation profile for case HL.

The migration of LNAPL due to precipitation can be easily studied from the LNAPL saturation profile by comparing the profile prior to and after precipitation. As can be seen, prior to precipitation (in the LNAPL infiltration stage), there are two distinct zones, which are contaminated (red) and uncontaminated (white) zones. This condition changed after the contaminated sand was subjected to precipitation. It can be seen that the LNAPL migrates dissipates downwards creating a new contamination plume boundary in the saturated capillary fringe zone due to precipitation. This boundary was defined by changes of LNAPL saturation, prior to and after precipitation. The changes in LNAPL saturation in terms of elevation were also taken into account while defining the boundary (Figure 3.19 and Figure 3.20). This means that the LNAPL saturation value ranges (must be continuously) from the top of the column to the bottom of the newly defined boundary. This screening procedure is taken into consideration to ensure that the migration of LNAPL is the actual physical migration, and not the value due to error in the method.

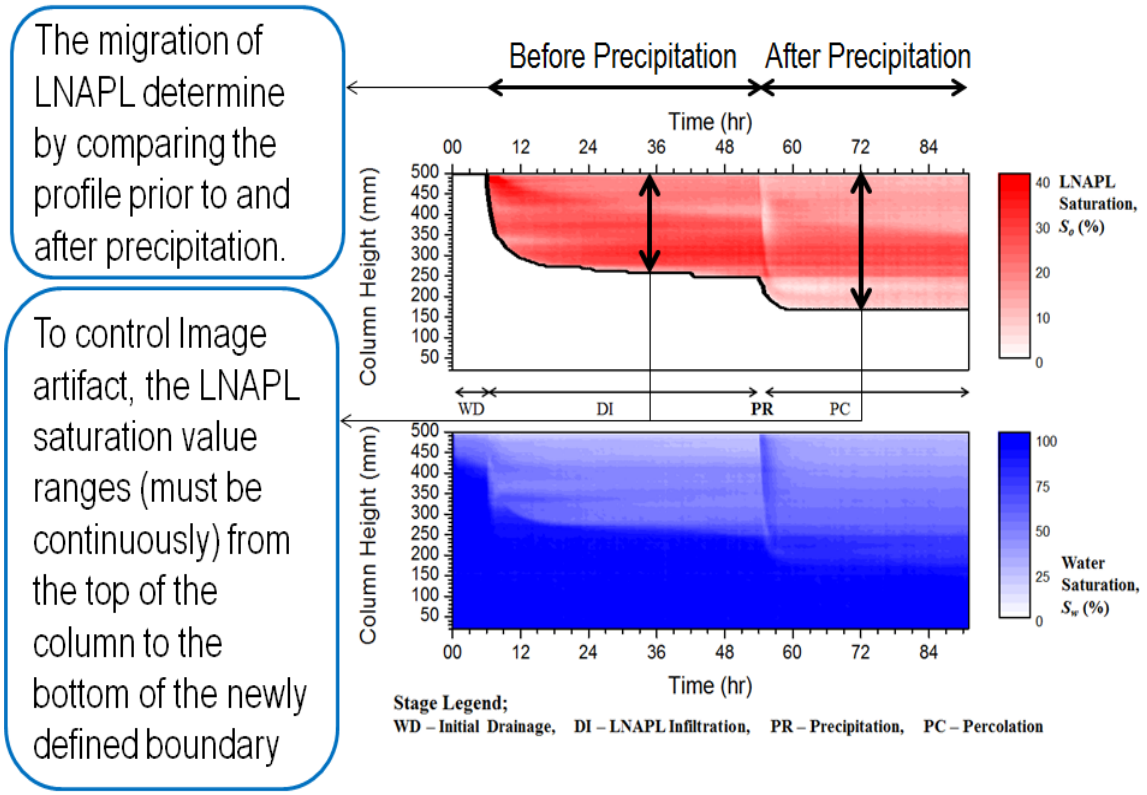

Figure 3.19 LNAPL migration boundary.

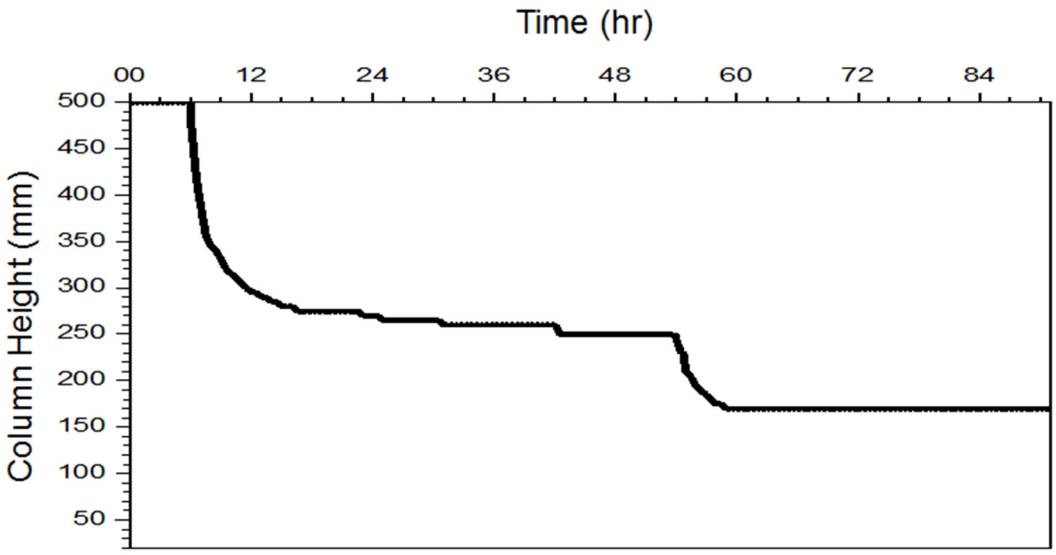

Figure 3.20 LNAPL migration boundary obtain from LNAPL saturation profile.

3.6.3 Capillary Depression due to LNAPL Infiltration

At the start of the experiment, the fully saturated sand was allowed to drain by gravitational force. Due to the fact that sand has high permeability, the water drained relatively quickly, and the stable capillary fringe height could be seen in less than 6 hours. The high capillarity is due to the effect of fine grain size distribution in Toyoura sand and can be seen clearly in all cases. The saturated capillary fringe could reach up to 350 mm of column height, which left only 150 mm of the unsaturated zone.

When the LNAPL spilled from the top of the column, it migrated downward due to the gravitational force and capillarity. Therefore, deeper LNAPL migration occurs in a larger spilled volume (Table 3.1), because it has sufficient pressure to overcome the capillary forces in order to advance into the finer pores filled with water. In the experiment, LNAPL could migrate from about 200 mm and 250 mm deep for 2.04 mL/cm^2 and 4.08 mL/cm^2 of spilled LNAPL, respectively.

While LNAPL infiltrated and migrated deeper, it had to overcome the capillary force; LNAPL ceases to migrate when it reaches equilibrium at interfacial tension. Although LNAPL density is lighter than water, due to the aforementioned mechanism, capillary depression occurred before equilibrium is reached. In the experiment, once the LNAPL infiltrated the sand and reached the top of the capillary fringe, the height of the capillary

fringe was depressed for about 50 mm and 100 mm for 2.04 mL/cm^2 and 4.08 mL/cm^2 of spilled LNAPL, respectively Figure 3.21. A similar condition was also found by Chevalier et al. (1998), when an unleaded gasoline caused a 34 mm capillary depression of the water table. The result from this experiment is higher perhaps due to the higher LNAPL volume.

Table 3.1 Capillary depression due to LNAPL infiltration

LNAPL Spill Volume	Capillary Depression
2.04 mL/cm^2	50 mm
4.08 mL/cm^2	100 mm

In Figure 3.21, it can be seen that the infiltration was faster for 4.08 mL/cm^2 of LNAPL than for 2.04 mL/cm^2 of LNAPL. This is mainly because the 4.08 mL/cm^2 had a higher volume and weight, which provided more pressure to push the LNAPL wetting front at a faster rate. It took about 6 hours for 4.08 mL/cm^2 to reach its stable depth compared to nearly 24 hours for 2.04 mL/cm^2 to reach its stable depth.

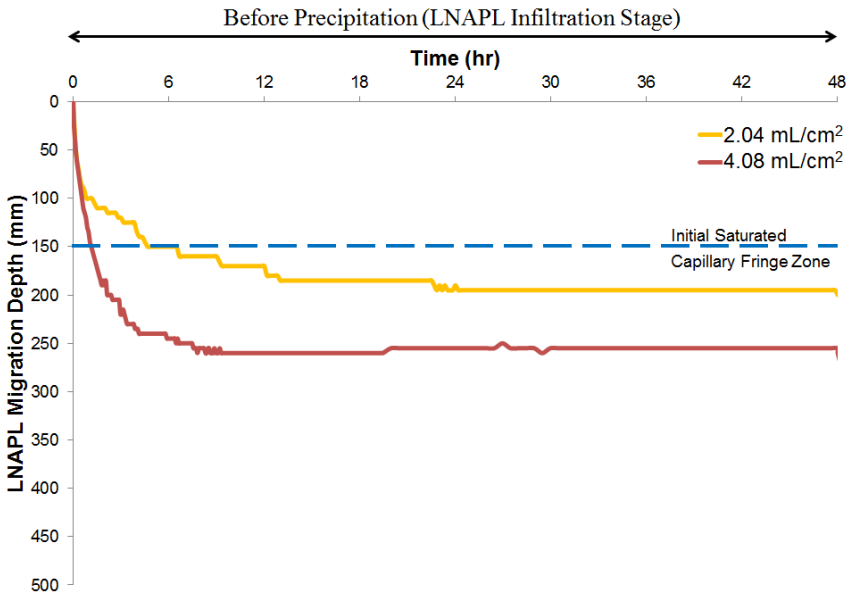

Figure 3.21 Contamination plume profile for 2.04 mL/cm^2 and 4.08 mL/cm^2 LNAPL infiltration cases.

3.6.4 LNAPL Migration due to Precipitation

When the infiltrated LNAPL reached a stable depth, it no longer migrated deeper, because the two immiscible liquids, LNAPL and groundwater, had reached its interfacial tension equilibrium. This condition changes as soon as precipitation infiltrates the contaminated sand layer (Figure 3.22). The infiltrating water is subjected to gravitational force; as it tries to flow towards groundwater level, it will push down any LNAPL that it encounters. The mobilized LNAPL will be entrapped within the saturated capillary zone. Since LNAPL solubility is low, this condition causes a prolonged groundwater contamination risk of carcinogen and toxic compound release from LNAPL degradation.

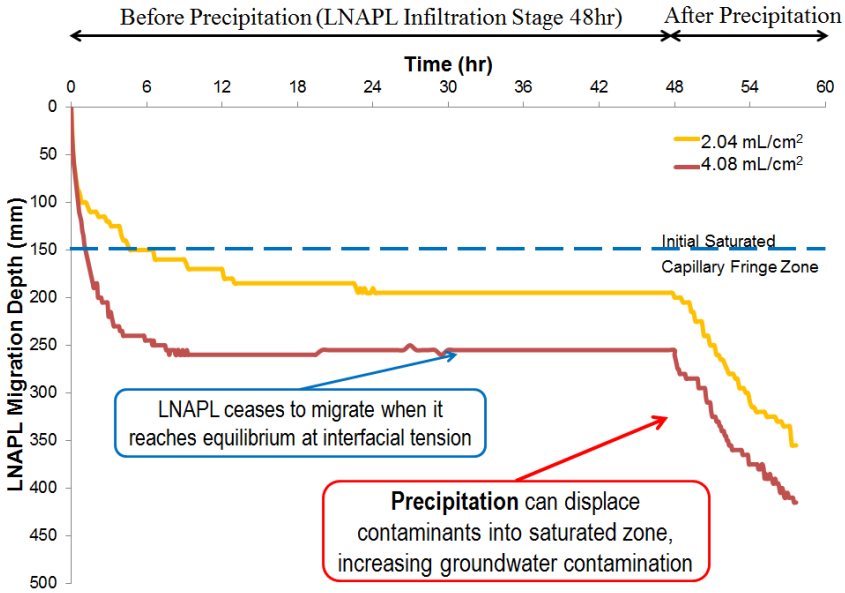

Figure 3.22 Contamination plume profile changes due to precipitation.

The infiltrated water also caused the contamination plume to further depress into the capillary fringe around 50 mm downward in the saturated zone (Figure 3.23). In comparison with other LNAPL contamination study cases, a depression of capillary fringe up to 50 mm was also found for surfactant infiltrated gasoline (Chevalier et al. 1998) and 1-Butanol (Henry and Smith 2002). This means that, even without considering fluctuations of groundwater, the contamination plume can migrate deeper into the saturated capillary fringe zone and contaminate the groundwater.

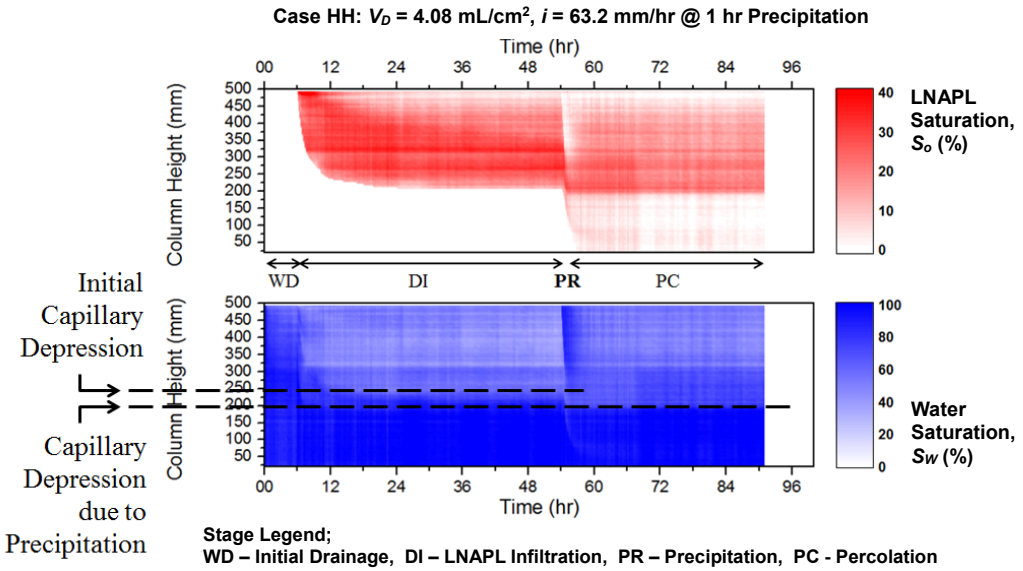

Figure 3.23 Further capillary depression.

3.6.5 Effects of LNAPL Infiltration Volume

In general, it can be said that the more LNAPL contaminated the sand, the more LNAPL migrated deeper due to precipitation. Although LNAPL is lighter than water, when LNAPL migrates downward due to gravitational force, it will occupy the available pores. Once precipitation water infiltrates the contaminated sand, it may encounter pores filling with LNAPL. Since both liquids are immiscible, the infiltrated water will push the LNAPL down until the migrated LNAPL becomes entrapped in deeper soil pores, or it will stop due to capillarity.

Comparing the low and high LNAPL spilled volume, more mobile LNAPL was spread through the contamination plume when subjected to precipitation in low LNAPL infiltration cases (Figure 3.24). In high LNAPL infiltration cases, LNAPL migrated downward and concentrated near the LNAPL wetting front region (Figure 3.25). Consequently, deeper high LNAPL saturation regions were created. There are two possible mechanisms that affected LNAPL migration in these low and high LNAPL volumes. The first mechanism is related to the LNAPL occupancy condition in soil pores from macro scale point of view. The second mechanism is related to saturation distribution within the contamination plume during LNAPL infiltration.

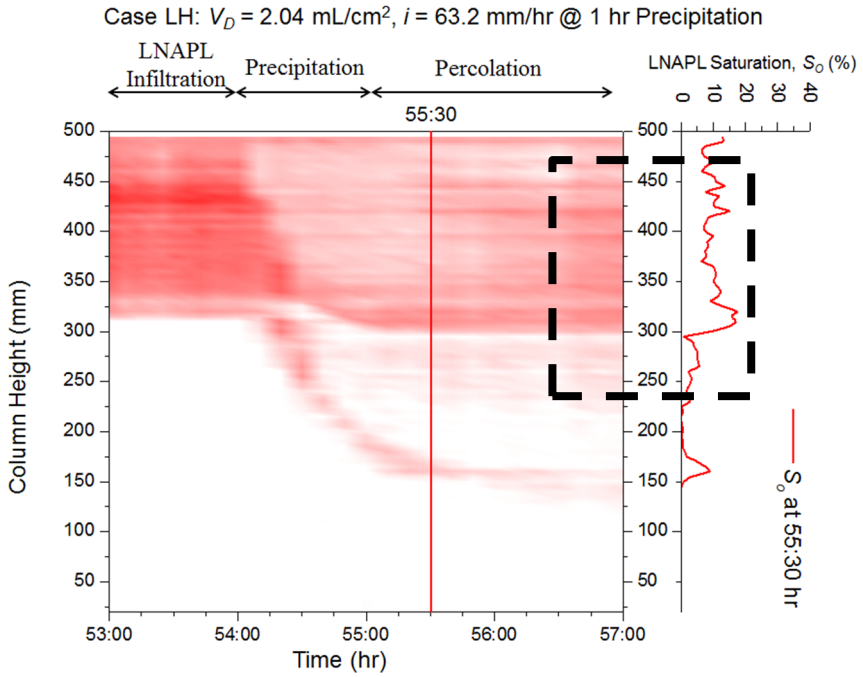

Figure 3.24 Mobile LNAPL spread through contamination plume in low LNAPL infiltration case.

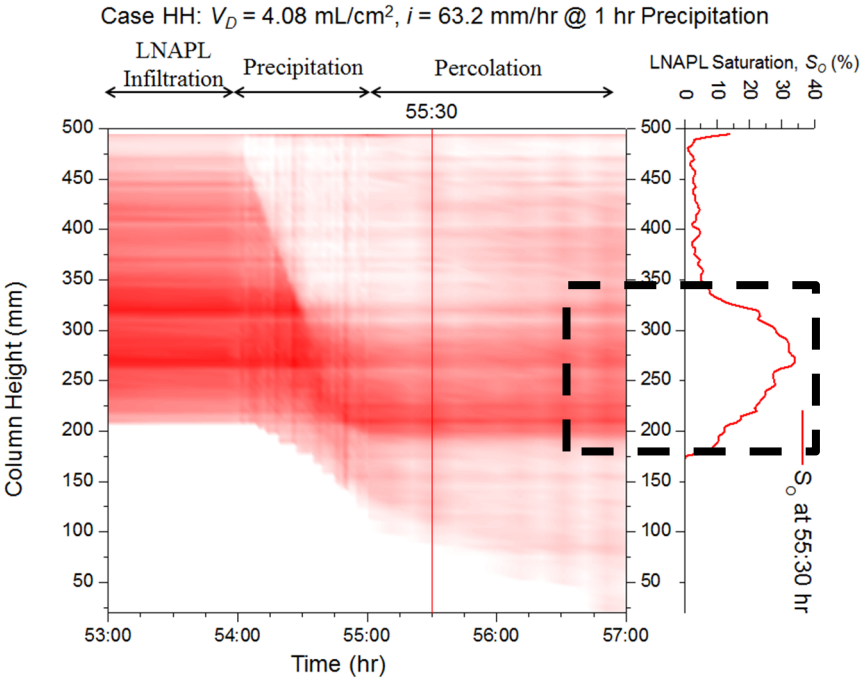

Figure 3.25 Mobile LNAPL concentrated near LNAPL wetting front region in high LNAPL infiltration case.

In the first mechanism, the availability of a contamination interconnecting bridge within soil pores affects how the precipitation water causes contamination migration. The interconnecting bridge of non-wetting (LNAPL) liquid is more likely to develop when the available liquid is sufficient. In other words, the greater the volume of LNAPL, the more it will occupy the void within soil pores. When more void is filled with LNAPL, the more likely it will be connected. This created a bridge within the water surface inside the pores, since water and LNAPL are immiscible, and soil is not in a dry state.

In relation to non-wetting interconnection with soil pores, soil pores being filled with LNAPL could also create variations in the saturation region. Based on the results of a column test, the saturation variation can be grouped into two conditions: low saturation regions and medium saturation regions. Low and medium saturation regions are defined based on three sections of the *S-p* relation curve: the residual stage, the desaturation zone, and the saturation zone (Figure 3.26). For Toyoura sand, LNAPL saturation of less than 20% would fall into the saturation zone and be considered a low saturation region. When the LNAPL is at 20% to 70% saturation, it would fall into the desaturation zone and be considered a medium saturation region. LNAPL saturation of above 70% would fall into the residual stage and be considered a high saturation region. In a high saturation region, most of the available water saturation (less than 30%) is probably from a 14% fraction of irreducible water saturation for Toyoura sand, which is similar to Kamon et al. (2004) and to entrapped water and air. In this study, the entrapped air is at up to 15% saturation, as shown in Figure 3.27.

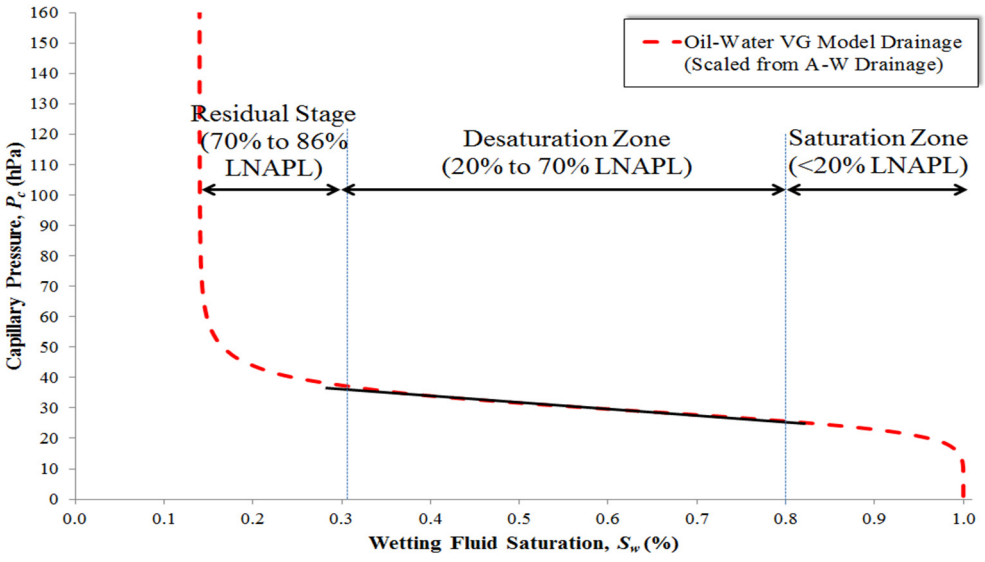

Figure 3.26 Three main parts of *S-p* relations.

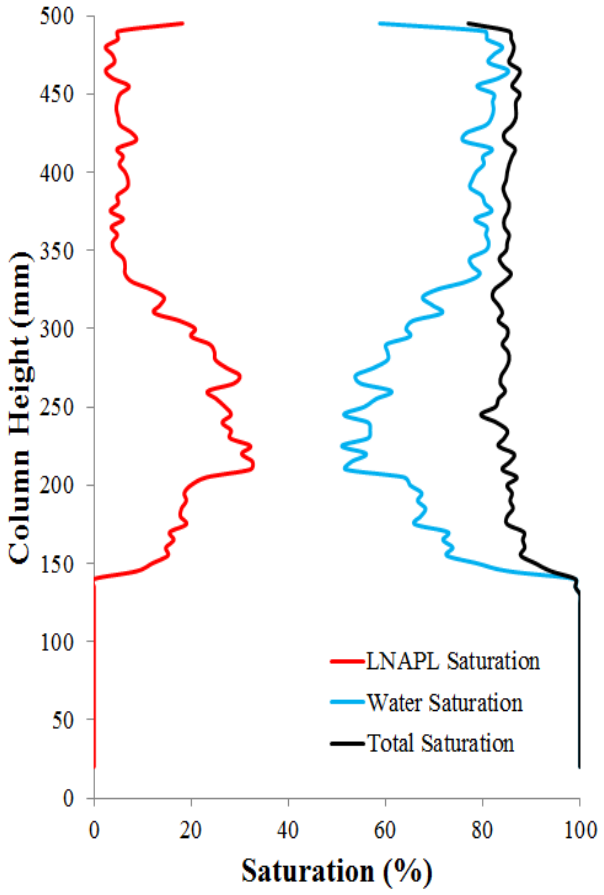

Figure 3.27 LNAPL saturation, water saturation, and total saturation in soil pores during precipitation in the HH case.

Based on the results of the column test, as shown in Figure 3.28, a low saturation region of around 15% to 20% is more pronounced in the case of low LNAPL infiltration. In all two low LNAPL infiltration cases (LL and LH), the contamination plume was more prone to be vertically mobilized by precipitation, because less LNAPL volume occupied the pores within the interconnection bridge. Furthermore, there is the possibility that very few non-wetting (LNAPL) interconnecting bridges developed within the contamination plume. As Wipfler and van der Zee (2001) suggest, only an excess of oil can cause the rings (film) to form interconnecting bridges. Therefore, the volume of mobile (non-entrapped) LNAPL is likely high.

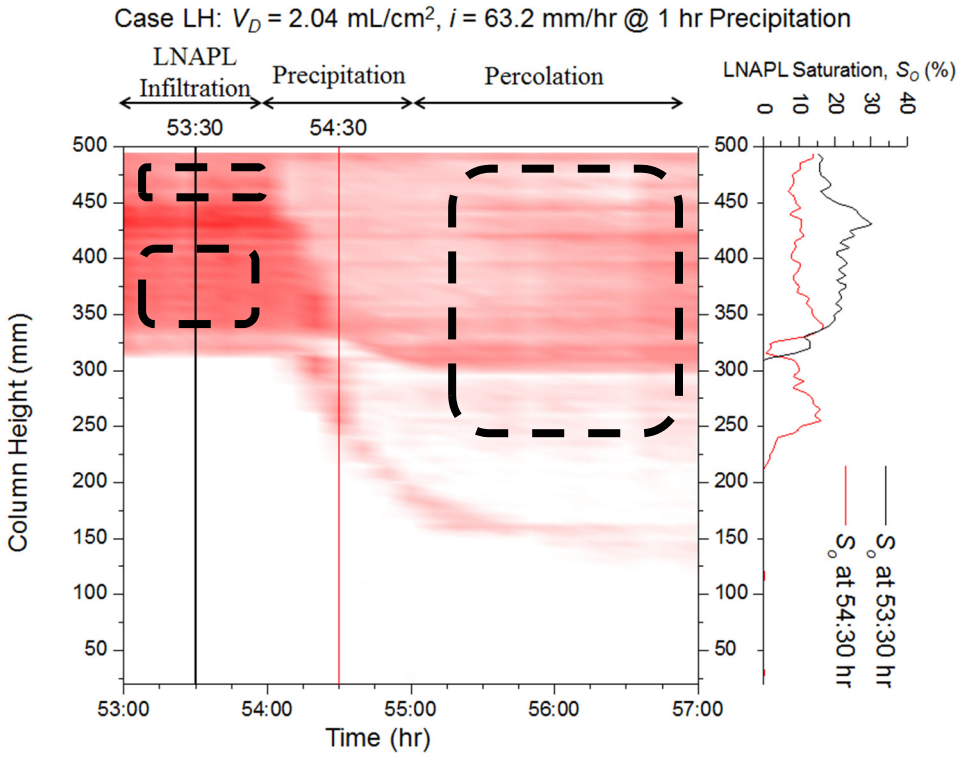

Figure 3.28 Low saturation region in the LH case.

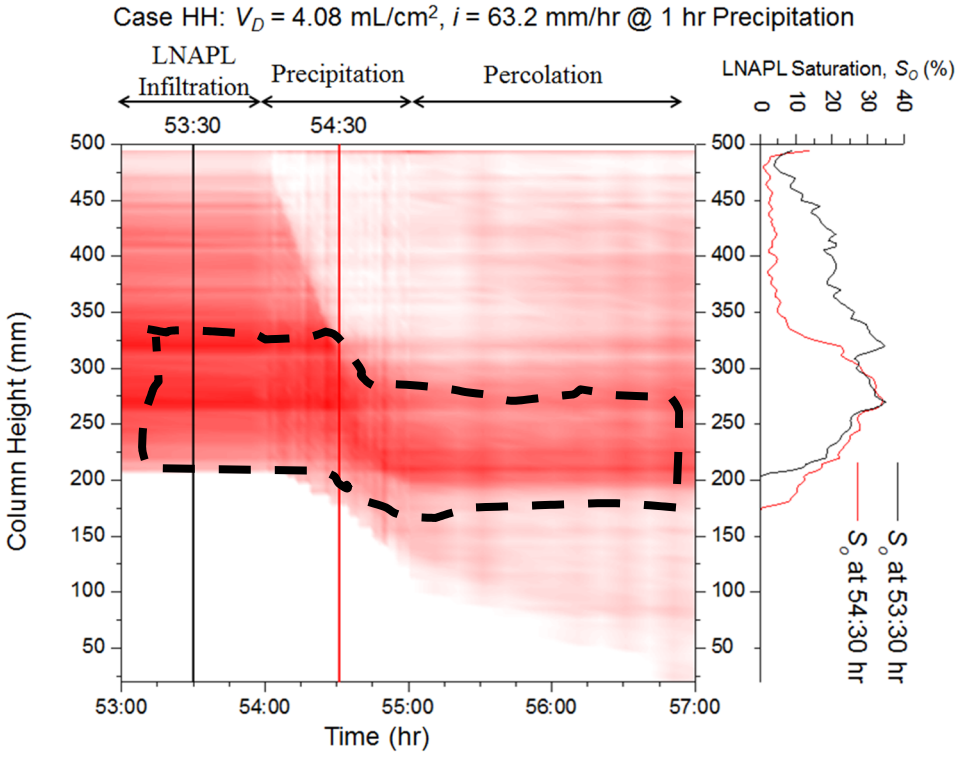

Figure 3.29 Medium saturation region in the HH case.

A medium saturation region with LNAPL saturation ranging from 20% to 30% will be more pronounced in the case of high LNAPL infiltration, as shown in Figure 3.29. In the case of high LNAPL infiltration (HL and HH), mobile LNAPL migrated downward together as the infiltration water pushed it deeper. Consequently, the contamination saturation is higher at deeper elevations, increasing the groundwater contamination risk.

In the second suggested mechanism, the initial distribution of contamination saturation affects how the precipitation water causes contamination migration. When the spilled LNAPL volume is high, it will infiltrate deeper at a relatively fast rate due to the high LNAPL volume that pushes the LNAPL wetting front. While LNAPL migrates deeper, some LNAPL will occupy soil pores due to capillarity. Consequently, LNAPL saturation will be gradually reduced from medium saturation concentrated in the wetting front region to low saturation near the top surface. For a low volume of spilled LNAPL, the LNAPL infiltration will be shallow. Therefore, the LNAPL saturation will be spread almost evenly within the height of the contamination plume. As these two conditions create different LNAPL saturation distributions, they also affect the available pores in the unsaturated zone, especially near the top surface.

The high LNAPL spilled volume case has more available pores near the top surface since the LNAPL saturation in this region is low compared to the low volume case. Therefore, when the contaminated sand is subjected to precipitation, it is much easier for infiltration water to accumulate when the available pores are high. Later, this accumulation of water will push the LNAPL when water infiltrates downward.

3.7 Conclusions for this Chapter

In this chapter, one-dimensional column test were conducted in order to understand the effect of LNAPL spill volume once the contaminated sand were subjected to the precipitation. As the flow and migration of LNAPL is closely related to soil saturation, the variation of high and low in LNAPL spill volume was studied. The spill of 4.08 mL/cm^2 and 2.04 mL/cm^2 of LNAPL were used to simulate the condition of high and low spill volume, respectively. The contaminated sand was subjected to the light precipitation intensity of 6.5 mm/hr and very heavy precipitation intensity of 63.2 mm/hr in one-dimensional column test.

When the LNAPL spilled from the top of the column, it migrated downward due to the gravitational force. Therefore, the high LNAPL spill volume case caused deeper LNAPL migration at faster rate compared to the low LNAPL spill volume case because it has sufficient pressure to overcome the capillary forces in order to advance into the finer pores filled with water. In the experiment, LNAPL could migrate from about 200 mm and 250 mm deep for 2.04 mL/cm^2 and 4.08 mL/cm^2 of spilled LNAPL, respectively. While LNAPL infiltrated and migrated deeper, it had to overcome the capillary force; LNAPL ceases to migrate when it reaches equilibrium at interfacial tension. Although LNAPL density is lighter than water, due to the aforementioned mechanism, capillary depression occurred before equilibrium is reached. The height of the capillary fringe was depressed for about 50 mm and 100 mm for 2.04 mL/cm^2 and 4.08 mL/cm^2 of spilled LNAPL, respectively.

When the infiltrated LNAPL reached a stable depth, it no longer migrated deeper, because the two immiscible liquids, LNAPL and groundwater, had reached its interfacial tension equilibrium. This condition changes as soon as precipitation infiltrates the contaminated sand layer. The infiltrating water is subjected to gravitational force; as it tries to flow towards groundwater level, it will push down any LNAPL that it encounters, and caused entrapment of LNAPL in the saturated zone. In general, it can be said that the more LNAPL contaminated the sand, the more LNAPL migrated deeper due to precipitation. Comparing the low and high LNAPL spilled volume, more mobile LNAPL was spread through the contamination plume when subjected to precipitation in low LNAPL infiltration cases. In high LNAPL infiltration cases, LNAPL migrated downward and concentrated near the LNAPL wetting front region. Consequently, deeper high LNAPL saturation regions were created. There are two possible mechanisms that affected LNAPL migration in these low and high LNAPL volumes.

In the first mechanism, the availability of a contamination interconnecting bridge within soil pores affects how the precipitation water causes contamination migration. The interconnecting bridge of non-wetting (LNAPL) liquid is more likely to develop when the available liquid is sufficient. In other words, the greater the volume of LNAPL, the more it will occupy the void within soil pores. When more void is filled with LNAPL, the more likely it will be connected. This created a bridge within the water surface inside the pores, since water and LNAPL are immiscible, and soil is not in a dry state.

In the second suggested mechanism, the initial distribution of contamination saturation affects how the precipitation water causes contamination migration. When the spilled LNAPL volume is high, LNAPL saturation will be gradually reduced from medium saturation concentrated in the wetting front region to low saturation near the top surface. For a low volume of spilled LNAPL, the LNAPL infiltration will be shallow. Therefore, the LNAPL saturation will be spread almost evenly within the height of the contamination plume. The high LNAPL spilled volume case has more available pores near the top surface since the LNAPL saturation in this region is low compared to the low volume case. Therefore, when the contaminated sand is subjected to precipitation, it is much easier for infiltration water to accumulate when the available pores are high. Later, this accumulation of water will push the LNAPL when water infiltrates downward.

CHAPTER 4: EFFECTS OF INTENSITY AND EQUAL VOLUME OF PRECIPITATION

4.1 General Remarks

Precipitation is one of the main parts in the hydrologic cycle that transports water from the atmosphere to the surface of the earth, and then percolates it down to groundwater. Thus, precipitation helps to recharge the abstracted groundwater. In many parts of the world, groundwater is the primary source of drinking water. However, as discussed in Chapter 3, precipitation also causes LNAPL to migrate into the saturated zone, thus, precipitation could also have a negative impact if it falls on contaminated land that is also situated in an aquifer system used for water supply.

Once LNAPL is introduced into the subsurface, it will migrate further from it source following the groundwater flow. Even worse, if the contamination discharge occurs underground, such as in the case of leaking underground storage tanks, it will remain unnoticed until a nearby drinking water well becomes contaminated (Nadim et al. 2001). A study by Schubert et al. (2007) showed that leaking from storage tank in petrol station cause LNAPL migrate very far from it source and contaminate the groundwater as it migrate farther. Thus, with the effect of precipitation, the degree of contamination will increase with time if the contaminated area is subjected to precipitation for a long period of time, unnoticed and un-remediate, until the nearest well is contaminated.

With global warming issues and unpredicted weather condition nowadays, precipitation will definitely increase contaminant mobilization where LNAPL spills occur. Global warming is suggested to be linked to the recent increase of heavy precipitation events due to the increased atmospheric water vapor and warmer air (Bocheva et al. 2009). Annual precipitation totals also show an upward trend in many regions in the world (Dai et al. 1997). The upward tendency of damages caused by natural disasters supports the idea that extreme events, such as torrential precipitation, associated with the effects of climate change, occur with greater frequency (Easterling et al. 2000). Thus in this chapter, the effects of precipitation intensity from light precipitation to very heavy precipitation was studied. Since precipitation intensity is directly related to precipitation volume, the one-dimensional column studies were also conducted.

4.2 Experimental Program and Procedure

4.2.1 Experimental Program

Whenever LNAPL spills, it will infiltrate deeper until it reaches the capillary fringe due to gravitational force. However, due to capillarity and the low density of LNAPL, migration becomes difficult and it will cease at the stable migration depth. This condition changes as soon as precipitation infiltrates the contaminated sand layer. Chapter 3 demonstrated that, although LNAPL density is lighter than water, precipitation can displace low-density contaminants further downward into the saturated zone, thus increasing the contamination degree of the groundwater. The experimental program in this chapter was more focused on the main characteristic of precipitation, which are the precipitation intensity and volume.

In order to appreciate how precipitation affects the behavior of LNAPL migration, the design precipitation intensity should be relatively similar to the natural precipitation. The precipitation intensity actually varies among locations and is closely related to the climate condition. The climate however, is a very complex system; and for each location in the world it can be categorized based on a climate classification system such as the aridity index (Lang 1920), the Holdridge life zones classification system (Holdridge 1967), and the Köppen climate classification (Köppen 1918). The last is the most widely used climate classification system (Chen and Chen 2013) because of its simplicity (Wilcock 1968). In the climate map generated by Köppen climate classification, it is clear that in one country it is possible to have more than one climate type. Considering this factor, and the availability of the appropriate technology, it is difficult for most countries to classify their precipitation based on precipitation intensity. Thus, a more practical approach is to classify the precipitation based on precipitation volume. According to the World Meteorological Organization, if precipitation is more than 50 mm in 24 hours, it is classified as heavy rain. Some countries, such as India, use even more specific precipitation classes (Figure 4.1). Malaysia is one of the few countries that have only one climate system: the tropical rainforest climate. Thus it is possible to specify classes for different precipitation intensities (Figure 4.1). Therefore, the applied precipitation intensity in this study can be compared with the actual rainfall condition based on the precipitation intensity classifications provided by the Malaysia Drainage and Irrigation Department Standard.

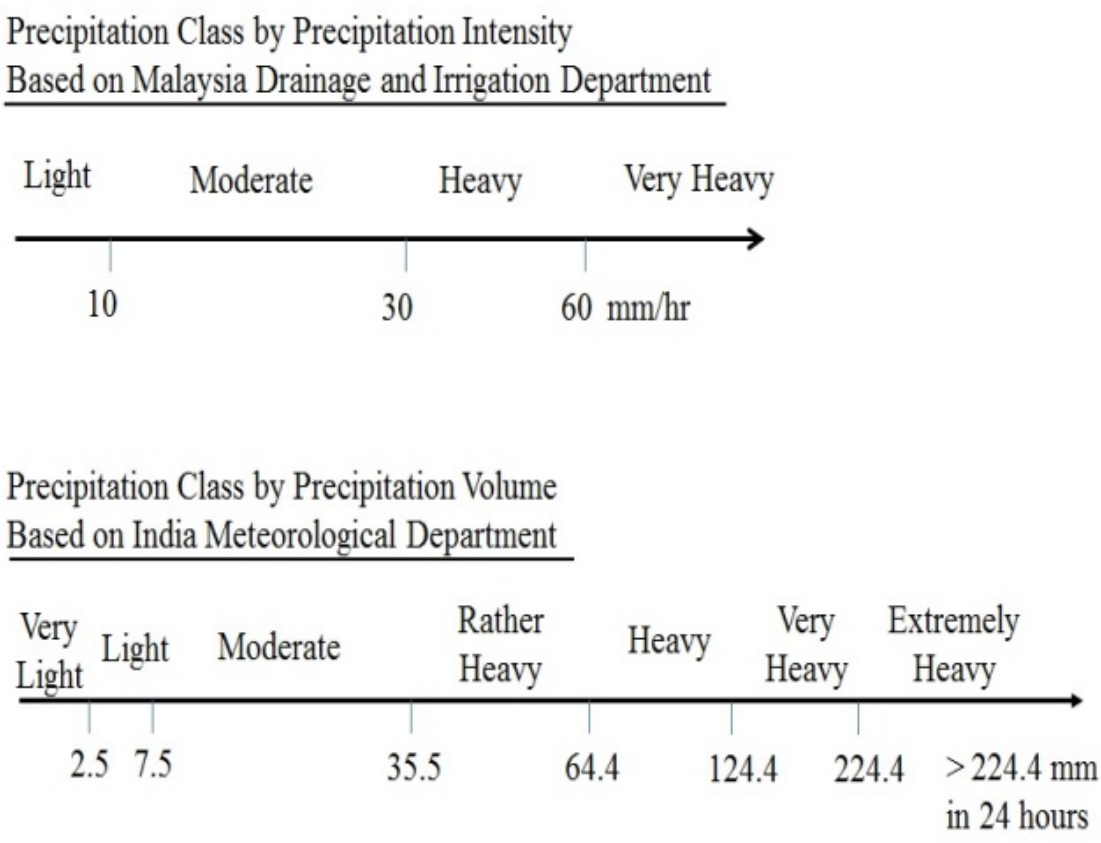

Figure 4.1 Precipitation classification system of Malaysia (DID Malaysia 2013) and India (IMD 2013).

When the infiltrated LNAPL reached a stable depth, it no longer migrated deeper, because it had reached its equilibrium at interfacial tension. It was the precipitation-infiltrated water that causes the migration of the LNAPL further into saturated zone. In relation to that, precipitation plays a direct role in causing the migration of the LNAPL; otherwise, LNAPL is simply entrapped at the stable migration depth. There were two areas of study focus in this chapter, which were the effect of precipitation intensity and the effect of equal precipitation volume. Figure 4.2 shows the ranges of precipitation intensity that were explored for the precipitation intensity study focus. A total of 91 hours was required for this study focus. In order to accurately simulate the actual rainfall, the experiment designed a precipitation range from light to very heavy precipitation based on the Malaysia Drainage and Irrigation Department Standard. To better appreciate LNAPL migration due to precipitation, a simple approach was followed to determine the precipitation duration. The duration chosen was one hour, similar to the time unit of intensity, which was also per hour.

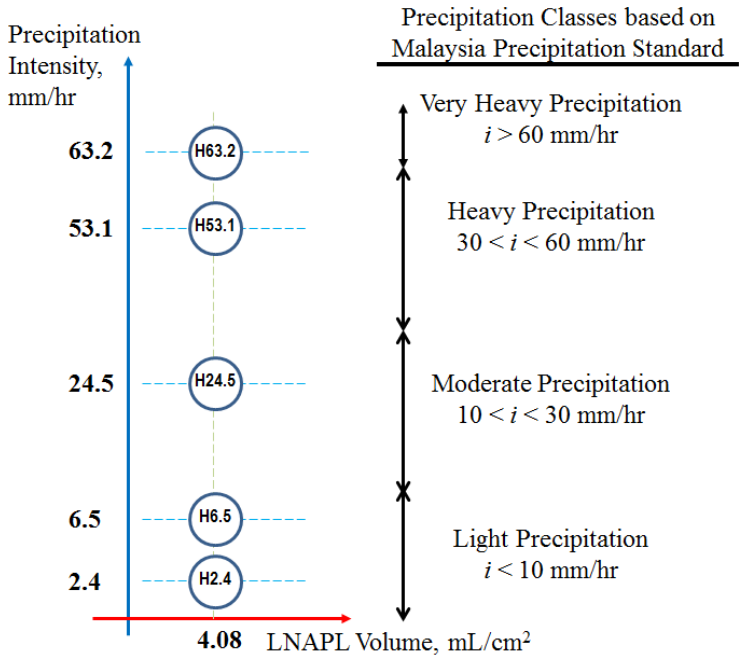

Figure 4.2 The experiment conducted for the precipitation intensity focus study.

Based on the one-dimensional column test results, it was proven that, instead of floating upward, LNAPL moves downward when subjected to precipitation. The laboratory results in Chapter 3 also revealed that a higher LNAPL spilled volume would further increase the degree of contamination in the saturated capillary zone due to precipitation. This happened due to a layer of highly saturated LNAPL that is created in the saturated capillary zone due to precipitation. Therefore, the experimental programs in the precipitation intensity study's focus were concentrated upon the migration of the LNAPL due to various precipitation intensities, i, on a high LNAPL spilled volume condition (V_D = 4.08 mL/cm^2).

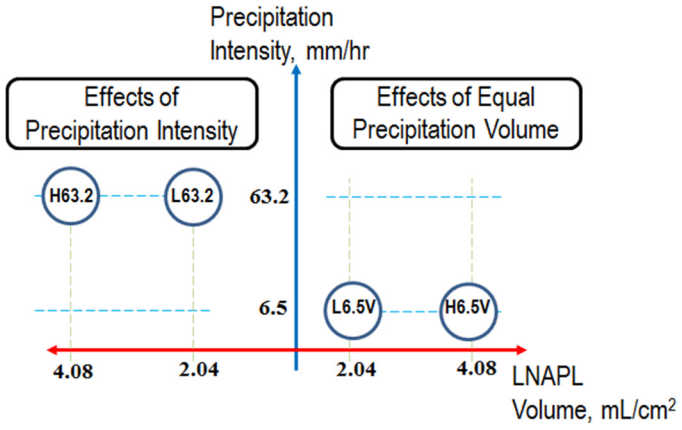

Figure 4.3 The experiment conducted for the equal precipitation volume focus study.

Since precipitation intensity is directly related to precipitation volume, the effects of both parameters on LNAPL migration remain unknown. Therefore, an equal precipitation volume study was conducted by using the light precipitation intensity for a longer period of precipitation to achieve the same precipitation volume as a very heavy precipitation intensity (i = 63.2 mm/hr). Figure 4.3 shows the ranges of precipitation intensity conducted for the equal precipitation volume study focus. A total of 100 hours was required for this study focus. The light precipitation intensities used in this study was 6.5 mm/hr, and the precipitation duration was about 10 hours. In order to evaluate the LNAPL migration behavior due to long precipitation condition for various spill volume conditions, the low and high LNAPL spilled volume (V_D = 2.04 and 4.08 mL/cm^2) conditions were evaluated. The 6.5 mm/hr of precipitation intensity case was chosen for this purpose.

4.2.2 Experimental Procedure

The Toyoura sand was packed into a test column to simulate the LNAPL migration behavior due to precipitation. The experimental setup for the one-dimensional column test conducted in this chapter was similar to the one-dimensional column experimental setup used in Chapter 3. Prior to starting the experiments, the sand was fully saturated with water. The sand was previously saturated with blue-dyed water and left for 24 hours in a vacuum chamber to remove air from it and ensure complete saturation. Then, the saturated sand was slowly poured with the help of a spoon into the column that was filled with de-aired water. Throughout the pouring process, the column was put on top of a vibrator to ensure uniform compaction until the final elevation was reached.

The experiment started as soon as the drainage valve was opened and the soil-saturated water was drained out of the column. The flow chart for the study focus, precipitation intensity and equal precipitation volume, is shown in Figure 4.4. The drained-out liquids were collected in a square bottle. Two 6-mm diameter holes were made in the bottle cap to receive a 4-mm diameter glass tube that connected to the drainage line. The rate of liquid lost inside the bottle due to evaporation was about 1 g per 10 days. The elevation of the outflow was 50 mm below the bottom of the column. The outflow was automatically measured by an electronic scale and recorded every 15 seconds. Throughout the experimental

period, the drainage valve was never closed, and the outflow elevation was never changed. The room temperature was kept at 20°C and the humidity was maintained at 70%.

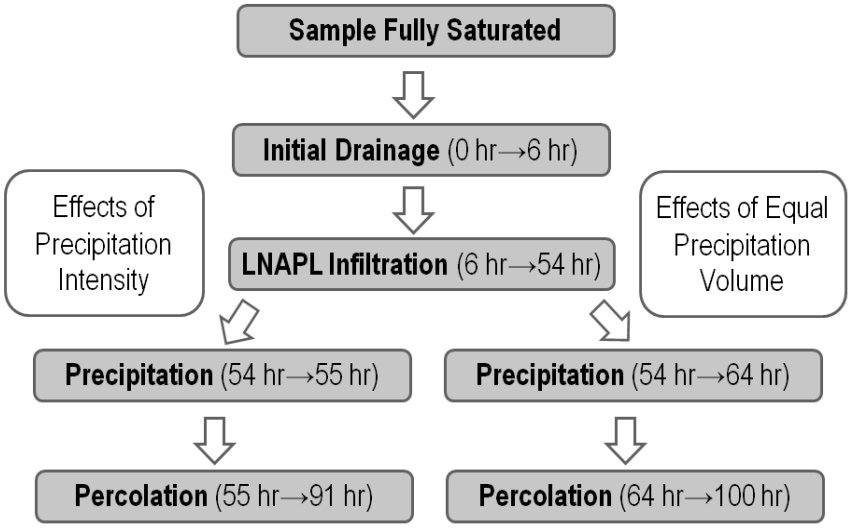

Figure 4.4 One-dimensional column test procedure.

When the bottom drainage valve was opened, the fully water-saturated Toyoura sand was drained for 6 hours. Then, designated volumes of LNAPL were released using a pipette from the top of the column. The LNAPL was allowed to migrate downward for 48 hours. Then, in the precipitation stage, the blue dye water was poured from the top of the column according to designated precipitation intensity and precipitation duration. The precipitation intensity and supply volume were controlled using a digital peristaltic pump. The precipitation water supplies were taken from a graduated cylinder to check if the precipitation volume is similar to the designed level. Finally, during the percolation stage, the LNAPL contaminants and precipitation water were allowed to drain for 36 hours.

Digital pictures were taken every 5 minutes during the first hour of each stage and every 30 minutes after that until the end of the stage. The cameras were set in manual mode, and the aperture, shutter speed, and white balance were defined and maintained constant throughout the experiment. The cameras were remotely controlled using Nikon Camera Control Pro 2 software to avoid vibrations and camera displacement. The two LED floodlights were turned on 30 seconds prior to taking picture and turned off 30 seconds afterwards.

4.3 Effects of Precipitation Intensity

4.3.1 LNAPL and Water Saturation Profile

The saturation profile developed from data obtained using SIAM analysis has allowed the study of LNAPL migration behavior due to precipitation. This allowed the LNAPL and water saturation from all 250,000 data obtained from each 91-hour experiment to be evaluated in a simple time history scale. Since the saturation profile is in time scale, the saturation changes between before and after the precipitation can be compared. Thus, the changes in LNAPL behavior can be studied more accurately according to the elapsed time during the experiment. The results of the one-dimensional column tests for the effects of the precipitation intensity study are shown in Figure 4.5 to Figure 4.9.

According to the Malaysia Drainage and Irrigation Department Standard for precipitation classes based on precipitation intensity, the precipitation intensity used in this study ranges from light to very heavy precipitation. Case H63.2 (Figure 4.5) is classified as very heavy, H53.1 (Figure 4.6) as heavy, and H24.5 (Figure 4.7) as moderate. Two cases were classed as light precipitation, which were case H6.5 (Figure 4.8) and H2.4 (Figure 4.9).

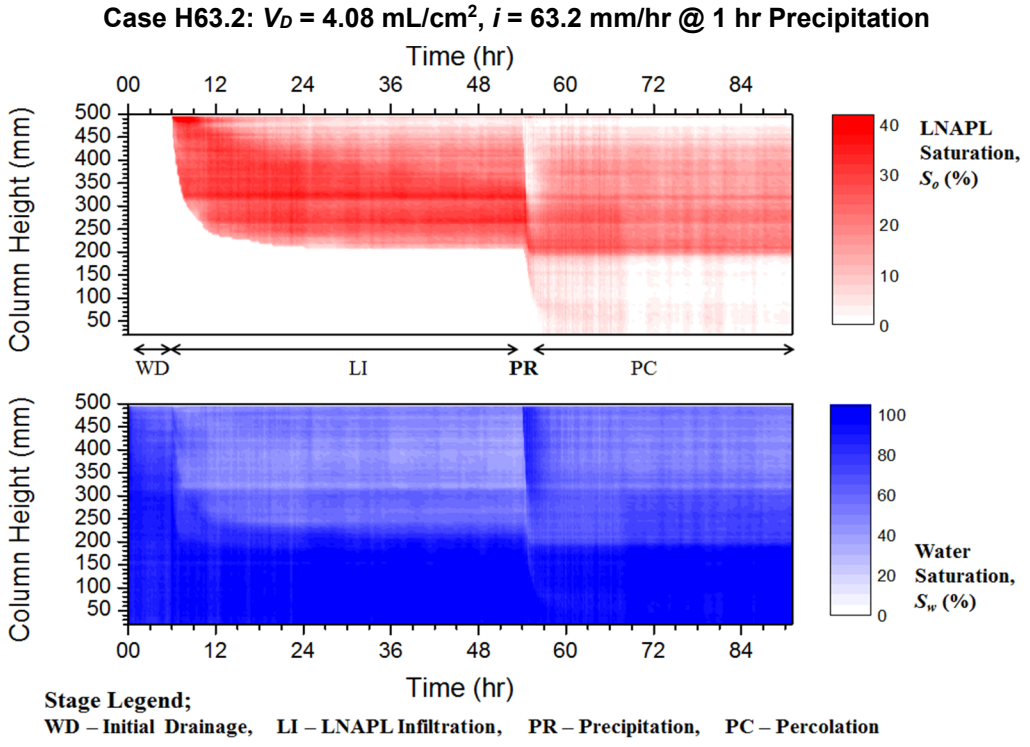

Figure 4.5 LNAPL and water saturation profile for case H63.2.

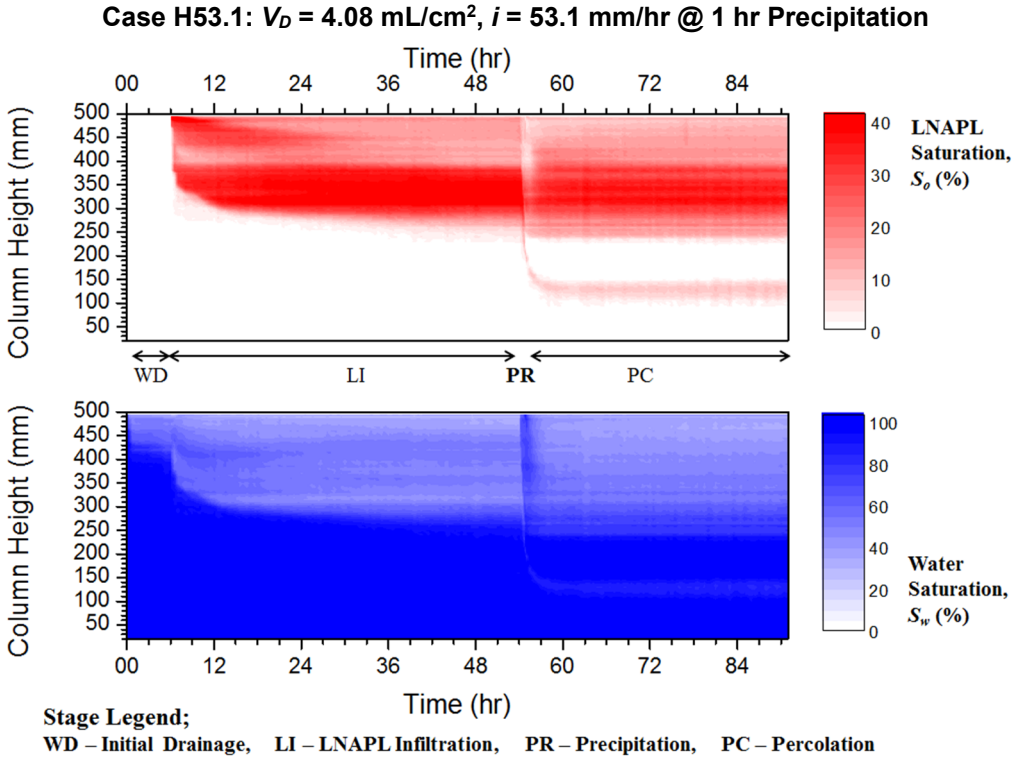

Figure 4.6 LNAPL and water saturation profile for case H53.1.

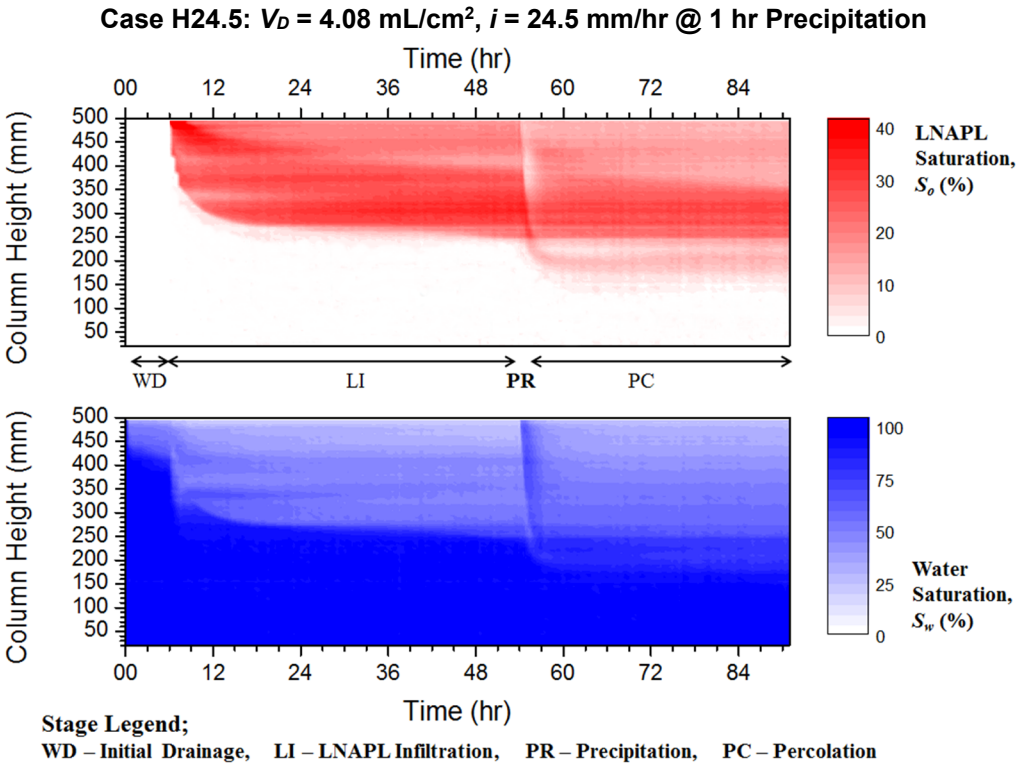

Figure 4.7 LNAPL and water saturation profile for case H24.5.

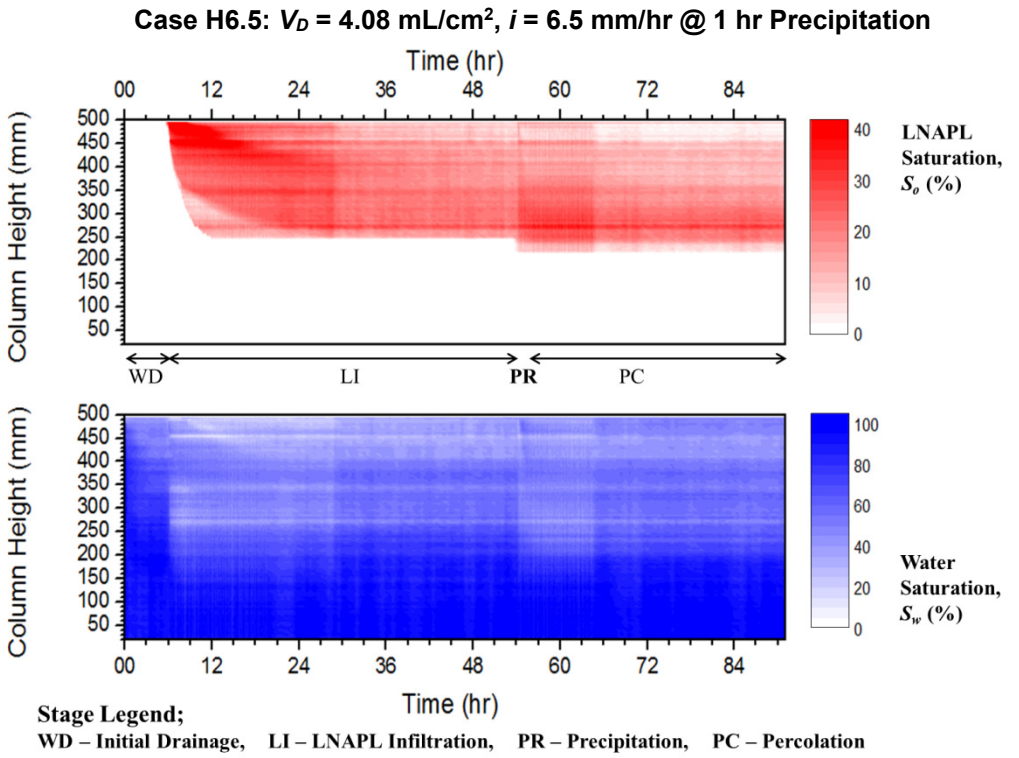

Figure 4.8 LNAPL and water saturation profile for case H6.5.

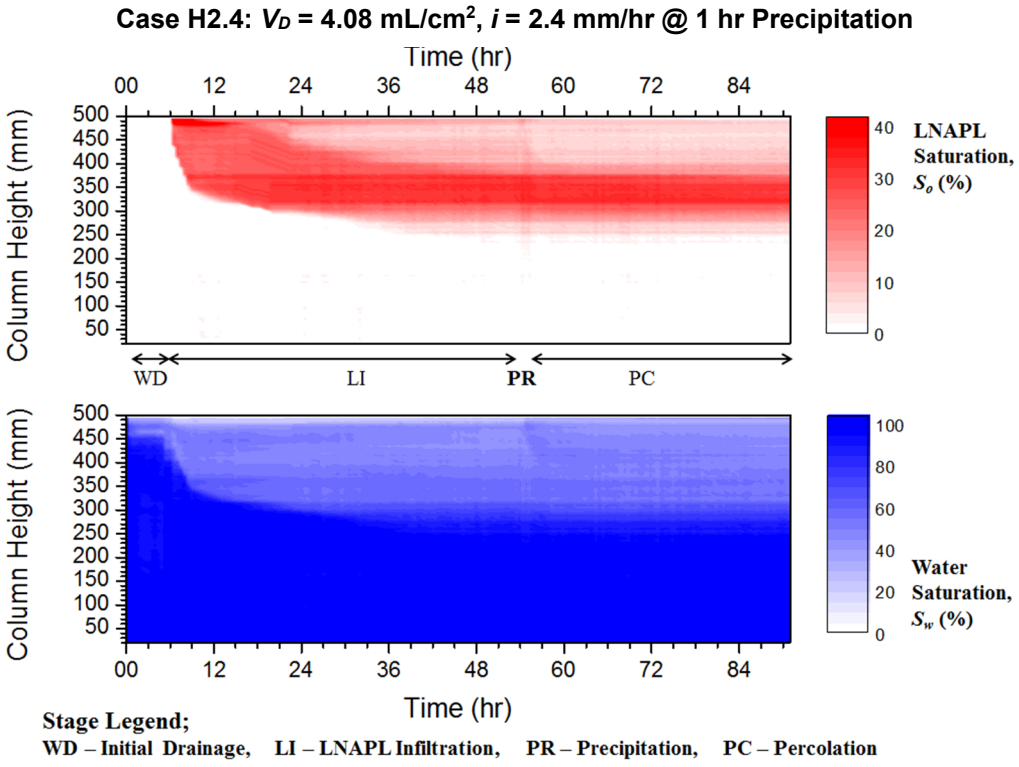

Figure 4.9 LNAPL and water saturation profile for case H2.4.

The migration of LNAPL due to precipitation can be easily studied from the LNAPL saturation profile by comparing the profile prior to and after precipitation. As can be seen, prior to precipitation (in the LNAPL infiltration stage), there are two distinct zones, which are contaminated (red) and uncontaminated (white) zones. This condition changed after the contaminated sand was subjected to precipitation. It can be seen that the LNAPL migrates downwards creating a new contamination plume boundary in the saturated capillary fringe zone due to precipitation. This boundary was defined by changes of LNAPL saturation, prior to and after precipitation. The changes in LNAPL saturation in terms of elevation were also taken into account while defining the boundary. This means that the LNAPL saturation value ranges (must be continuously) from the top of the column to the bottom of the newly defined boundary. This screening procedure is taken into consideration to ensure that the migration of LNAPL is the actual physical migration, and not the value due to error in the method.

4.3.2 LNAPL Migration Behavior

Although LNAPL is lighter than water, this study has demonstrated that, instead of floating upward, LNAPL moves downward when subjected to precipitation. In that sense, it is the precipitation that causes the migration of LNAPL; otherwise, LNAPL is simply entrapped at the stable migration depth. In Figure 4.10, the initial LNAPL saturation was around 20% at 400 mm of column elevation. The saturation value was constant from an elapsed time of 53 hours until 54 hours. The same condition also occurred at 350 mm of column elevation. At this elevation, the LNAPL saturation was around 26% and the value remained constant until 54 hours of experimental elapsed time.

Table 4.1 Changes of LNAPL saturation incase H63.2 due to precipitation.

Elevation	Before Precipitation	During Precipitation	After Precipitation
400 mm	20%	4%	11%
350 mm	26%	2%	10%

The constant value reflects that there was no increase or reduction in the volume of LNAPL within the soil pores at this elevation. This means that the two immiscible liquids have reached the equilibrium condition of capillary pressure between them at interfacial tensions. The stable conditions however, change due to precipitation. In the precipitation

stage, precipitation water infiltrates the contaminated sand from the top layer in the column downward due to gravitational force. As the precipitation water infiltrates downward, it has to overcome the LNAPL layer in the soil pores. Due to the fact that both liquids are immiscible, the infiltrated water pushes any mobile LNAPL that it overcomes when it infiltrates downward. Consequently, the mobile LNAPL migrates into a deeper soil layer.

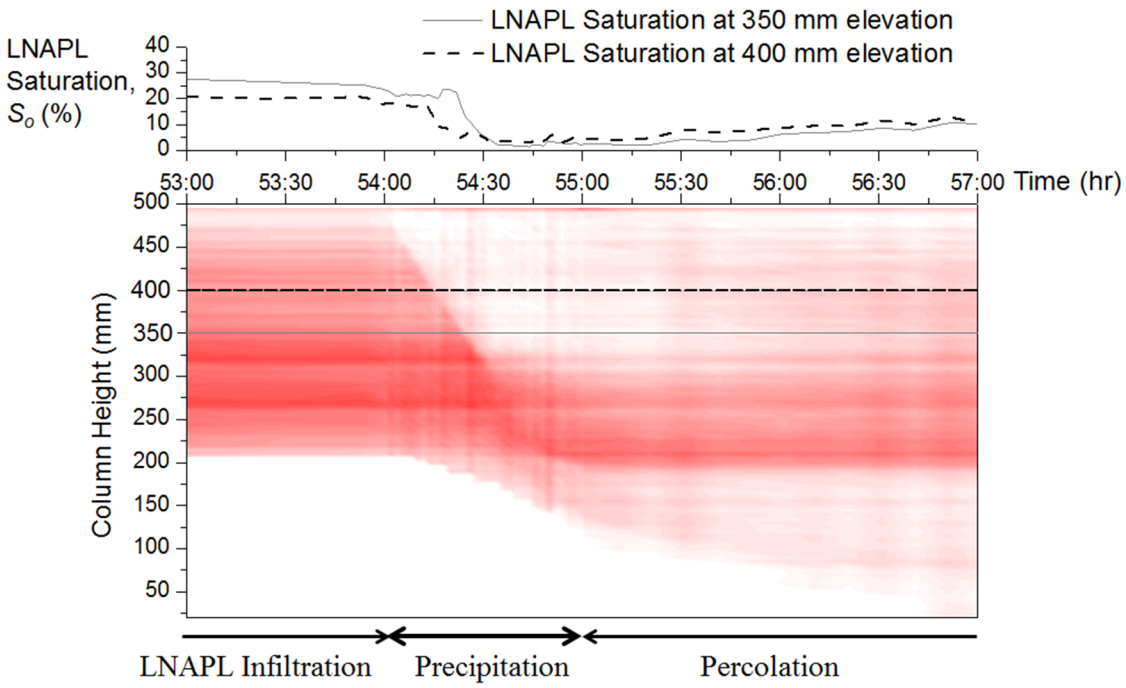

Figure 4.10 LNAPL saturation before and after precipitation for case H63.2.

The effect of precipitation was clearly shown in Figure 4.10: during the precipitation stage (54 to 55 hours), the LNAPL saturation reduced significantly. Between 400 and 350 mm elevation, the former shows the extent of early reduction in LNAPL saturation compared to the latter. This is due to the migration of the mobile LNAPL, which started at the upper column layer, as the precipitation water infiltrated the soil column from the top to bottom. The precipitation water infiltrated downward due to the gravitational force. As both liquids are immiscible, the infiltrated water pushed the LNAPL even deeper as it infiltrated due to gravitational force.

The LNAPL migration occurred due to high wetting front propagation force during precipitation. In case H63.2, layers of medium LNAPL saturation (20% to 30% of saturation) at around 325 mm to 450 mm elevation diminished. At the same time, the contamination

plume's vertical width reduced from 225 mm to 100 mm in height. The reduction of the contamination plume's vertical width can be considered as proof that high wetting front propagation force rapidly pushes down mobile LNAPL until it reaches the contamination plume boundary. The reduction occurred rapidly after 30 minutes of precipitation. Consequently, a significant volume of LNAPL was pushed downward until it reached the bottom of the column and immobilized in the soil pores in the bottom layer inside the column. Since the intensity was high (i = 63.2 mm/hr), the water remaining in the column kept pushing the LNAPL until it reached a final stable condition, 80 mm deeper, one hour after the end of precipitation. Thus, LNAPL with a saturation value of 10% to 15% can migrate into the saturated zone, extend the contamination deeper, and increase the groundwater contamination risk.

Considering that the downward flow of precipitation water during infiltration was the main mechanism that caused the migration of LNAPL, the volume of water supplied from precipitation certainly affects the migration behavior. In this study focus, as the volume of supplied water was based upon precipitation intensity, a significant migration depth trend can be seen from very heavy precipitation intensity (Figure 4.5) to light precipitation intensity (Figure 4.9). The higher the precipitation intensity, the deeper LNAPL will migrate due to precipitation. This is because more pressure and force was applied to the LNAPL by infiltrating water in the higher precipitation intensity cases.

In all high precipitation intensity cases (H63.2, H53.1 and H24.5), once precipitation started, a high volume of water supplied from high precipitation intensity infiltrated the sand and flowed downward due to gravitational force. This high amount of infiltrating water provided a high wetting front propagation force that pushed down any LNAPL within its flow path. This mechanism helped LNAPL migrate easily into the saturated zone. In case H6.5, it was found that precipitation can cause the migration of LNAPL into the saturated zone. However, in case H2.4, due to the low volume of supplied water during precipitation, the infiltration of precipitation water was not able to cause LNAPL migration into the saturated zone. The water saturation profile also shows that the light precipitation intensity, in this case, is only able to cause small increases in the water saturation (Figure 4.9). At this intensity, it was only able to wet the soil, but was not able to initiate the migration of LNAPL.

4.4 Effects of Equal Precipitation Volume

Climate conditions are very complex systems that affect the precipitation characteristics between one location and another. This condition affects the intensity and volume of precipitation throughout the whole year. There can be conditions where very heavy precipitation occurs in a relatively short period of time during light precipitation. This type of precipitation is normally called torrential or extreme precipitation, where the intensity is around 60 to 130 mm/hr (Bocheva et al. 2009; Deshpande et al. 2012; Zanon et al. 2010; Zhou and Ran 2012). It is very rare to have a very long period of heavy precipitation intensity, unless it is during rainstorms (due to strong winds), such as the case reported in Mumbai, India by Jenamani et al. (2006) where the precipitation intensity was between 60 mm/hr to 191 mm/hr in 6 hours with a total of 944 mm of precipitation volume during 24 hours of precipitation. A long duration of precipitation normally occurs with light precipitation intensity (< 10 mm/hr). It can be said in general that, the longer the precipitation duration, the lower the precipitation intensity. There is, however, a condition where precipitation intensity around 25 mm/hr occurred for almost 9 hours in Barcelona, Spain (Llasat 2001). That condition rarely, however, occurs, and this study focuses more on long precipitation durations of light precipitation intensity; which, in general, normally occurs. The precipitation intensity chosen for the long precipitation duration in this study was 6.5 mm/hr.

The precipitation intensity is directly related to precipitation volume; where the former consider volume of water per time (per hour), whereas the latter consider the total volume of water due to precipitation. In section 4.3, it has been demonstrated that a higher precipitation intensity helped LNAPL migrate deeper. The LNAPL migration depth was less significant in the light precipitation intensity case compared with the heavy precipitation case. In natural conditions, however, the light precipitation intensity occurs most often in most parts of the world, and commonly the precipitation duration is much longer than an hour. Thus, the LNAPL migration behavior due to long precipitation duration of light precipitation intensity was assessed, and the precipitation volume of very heavy precipitation intensity cases (i = 63.2 mm/hr) was chosen for comparison. The effects under equal precipitation volume study was conducted by using the light precipitation intensity (i = 6.5 mm/hr) for a longer period of precipitation to achieve the same precipitation volume as very heavy precipitation intensity (i = 63.2 mm/hr) (Figure 4.11 to Figure 4.14).

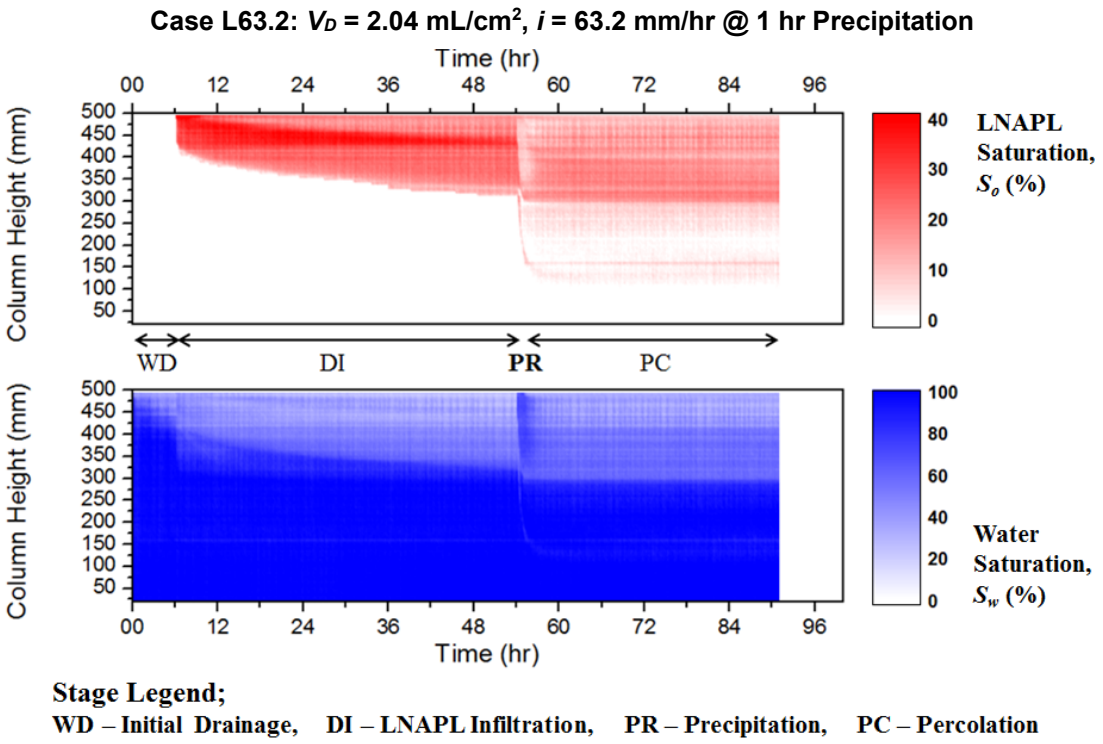

Figure 4.11 LNAPL and water saturation profile for case L63.2.

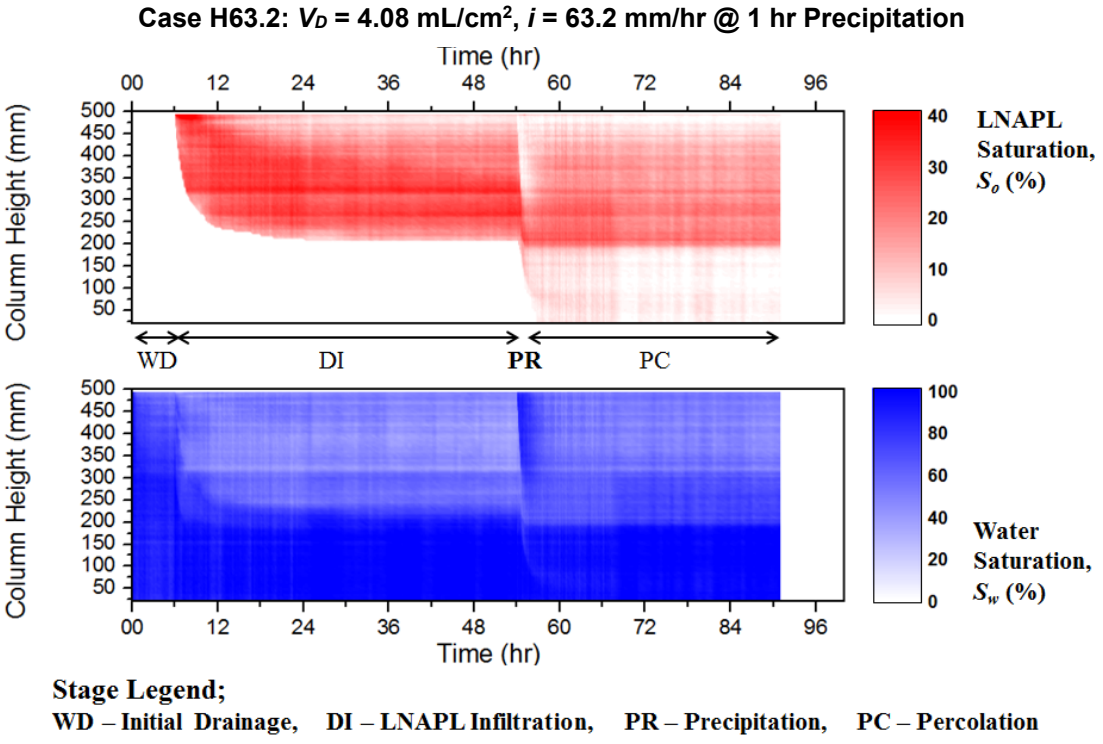

Figure 4.12 LNAPL and water saturation profile for case H63.2.

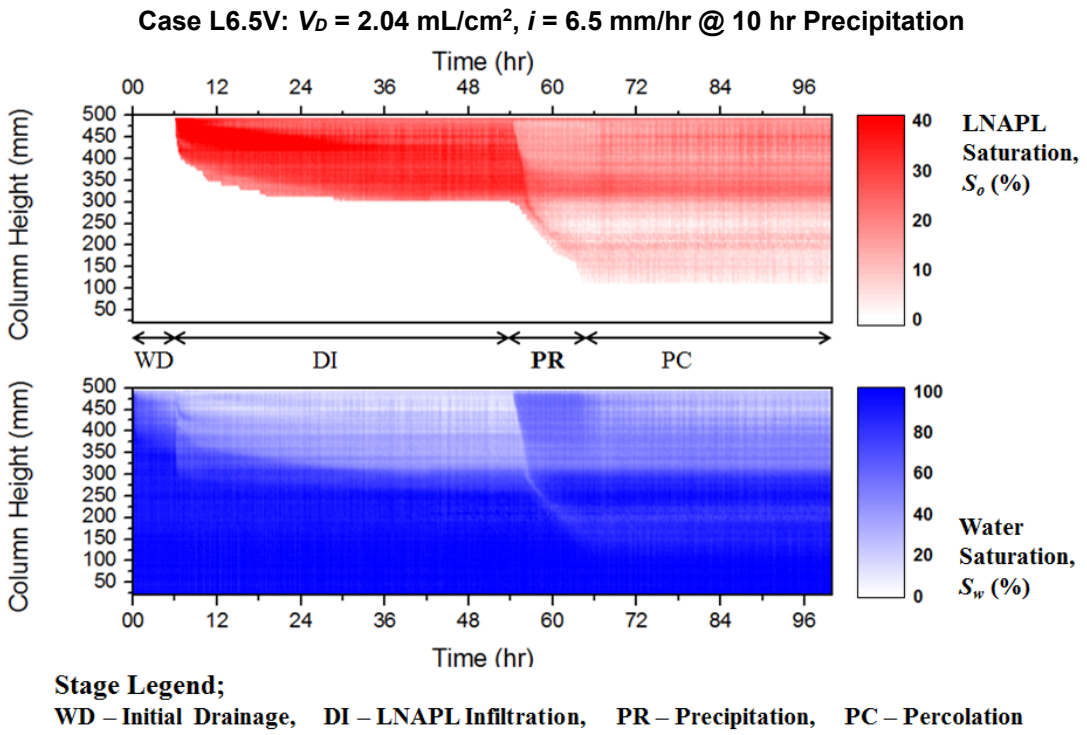

Figure 4.13 LNAPL and water saturation profile for case L6.5V.

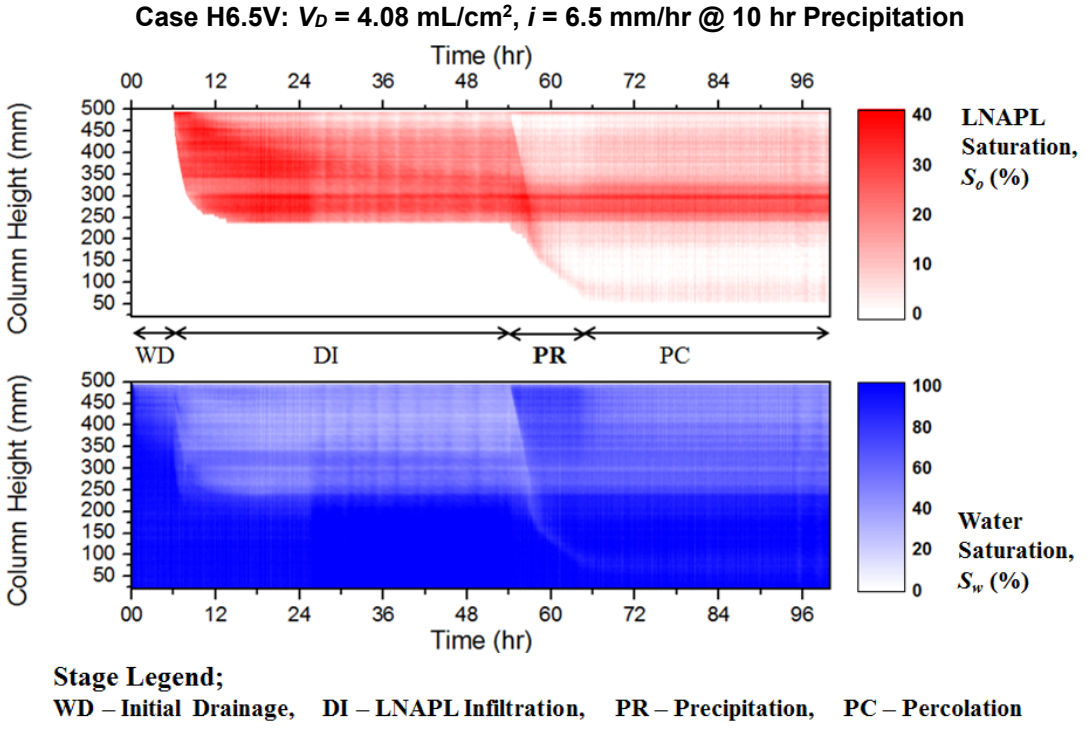

Figure 4.14 LNAPL and water saturation profile for case H6.5V.

Based on the saturation profile, there was similarity in the LNAPL migration behavior between both precipitation intensity cases; the very heavy intensity (L63.2 and H63.2 cases) and light intensity (L6.5V and H6.5V cases). Although the amount of water infiltrated per time was almost 10 times lower in the light precipitation intensity cases, the constant water infiltration from the 10 hours of precipitation consequently gave a similar effect as in very heavy precipitation intensity cases. This is due to the increasing amount of supplied water from continuous long precipitation, which caused an increase in as well as an accumulation of infiltrated water. This accumulation of water consequently pushed the mobile LNAPL deeper into the saturated zone, similarly to very heavy precipitation intensity cases.

The LNAPL migration behavior due to the pushing mechanism by the infiltrated precipitation water can be seen during the precipitation stage (Figure 4.15). In the saturation profile, the sharp triangle pattern during precipitation was the evidence of liquid movement within the increasing time. This triangle pattern reflects the displacement of mobile LNAPL in the soil pores due to the infiltration of water. As the time increases, the blue (water profile) triangle gets deeper, the red triangle (LNAPL profile) gets shorter. The downward infiltration of water due to the gravitational force has caused the wetting front force to push any LNAPL that water overcomes during infiltration.

The similar pushing mechanism also occurred in the light intensity with long duration precipitation cases (L6.5V and H6.5V cases). Figure 4.16 shows the saturation profile one hour before and after precipitation, as well as during the 10 hours of precipitation. The similar sharp triangle pattern due to the wetting front of infiltration water clearly appeared in the saturation profile. This indicated that the similar LNAPL migration mechanism and behavior occurred in these cases.

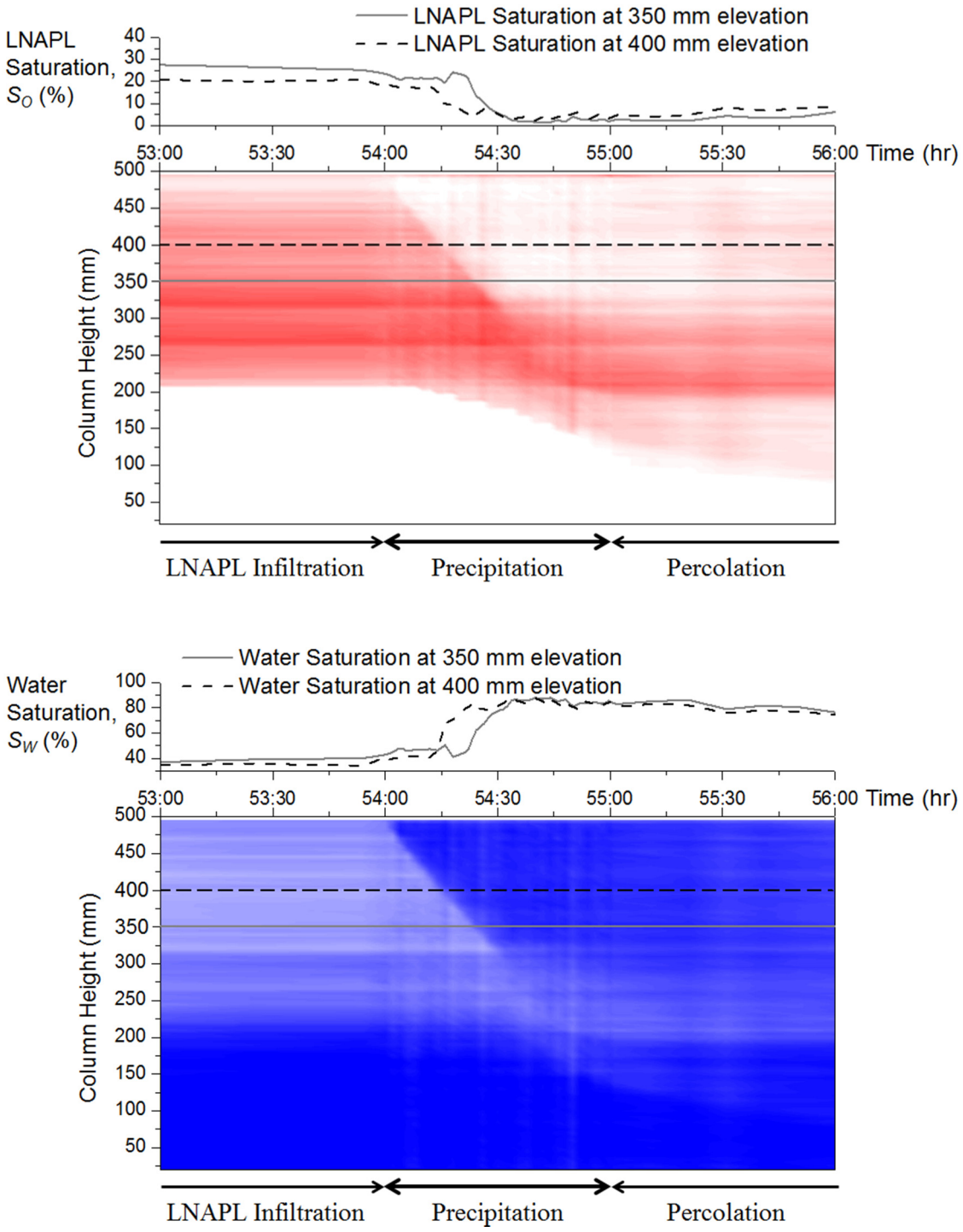

Figure 4.15 Saturation profile of one hour before, during and after precipitation for the case H63.2; (a) LNAPL saturation profile (b) water saturation profile.

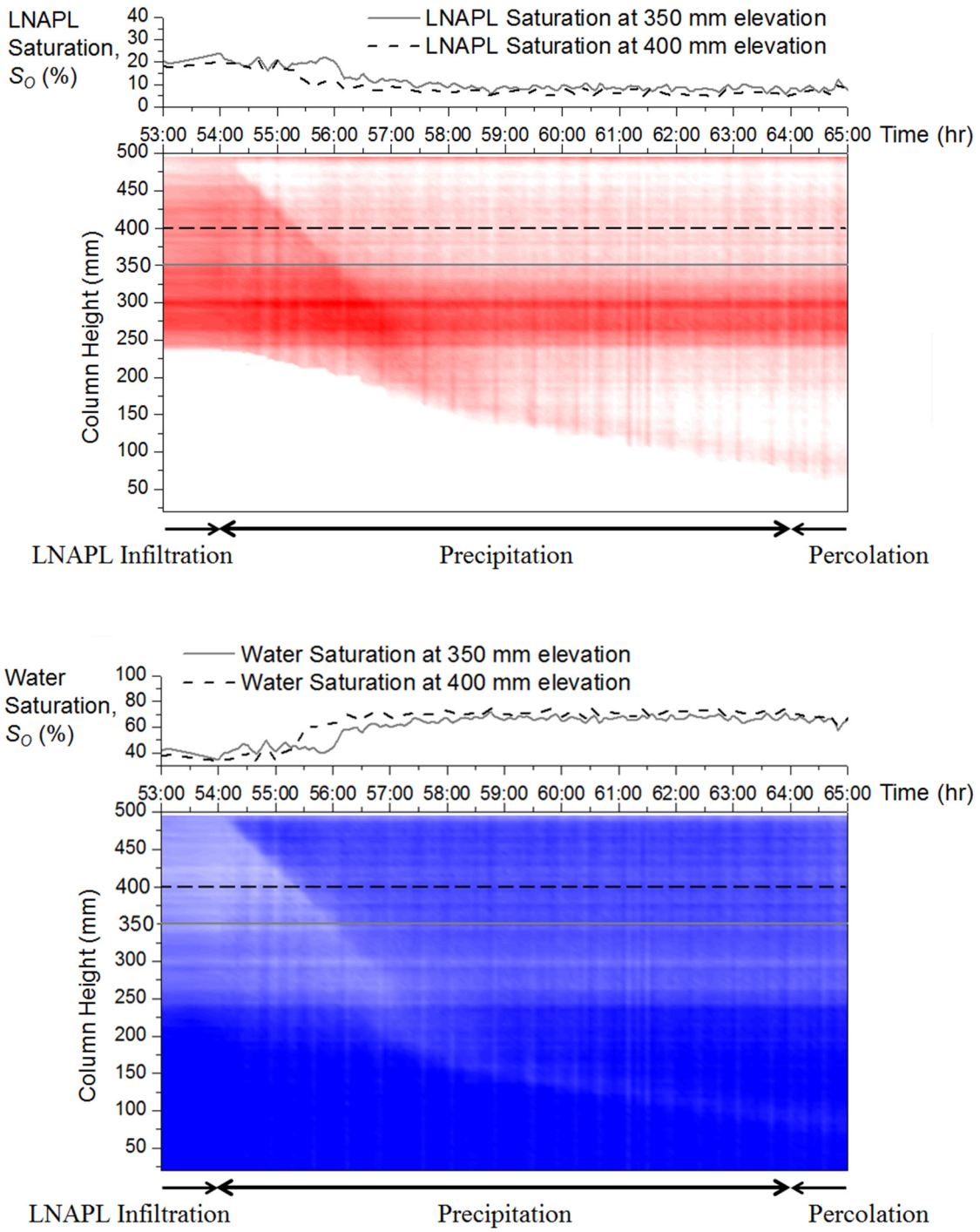

Figure 4.16 Saturation profile of one hour before and after precipitation, as well as during precipitation (10 hours) for the case H6.5V: (a) LNAPL saturation profile and (b) water saturation profile.

There was also similarity in the saturation changes behavior for both conditions cases; the light intensity with long duration precipitation case and very heavy intensity with normal duration precipitation case. This can be shown by comparing the saturation changes of two different elevations for both cases (H63.2 and H6.5V cases). In Figure 4.15 and Figure 4.16, the saturation value with respect to the experiment time for 400 mm and 350 mm elevations were shown in the graph above the saturation profile. In the H6.5V case, the initial stable saturations were around 19% for LNAPL and 36% for water at 400 mm elevation before precipitation stage. Eighty-five minutes after the precipitation, the wetting front of the infiltration water reached the 400 mm elevation. The infiltration water pushed down any mobile LNAPL that it encountered as water infiltrated deeper due to gravitational force. The saturation graph in Figure 4.16 for 400 mm elevation shows that the water saturation started to increase rapidly and LNAPL saturation started to reduce. The LNAPL saturation was around 10% and reducing, whereas the water saturation was around 50% and increasing.

At the same time, there was no significant saturation change at 300 mm elevation. This was because the pushing mechanism by infiltrated water that caused the migration of LNAPL had not yet reached 300 mm elevation. Once the infiltration water reached this elevation, the similar migration behavior that occurred at 400 mm elevation during the same situation also occurred. The similar pattern, where the LNAPL saturation reduced as water saturation increased, is shown in the saturation graph (Figure 4.16).

The pushing mechanism by infiltration water had caused LNAPL volume accumulation at the wetting front and thus caused liquid weight to increase at the wetting front. Together with increased volume of water with time at the vadose zone, the saturated capillary boundary had to adapt to the new pressure changes from above. Consequently, LNAPL started to infiltrate into saturated zone. As the precipitation water continued to infiltrate downward due to the gravitational force, it reached the saturated capillary layer. Since LNAPL and water are immiscible, the pushed LNAPL kept being pushed by the infiltration water into the saturated zone. Consequently, some of the mobile LNAPL became entrapped inside the soil pores in the saturated zone, whereas some other mobile LNAPL had still migrated due to the pushing of infiltrated water until it reached the stable condition when the pushing force was balanced with the local capillary force. The similarity of LNAPL migration behavior due to pushing mechanism by infiltration water in both the very heavy

intensity (L63.2 and H63.2 cases) and light intensity (L6.5V and H6.5V cases) cases was clearly shown in Figure 4.15 and Figure 4.16

Besides the LNAPL migration behavior similarity due to the pushing mechanism, it was also found that the total precipitation volume plays an important role in determining the depth of migrated LNAPL. A mentioned earlier, precipitation intensity is directly related with precipitation volume. It can be seen that whether the contaminated sand is subjected to either low or high precipitation intensity, if the precipitation total is the same, then the total depth of LNAPL migration will also be the same (Figure 4.17). Based on this study, the infiltrating water is one of the main mechanisms pushing the LNAPL to migrate deeper into the saturated zone. If subjected to high precipitation, the high wetting front force will help LNAPL migrate at a faster rate.

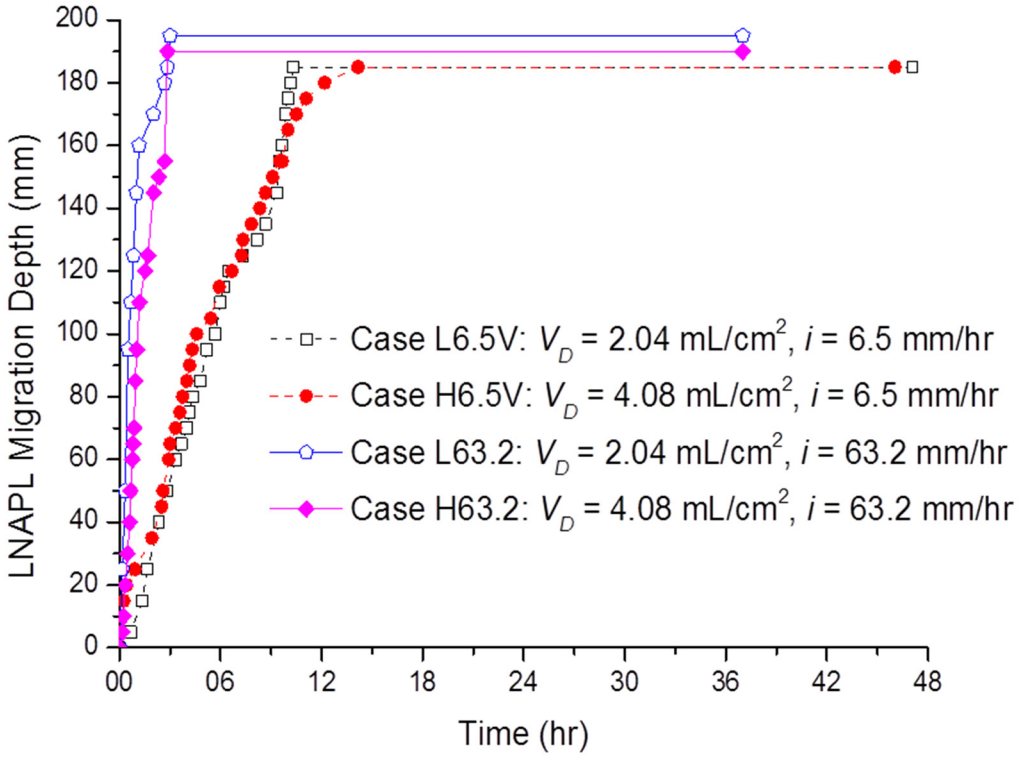

Figure 4.17 LNAPL total migration depth for the same total precipitation volume but different precipitation intensity and duration (cases L6.5V, H6.5V, L63.2 and H63.2).

4.5 The Mechanism of LNAPL Migration due to Precipitation

Based on the experiment results, it was shown that when the infiltrated LNAPL reached a stable depth, it no longer migrated deeper. LNAPL ceased to migrate when it reached equilibrium at interfacial tension. However, once the contaminated sand was subjected to precipitation, the LNAPL was able to migrate deeper into the saturated capillary fringe zone. With the help of saturation profile, the mechanism of LNAPL migration due to precipitation can be seen clearly. A sharp triangle profile developed in both LNAPL and water saturation profile due to the movement of liquid within increased time during the experiment in the precipitation stage. The movement of liquid was found to be downward as the time increased, where the water profile triangle was getting deeper and the LNAPL profile triangle was getting shorter. These triangle patterns reflect the displacement of mobile LNAPL in the soil pores due to the infiltration of precipitation water. The infiltration of precipitation water was found to be the main mechanism that pushes the LNAPL deeper into the saturated capillary zone.

Despite the low density of LNAPL, the infiltration of precipitation water was able to push the mobile LNAPL deeper into saturated zone. This occurred due to the fact that both liquids are immiscible, and thus additional volumes of water don't cause mixture of liquid. The precipitation water simply infiltrated downward due to gravitational force. Since the additional water came from above and both liquids are immiscible, the precipitation water pushed any LNAPL that it overcomes as it infiltrated downward.

Once the precipitation water has infiltrated the soil pores, it tends to flow in the main channel (the bigger space in between pores) rather than narrow soil pores. The main channel has a bigger pore radius compared with the pores in the smaller space; this also means that liquid in the main channel is subjected to less capillary pressure. Therefore, as the precipitation water infiltrated downward, the water was more able to displace LNAPL in this location since only low pressure was required to mobilize the LNAPL. The LNAPL in narrow soil pores would present more difficulty in being mobilized, as it would require higher pressure because it was subjected to the higher capillary pressure.

Since infiltration of precipitation water was the cause of migration of LNAPL, it is considered to be the applied pressure that pushed and caused the migration of LNAPL. Therefore, as volume of infiltrated precipitation water increases, so does the applied pressure. This mechanism can be correlated to the precipitation intensity. It has been discussed in section 4.3 that the higher precipitation intensity class was able to push more LNAPL into the saturated capillary zone. In general, the higher the precipitation intensity, the deeper LNAPL will migrate due to precipitation. This was because more pressure and force was applied to the LNAPL in the higher precipitation intensity cases. In all high precipitation intensity cases (H63.2, H53.1 and H24.5), once precipitation started, a high volume of water supplied from high precipitation intensity infiltrated the sand and flowed downward due to gravitational force. This high amount of infiltrating water provided a high wetting front propagation force that pushed down any LNAPL within its flow path. This mechanism helped LNAPL migrate easily into the saturated zone.

4.6 Conclusions for this Chapter

The intensity and volume of precipitation are the two parameters that govern the applied water volume during precipitation. Therefore, in order to understand the mechanism that cause the migration of LNAPL due to precipitation, two series of one-dimensional column test that focused on the precipitation intensity and volume were conducted in this chapter. The experimental programs in the precipitation intensity study's focus were concentrated upon the migration of the LNAPL due to various precipitation intensities. Since precipitation intensity is directly related to precipitation volume, the effects of both parameters on LNAPL migration remain unknown. Therefore, an equal precipitation volume study was conducted by using the light precipitation intensity for a longer period of precipitation to achieve the same precipitation volume as very heavy precipitation intensity.

In general, the higher the precipitation intensity, the deeper LNAPL will migrate due to precipitation. This is because more pressure and force was applied to the LNAPL by infiltrating water in the higher precipitation intensity cases. In all high precipitation intensity cases, once precipitation started, a high volume of water supplied from high precipitation intensity infiltrated the sand and flowed downward due to gravitational force. This high amount of infiltrating water provided a high wetting front propagation force that pushed

down any LNAPL within its flow path. This mechanism helped LNAPL migrate easily into the saturated zone. In case H2.4 (i = 2.4 mm/hr), due to the low volume of supplied water during precipitation, the infiltration of precipitation water was not able to cause LNAPL migration into the saturated zone. The water saturation profile shows that it only able to cause small increases in the water saturation. At this intensity, it was only able to wet the soil, but was not able to initiate the migration of LNAPL.

In the equal precipitation volume study's focus, it was found that there was similarity in the LNAPL migration behavior between both precipitation intensity cases; the very heavy intensity and light intensity. Although the amount of water infiltrated per time was almost 10 times lower in the light precipitation intensity cases, the constant water infiltration from the 10 hours of precipitation consequently gave a similar effect as in very heavy precipitation intensity cases. This is due to the increasing amount of supplied water from continuous long precipitation, which caused an increase in as well as an accumulation of infiltrated water. This accumulation of water consequently pushed the mobile LNAPL deeper into the saturated zone, similarly to very heavy precipitation intensity cases. Besides the LNAPL migration behavior similarity due to the pushing mechanism, it was also found that the total precipitation volume plays an important role in determining the depth of migrated LNAPL. It can be seen that whether the contaminated sand is subjected to either low or high precipitation intensity, if the precipitation total is the same, then the total depth of LNAPL migration will also be the same. Based on this study, the infiltrating water is the main mechanisms pushing the LNAPL to migrate deeper into the saturated zone. If subjected to high precipitation, the high wetting front force will help LNAPL migrate at a faster rate.

In both experimental programs, a sharp triangle profile developed in both LNAPL and water saturation profile due to the downward movement of liquid within increased time during the experiment in the precipitation stage. These triangle patterns reflect the displacement of mobile LNAPL in the soil pores due to the infiltration of precipitation water. Since the additional water came from above and both liquids are immiscible, the precipitation water pushed any LNAPL that it overcomes as it infiltrated downward due to gravitational force. Based on both intensity and volume of precipitation study focus, it is found that the pushing mechanism by the precipitation infiltrated water is the main mechanism that caused the migration of LNAPL due to precipitation.

CHAPTER 5: TWO-DIMENSIONAL STUDY OF LNAPL MIGRATION DUE TO PRECIPITATION AND SATURATION-CAPILLARY PRESSURE RELATION

5.1 General Remarks

When aquifers become polluted, contamination is persistent and difficult to remediate due to their large storage, long residence times, and physical inaccessibility (Foster and Chilton 2003). Moreover, groundwater contamination is an imperceptible and irreversible process, and prohibitive costs and time requirements may limit efforts to improve the groundwater condition (Causapé et al. 2006; Yu et al. 2010). As discussed in Chapters 3 and 4, precipitation can cause LNAPL to migrate into saturated capillary zone even though it is lighter than water. Therefore, the investigation continued in a two-dimensional study to ensure that this condition exits.

Further in this chapter, the analysis of saturation-capillary pressure relation (*S-p* relations) was also discussed. The *S-p* relations data were obtained from a one-dimensional column and two-dimensional tank test. These data were compared to the van Genuchten (1980) model to assess the LNAPL migration behavior due to precipitation in both one-dimensional and two-dimensional studies.

5.2 Materials and Methods

5.2.1 Materials

Toyoura sand was used as a porous medium in the two-dimensional study. The sand can be classified as SP according to the Unified Soil Classification System. The sand particle density, ρ, is 2.65 g/cm^3, equivalent grain size, D_{50}, is 0.18 mm and void ratio, e, is 0.66. The LNAPL used in the two-dimensional study is diesel. The density of the diesel used in this research is 0.865 g/cm^3, with viscosity of 7 mm^2/s, surface tension of 0.2675 N/m, and vapor pressure of 0.40 mm-Hg.

5.2.2 Experimental Apparatus

A 500 × 700 × 35 mm tank with a front transparent acrylic wall (Figure 5.1) was designed to study the LNAPL migration behavior in Toyoura sand affected by precipitation. The sand was packed inside the tank according to the sample size of 500 × 550 × 35 mm. A transparent glass wall was used to allow a clear view of liquid migration inside the sand tank. Simplified Image Analysis Method (SIAM) was used in this study to obtain the soil saturation value. Two consumer-grade digital cameras (Nikon D7000 and Nikon D90) with two different bandpass filters (λ = 450 and 656 nm) were placed in front of the sand column to capture the images throughout the test. Figure 5.2 shows the two-dimensional tank test set-up used in this study. Two LED floodlights were installed in the dark room as sole lighting sources and a Gretagmacbeth white balance card was located next to the tank for a constant white reference.

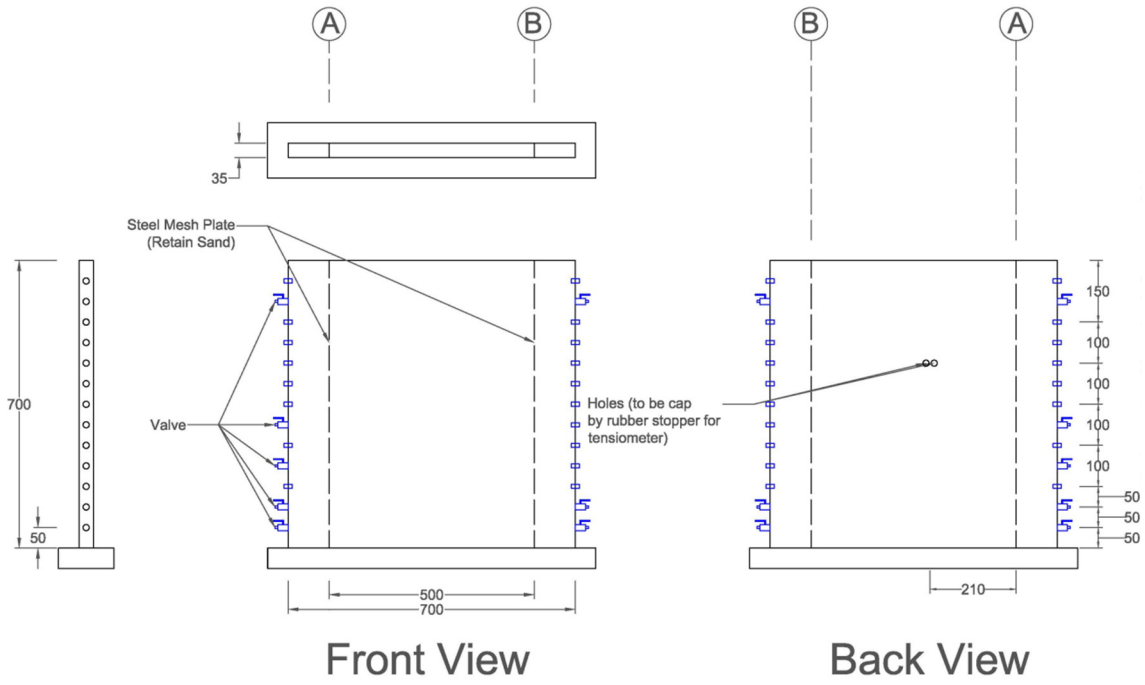

Figure 5.1 Tank design.

The groundwater level is at 50 mm elevation on both sides of the tank. It is thus considered that there is no hydraulic flow gradient below the groundwater level. The outflow water is collected in a square bottle where the mass of outflow is monitored for mass-balance check. Two 6-mm diameter holes were made in the bottle cap to receive a 4-mm diameter

glass tube that connects to the drainage line. By having these small holes at the side of the bottle, the possibility of evaporation from the outflow collected can be minimized.

To obtain capillary pressure value changes due to precipitation, a set of tensiometers (hydrophobic and hydrophilic) was placed in the vadose zone. The tensiometers were placed vertically at an elevation of 450 mm, and horizontally at 210 mm from left, in the same alignment as the LNAPL spill point. The LNAPL pressure and water pressure measurement is taken for every minute throughout the experiment and stored by a data logger connected to the computer. The capillary pressure value is the non-wetting pressure minus the wetting pressure, thus, LNAPL pressure minus water pressure.

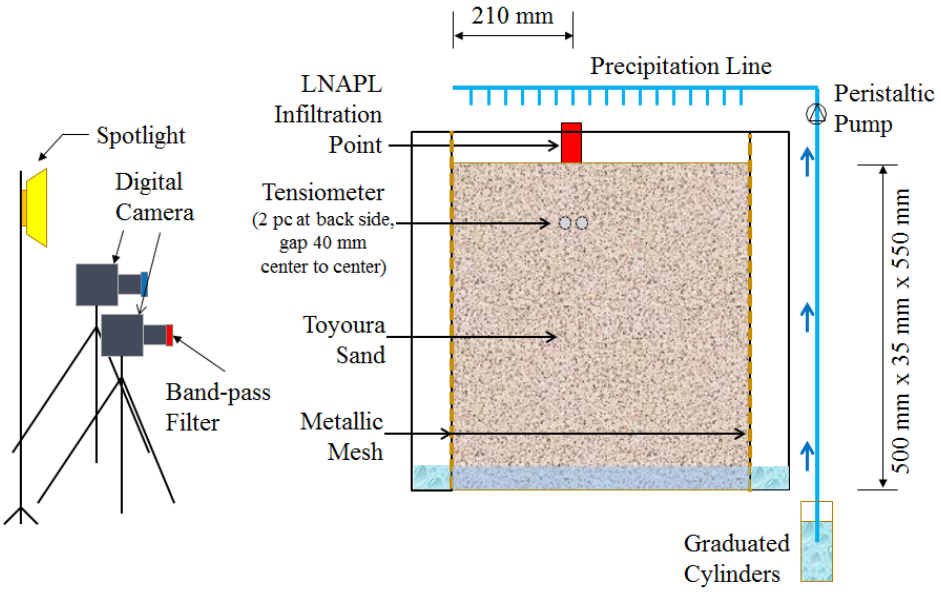

Figure 5.2 Two-dimensional tank test set-up.

5.2.3 Experimental Procedure

In Two-dimensional study, Toyoura sand was packed into a test tank to simulate the LNAPL migration behavior due to precipitation. Prior to starting the experiments, the sand was fully saturated with water. The sand was previously saturated with blue-dyed water and left for 24 hours in a vacuum chamber to remove air from it and ensure complete saturation. Then, the saturated sand was slowly poured with the help of a spoon into the column filled with de-aired water until the final elevation is reached. The room temperature was kept at 20°C and the humidity was maintained at 70%.

The experiment started as soon as the drainage valve was opened, and the soil-saturated water was drained out of the tank. The water levels that were initially at the top of the sample level were allowed to drain until reaching the final water level at 50 mm elevation. The flow chart for the two-dimensional tank test procedure is shown in Figure 3.8. The drained-out liquids were collected in a square bottle. Two 6-mm diameter holes were made in the bottle cap to receive a 4-mm diameter glass tube that connected to the drainage line. The rate of liquid lost inside the bottle due to evaporation was about 1 g per 10 days. The outflow was automatically measured by an electronic scale and recorded every 15 seconds. Throughout the experimental period, the drainage valve was never closed, and the water level was never changed. When the bottom drainage valve was opened, the fully water-saturated Toyoura sand was drained for 9 hours.

Then, 250 mL of LNAPL was released from the top of the tank. In order to ensure the release of LNAPL created a uniform contamination plume, and to avoid spreading at the top sand surface, the released point was assisted with a tube embedded about 10 mm below the top surface. This tube was connected to the 100 mL glass syringe where the LNAPL was supplied. The LNAPL was allowed to migrate downward for 72 hours.

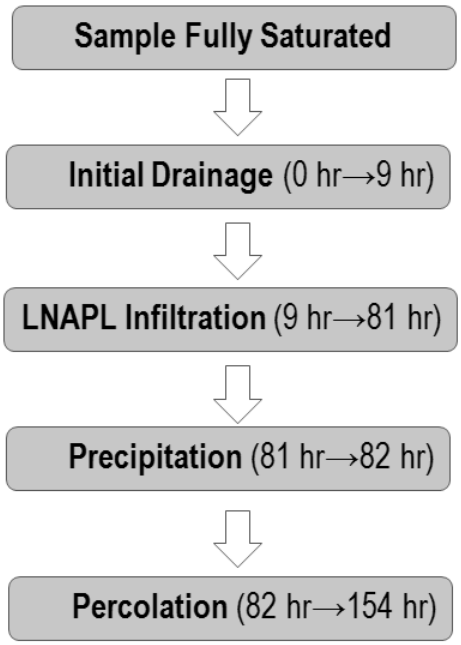

Figure 5.3 Two-dimensional tank test procedure.

Then, in the precipitation stage, the blue dye water was poured from the top of the tank with the precipitation intensity of 63 mm/hr. The precipitation intensity and supply volume were controlled using a digital peristaltic pump. The precipitation water supplies were taken from a graduated cylinder to check if the precipitation volume is similar to the designed level. Finally, during the percolation stage, the LNAPL contaminants and precipitation water were allowed to drain for 72 hours.

Digital pictures were taken every 5 minutes during the first hour of each stage and every 30 minutes after that until the end of the stage. The cameras were set in manual mode, and the aperture, shutter speed, and white balance were defined and maintained constant throughout the experiment. The cameras were remotely controlled using Nikon Camera Control Pro 2 software to avoid vibrations and camera displacement. The two LED floodlights were turned on 30 seconds prior to taking picture and turned off 30 seconds afterwards.

5.3 Two-Dimensional Tank Test Result

5.3.1 Capillary Depression due to LNAPL Infiltration

The experiment started when the fully saturated sand was allowed to drain until reaching the final water level at 50 mm elevation by gravitational force. Due to the fact that sand has high permeability, the water drained relatively quickly. After nine hours, by the end of initial drainage, the water saturation inside the tank was already in stable condition. Figure 5.4 shows the water and LNAPL saturation distribution inside the tank at the end of the initial drainage stage.

The high capillarity due to the effect of fine grain size distribution in Toyoura sand can be seen clearly in the water saturation contour. The saturated capillary fringe could reach up to 350 mm height, which left an unsaturated zone of only 150 mm. This condition was similar in the one-dimensional column study. The saturated capillary fringe zone was clearly formed from water level from 50 mm to 405 mm elevation. In the saturated capillary fringe zone, the water saturation is 100%. Above the capillary fringe was the continuous-capillary (funicular) zone. The water saturation in this region ranged from less than 100% to around

45% water saturation. In the initial drainage, LNAPL was not yet being spilled into the sand, thus there was no sign of LNAPL saturation.

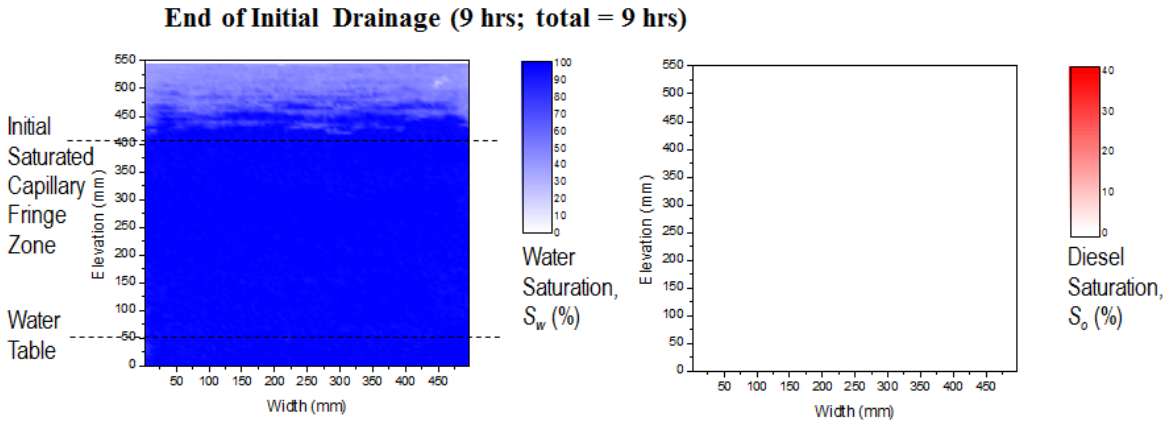

Figure 5.4 Water and LNAPL saturation at the end of initial drainage.

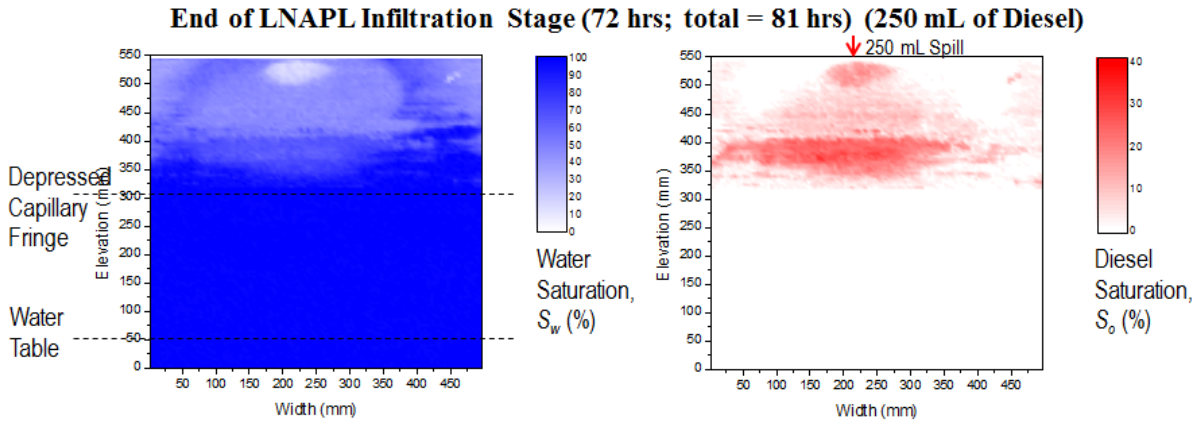

Figure 5.5 Water and LNAPL saturation at the end of the LNAPL infiltration stage.

5.3.2 LNAPL Migration due to Precipitation

When the infiltrated LNAPL reached a stable depth, it no longer migrated deeper, because the two immiscible liquids, LNAPL and groundwater, had reached interfacial tension equilibrium. This condition changes as soon as precipitation infiltrates the contaminated sand layer (Figure 3.22). The infiltrating water is subjected to gravitational force; as it tries to flow toward the groundwater level, it will push down any LNAPL that it encounters. The mobilized LNAPL will be entrapped within the saturated capillary zone.

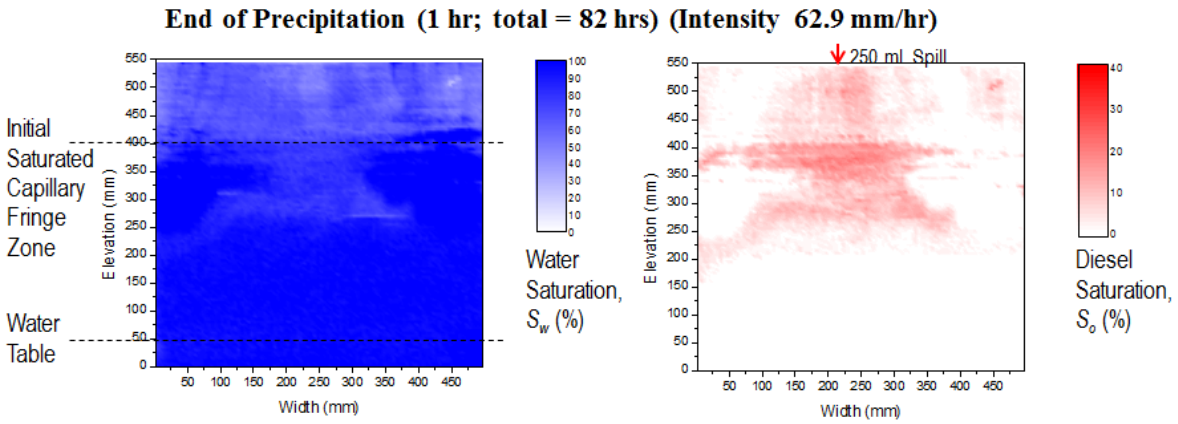

Figure 5.6 Water and LNAPL saturation at the end of the precipitation stage.

Once precipitation water infiltrates the contaminated sand, it may encounter pores filling with LNAPL. Since both liquids are immiscible, the infiltrated water will push the LNAPL down until the migrated LNAPL becomes entrapped in deeper soil pores, or stops due to capillarity. A high amount of infiltrating water during precipitation provided a high wetting front propagation force that pushed down any LNAPL within its flow path. This mechanism helped LNAPL migrate easily into the saturated zone.

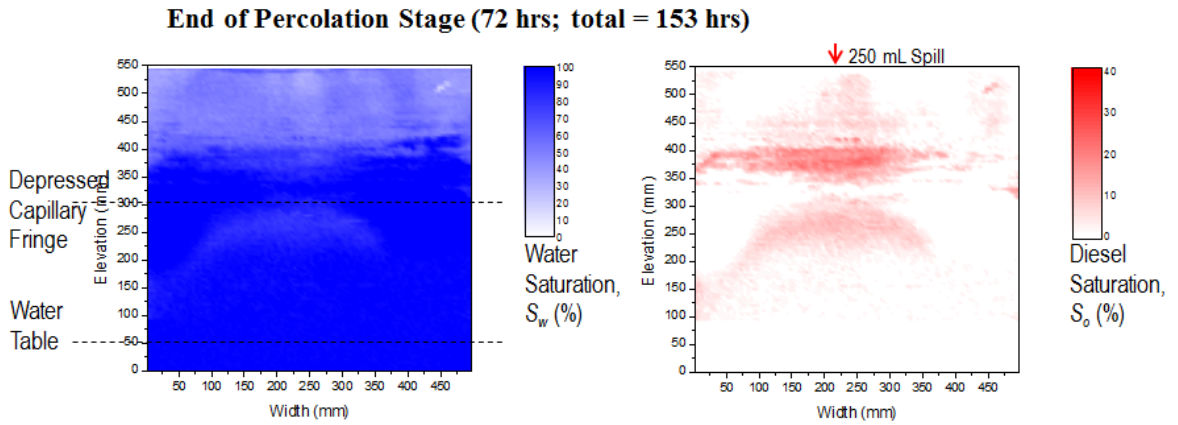

Figure 5.7 Water and LNAPL saturation at the end of the percolation stage.

After an hour of precipitation, the experiment was continued with a percolation stage as shown in Figure 3.23. In this stage, the precipitating water is allowed to drain until it reaches the water level for another 72 hours. During this stage, the infiltration water that remains above the water level will infiltrate downward due to gravitational force, and at the

same time it will push down any mobile LNAPL that it encounters. Therefore during this stage, there were still some changes to the LNAPL saturation, especially the mobile LNAPL, as it tried to obtain equilibrium at interfacial tension.

5.4 Saturation-Capillary Pressure Relation (*S-p* Relations) for LNAPL Migration Study

There are many ways to characterize soil physical properties, and saturation-capillary pressure relation (*S-p* relations) is one of the most commonly used in the NAPL study. The *S-p* relations was first introduced as water retention curve by Buckingham (1907), basically to understand the movement of soil moisture in the vadose zone which focuses on the two-phase system of air-water in soil. Adopting the same principle of capillary pressure (non-wetting and wetting phase pressure), the *S-p* relations prove suitable for characterization in NAPL study. The *S-p* relations is widely used because of the immiscible nature of NAPL and water that makes changes in saturation and pressure very distinctive.

In principle, the nearly symmetrical "*S*"-shaped curve of *S-p* relations (van Genuchten 1980) is actually about similar curve shape for any type of soil. Therefore, the migration behavior of LNAPL can be compared to other types of soils using the *S-p* relations. Although any type of soil would have similar "*S*"-shaped in the *S-p* relations, except for marine clay (Holtz et al. 2011), the main difference is its capillary pressure range value. In general, the finer the soil texture, the higher the capillary pressure value is. In this research, to determine the saturation and capillary pressure value for Toyoura sand, a laboratory element test for *S-p* relations was conducted.

5.4.1 Element Test for *S-p* Relations

The main principle in determining *S-p* relations is to obtain the changes of saturation corresponding to the changes in pressure. Basically, the capillary pressure in the initially saturated sample is increased incrementally by producing a negative water pressure at the bottom of the sample. Conventionally, in the Thomson et al. (1992) method, this increase is obtained by lowering the water tube connected to the bottom of the sample (in the cell). The capillary pressure is increased and water will leave the sample through the capillary barrier (porous stone). After equilibrium has been reached, following each incremental change in the

capillary pressure, the volume of water outflow is measured and the new water saturation computed. This procedure is repeated step-wise to generate points on the drainage capillary pressure curve.

To obtain saturation and capillary pressure for Toyoura sand, a laboratory set-up similar to Van Geel and Roy (2002) was constructed. A simple schematic of an experimental cell is illustrated in Figure 5.8. This set-up was chosen over the Thomson et al. (1992) method because it uses a peristaltic pump that can decrease the time taken to reach equilibrium during drainage and wetting of the sample.

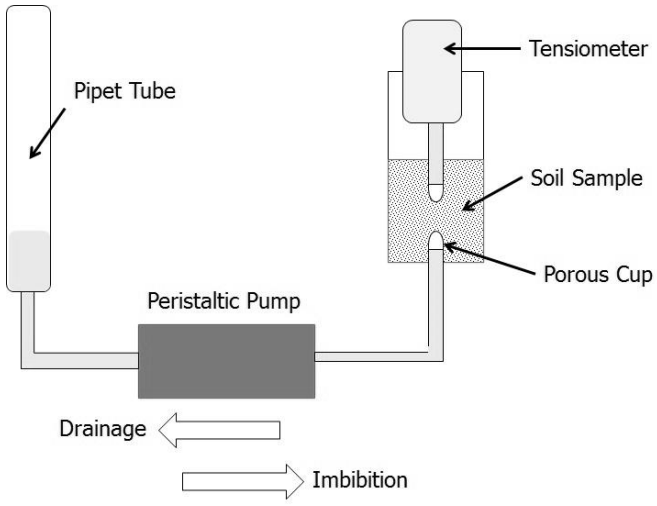

Figure 5.8 Experimental set-up for *S-p* relations elements test.

The top of the cell was kept open to the atmosphere to allow free air movement into or out of the cell in response to a change in water pressure. A tensiometer is attached at the top of the cell to measure the water pressure within the cell. The bottom of the cell is attached with a porous cup that is attached to a length of flexible tubing and glass pipet. Pipet is chosen over burette (conventionally used) because of better accuracy (± 0.1 mL) and smaller opening at top, which may reduce potential evaporation.

Prior to packing the sand in the cell, it was fully saturated with water in a beaker and left to stand for 24 hours in a vacuum chamber to remove air from the soil pores and ensure complete saturation. Then, the saturated sand was slowly poured, with the help of a spoon, into the cell filled with de-aired water to ensure uniformity until the final elevation was reached. Later, the cell was left for 24 hours in a vacuum chamber to ensure that there was no

entrapped air during the packing process and obtain the final elevation. The height of the cell was measured using digital micrometer caliper. The weight of the sand used inside the cell was obtained based on the difference between the values prior to saturation in a beaker and after packing.

To generate pressure-saturation data points, flexible tubing joining the cell and pipet was fed through a peristaltic pump, which was used to pump water out (drainage) and into (wetting) the cell. The pump generated a significant hydraulic gradient across the walls of the porous cup to increase the flow and decrease the time taken to reach equilibrium. At each stage of the experiment, the volumes and pressures were recorded to generate the drainage and wetting curves. During the entire experiment, a control was established to monitor evaporation losses.

5.4.2 *S-p* Relations in Air-Water System

The *S-p* relations curve for any type of soil can be model based on saturation and capillary-pressure data. In this research, the van Genuchten (1980) model was used for generating an *S-p* relations curve for both drainage and wetting conditions:

$$S_{we} = \begin{cases} \left[\frac{1}{1+(\alpha P)^n}\right]^m, & h > 0 \\ 1 \qquad\quad , & h \leq 0 \end{cases} \tag{5.1}$$

$$S_{we} = \frac{S_w - S_r}{1 - S_r} \tag{5.2}$$

where P is the capillary-pressure head, α and n are the curve-shape parameters with $m = 1 - 1/n$, S_w is the wetting saturation, and S_r is the residual or irreducible saturation. According to Kool and Parker (1987), constraints imposed on the parameter n and S_r for drainage and wetting conditions will not lead to an unacceptable loss in accuracy. Therefore, in this research, a constraint on the n and S_r parameter is imposed for drainage and wetting, as it is considered that the porous medium is rigid enough not to have any deformation or settlement during the experiment based on the observations from image analysis.

Through curve fitting, the saturation and capillary-pressure data points were fit to the van Genuchten equation. The *S-p* relations for air-water systems during drainage and wetting are shown in Figure 5.9.

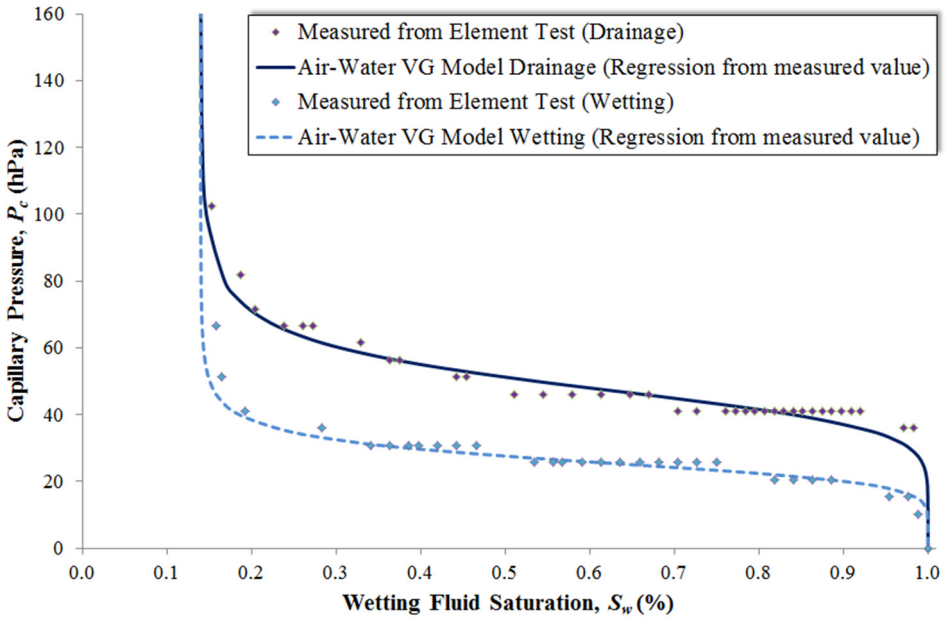

Figure 5.9 *S-p* relations for air-water systems during drainage and wetting.

The data points were fit to the van Genuchten model using the solver subroutine in Microsoft Excel, specified to nonlinear least squares optimization (Liu et al. 1998; Van Geel and Roy 2002) to minimizing the sum of squared errors (SSE). The coefficient of determination, R^2, for the resulting *S-p* relations-curve fit can be calculated using (Wraith and Or 1998):

$$R^2 = 1 - \frac{SSE}{N\sigma_S^2} \tag{5.3}$$

where σ_S^2 denotes the variance of the measurements on the independent variable, *S*, and *N* is the number of data points. The R^2 value ranges between 0 and 1, and it expresses the proportion of variance in the dependent variable explained by the independent variable. An R^2 value of 0 means that the independent variable (saturation) does not help to predict the dependent variable (capillary pressure). As the R^2 value increases towards 1 the more accurately the function fits the data (Brown 2001). The saturation and capillary-pressure data from the elements-test experiment fits the van Genuchten model very well with R^2 of 0.95.

5.4.3 Estimating *S-p* Relations in Air-LNAPL and LNAPL-Water Systems

The *S-p* relations for air-water phase systems would probably best describe the soil moisture movement in the natural vadose zone, in which no LNAPL contamination occurs. When LNAPL contaminates the subsurface, the LNAPL-water *S-p* relations would probably best describe moisture movement in the subsurface. Based on the Van Genuchten parameters value obtained from the air-water phase *S-p* relations together with the scaling factor, the *S-p* relations for LNAPL-water as well as air-LNAPL phase systems were estimated.

The scaling factor allowed the prediction of the *S-p* relations for the third system by only measuring one set of *S-p* relations (Parker et al. 1987). If scaling is predicted from one set of *S-p* relations, it is advisable that the scaling procedure be based on air-water rather than oil-water systems since air-water experiments are simpler to conduct and are less prone to error (Parker and Lenhard 1990). In this research, *S-p* relations for air-water systems were measured in a laboratory experiment, as explained in sections 5.4.1 and 5.4.2, whereas the *S-p* relations for the air-LNAPL and LNAPL-water were generated using the scaling procedure.

The scaling procedure used in this research is by Parker et al. (1987). This scaling procedure is frequently used in NAPL studies because of its good accuracy, and, for LNAPL studies specifically, Van Geel and Sykes (1994) have shown that this scaling would only cause a 0.5% underestimation of the LNAPL volume in a very complex analysis. This scaling procedure is able to extend the two-phase data to the three-phase systems using the following expression:

$$\beta_{aw}P_{aw} = \beta_{ow}P_{ow} = \beta_{ao}P_{ao} \tag{5.4}$$

and when employing an adaptation to the van Genuchten expression, the following are the scaled *S-p* relations for drainage and wetting according to Parker and Lenhard (1987):

$$S^{d*}(P^*) = \left(1 + \left(\beta_{ij}\alpha^d P_{ij}^*\right)^n\right)^{-m} \tag{5.5}$$

$$S^{i*}(P^*) = \left(1 + \left(\beta_{ij}\alpha^i P_{ij}^*\right)^n\right)^{-m} \tag{5.6}$$

where $S^*(P^*)$, is a scaled saturation-capillary head function with superscripts *d* and *i* being

used to denote drainage and wetting (imbibition) curves, respectively. According to Lenhard and Parker (1987), the following is fluid pair-dependent scaling factor, β_{ij}:

$$\beta_{aw} = 1 \tag{5.7}$$

$$\beta_{ow} = \frac{\sigma_{aw}}{\sigma_{ow}} \tag{5.8}$$

$$\beta_{ao} = \frac{\sigma_{aw}}{\sigma_{ao}} \tag{5.9}$$

where σ_{aw}, σ_{ao} and σ_{ow} are the interfacial tension of air-water, air-oil, and oil-water, respectively. For a rigid-porous medium, scaling coefficients are thus related:

$$\frac{1}{\beta_{ow}} + \frac{1}{\beta_{ao}} = \frac{1}{\beta_{aw}} \tag{5.10}$$

In this scaling factor, *S-p* relations of each of the pair systems are adjusted so as to obtain a unique function for a given porous medium. The flow chart for estimating *S-p* relations for air-LNAPL and LNAPL-water systems is shown in Figure 5.10.

The *S-p* relations for LNAPL-water during drainage were fitted using Equation (5.5) and during wetting using Equation (5.6). In order to generate these curves, the LNAPL-water scaling factor, β_{ow}, must be obtained, and it was calculated from Equation (5.8). The β_{ow} can be calculated from Equation (5.10) using the β_{ao} value calculated from σ_{aw} and σ_{ao} as in Equation (5.9), and β_{aw} as in Equation (5.7). The air-LNAPL (air-dye diesel) interfacial tension, σ_{ao}, value is 26.75 mN/m, which was obtained from a laboratory test conducted by a material specialist. Since the water was dye, the air-water interfacial tension, σ_{aw}, value was also obtained from a laboratory test conducted by a material specialist. The dye water interfacial tension value is 70.04 nN/m, which was 3.7% lower compared to standard value as recommended by the U.S. National Institute of Standards and Technology, which was 72.75 mN/m (Vargaftik et al. 1983) .

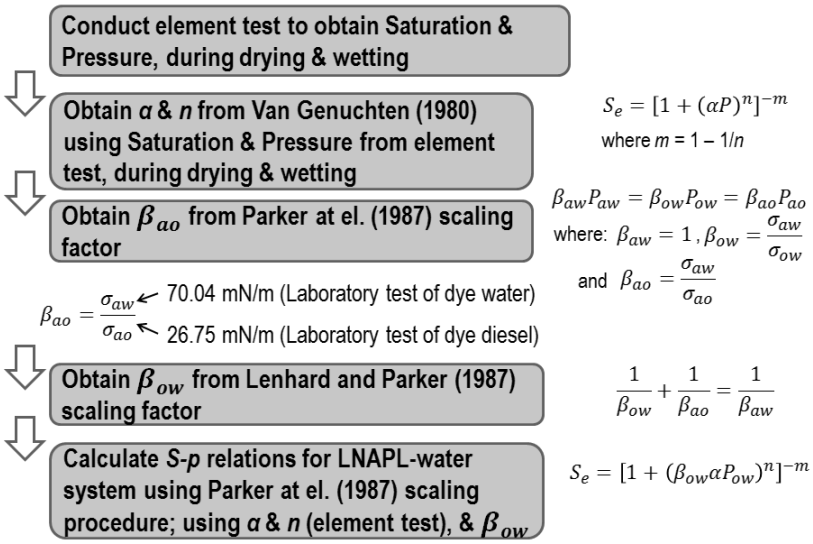

Figure 5.10 Flow chart for estimating *S-p* relations for air-LNAPL and LNAPL-water systems.

5.5 Mechanism of LNAPL Migration due to Precipitation in Relation to *S-p* Relations

5.5.1 Saturation-Capillary Pressure Relations before Precipitation

Based on the saturation and capillary-pressure data obtained from the Tank test, the *S-p* relations for each stage of the experiment were generated. The experiment started as soon as the saturated Toyoura sand was allowed to drain. This stage is called initial drainage, whereby water levels that were initially at the top of the sample level were allowed to drain until reaching the final water level at 50 mm elevation. The water level never changes thereafter until the end of the experiment. Since the Toyoura sand was initially saturated when this condition was reflected in the *S-p* relations, the starting point of the experiment is at the bottom right of the graph (Figure 5.11), where the capillary pressure is zero.

When the water was allowed to drain, it leaves the soil pores and is replaced by air. Consequently, air-water interfaces (menisci) were formed, and this was the point at which negative pore pressure or capillary pressure started to exist. The saturation and capillary-pressure changes during this stage can be referred to the generated air-water van Genuchten model (VG model) drainage curve. It can be seen in Figure 5.11 that as water saturation decreased, the capillary pressure increased. This is referring to the intrusion of air into soil pores where it was initially occupied by water.

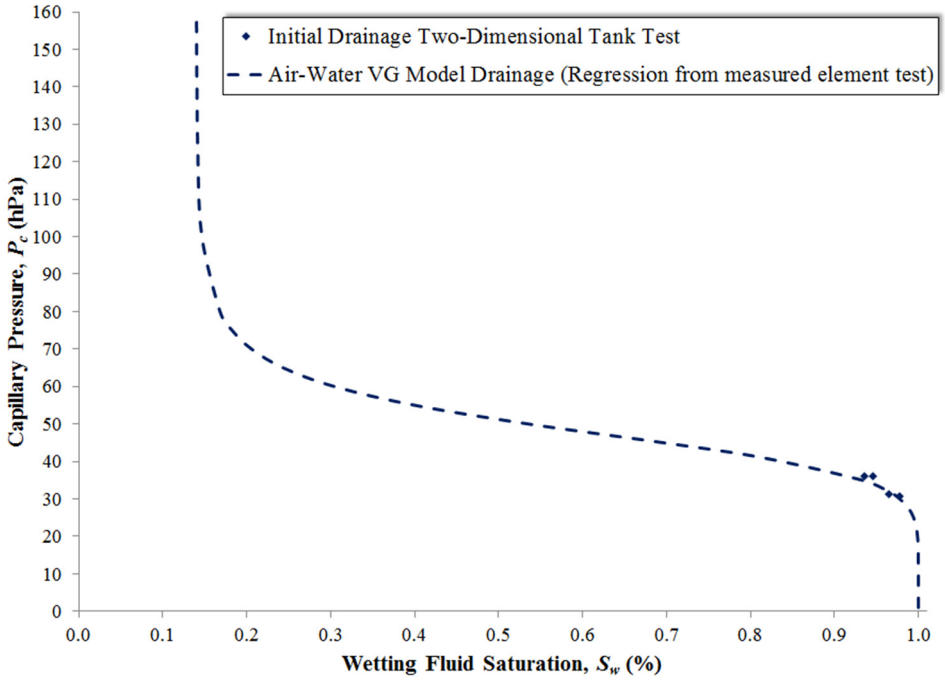

Figure 5.11 *S-p* relations for tank test during Initial drainage stage.

In the early stage of initial drainage, the water in the main channel (in between the soil pores) was the first to be drained. Apart from gravitational force that allowed this part to be easily drained, the main channel also has a large pore radius. Therefore, it was easy for air to empty into the channel at low capillary pressure. In general, pores have different dimensions and shapes. Consequently, they will not all empty at the same capillary pressure. The large pores (or throats of entry) will empty at low capillary pressures, while those with narrow channels of entry, supporting interfaces of a smaller radius of curvature, will empty at higher capillary pressures.

The capillary pressure and capillary rise are affected by the pore radius of soil pores. As Toyoura sand has a relatively small pore radius compared to typical coarse sand, it shows significant height of the capillary-fringe zone. The height of the saturated capillary-fringe zone was about 350 mm, and the tensiometer was located at 450 mm elevation (about 50 mm above capillary fringe). This means that the tensiometer was located in the continuous-capillary (funicular) zone. It can be seen in image analysis and *S-p* relations that, in this elevation, the water saturation is still high—around 90% saturation. This high water saturation changes as soon as LNAPL infiltrates the soil pores (Figure 5.12).

When LNAPL was spilled into the tank, the LNAPL infiltrated the Toyoura sand and migrated downward as gravitational force acted on the LNAPL mass. In this experiment, this stage is called the LNAPL infiltration stage. The *S-p* relations during this stage can be corresponded to the generated LNAPL-water van Genuchten model (VG model) drainage curve shown in Figure 5.12. As soon as this stage started, the saturation and capillary pressure was still at the air-water system curve and continuing from the previous stage.

As LNAPL infiltrated the sand and reached the tensiometer elevation, it invaded the pores filled with air and simultaneously displaced the water in the soil pores. This condition caused the pores-phase system to change from air-water interface to LNAPL-water interface. Starting from this moment, the reference-pressure system was changed to the LNAPL-water VG model drainage curve. The reference-pressure system was based on the drainage curve because the infiltration of LNAPL caused the water (which was the wetting fluid for the LNAPL-water system) saturation to reduce. Therefore, this is considered to be a drainage condition.

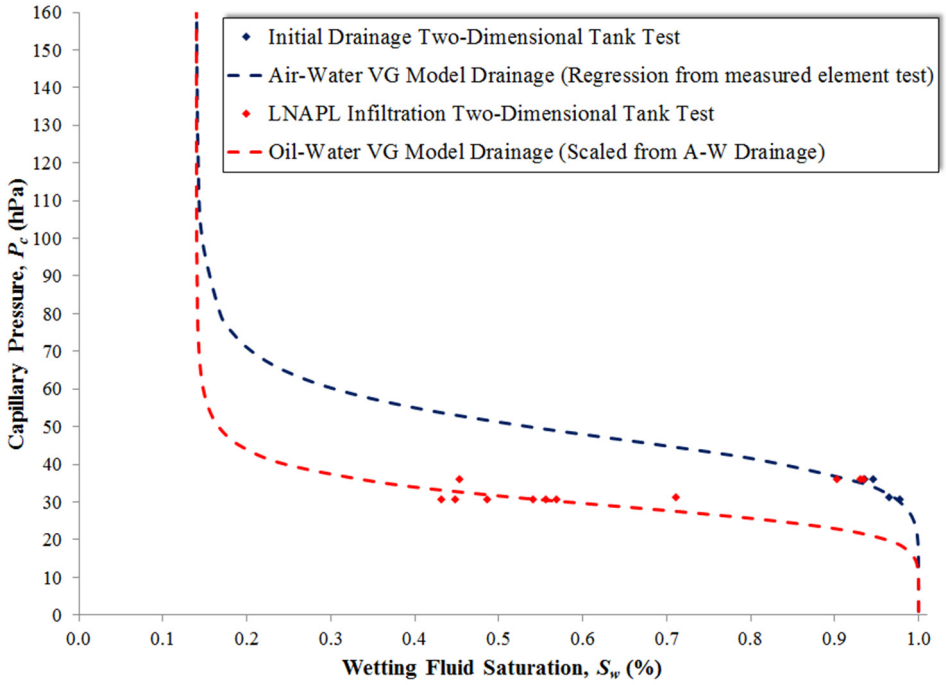

Figure 5.12 *S-p* relations for tank test during LNAPL infiltration stage.

Since the interfacial tension of LNAPL-water, σ_{ow}, is lower than the interfacial tension of air-water, σ_{aw}, the drainage curve of both systems also exhibits similar behavior in the *S-p* relations. The LNAPL-water interfacial tension, σ_{ow}, value is 46.35 mN/m, whereas the air-water interfacial tension, σ_{aw}, value is 72.75 mN/m. Therefore, in Figure 5.12, as the phase changed, the capillary pressure also reduced according to the reference LNAPL-water VG model drainage curve. When wetting saturation had been already reduced to around 71%, the measured capillary pressure was 31 hPa. This value is much lower in comparison to the air-water VG model drainage curve: the capillary pressure at the same saturation degree is about 45 hPa. If the current phase system is in the air-water system, a further wetting saturation reduction would require higher pressure. However, since the system already changes to the LNAPL-water system, it doesn`t require high pressure for LNAPL to displace water from the soil pores. When the increased volume of infiltrated LNAPL reaches the tensiometer elevation, the LNAPL has enough pressure to cause the further displacement of water. This condition is shown in the *S-p* relations in which wetting-fluid saturation is reduced until it reaches around 45% saturation. As LNAPL infiltrates the soil pores, it also has to overcome the capillary pressure from the water. The LNAPL ceased to migrate when it reached equilibrium at interfacial tension. The final wetting-fluid saturation at equilibrium during this stage was around 43%.

5.5.2 Saturation-Capillary Pressure-Relation Changes due to Precipitation

When the sand is subjected to precipitation, the precipitation water will infiltrate the soil layer from the top and infiltrate downward until it reaches water level. In principle, when precipitation occurs, the infiltrated water will fill up the empty pores, thus increasing the soil saturation. At the same time, the capillary pressure also reduces due to infiltrated water filling up the small-pores space, which contributes to the high capillary pressure. In the *S-p* relations, this condition corresponding to the increasing of wetting-fluid saturation can be described with the wetting curve. Since the sand condition during the precipitation stage in this experiment had already been contaminated with LNAPL, the reference pressure was the LNAPL-water system. Therefore, the *S-p* relations during this stage can be corresponded to the generated LNAPL-water VG model wetting curve shown in Figure 5.13.

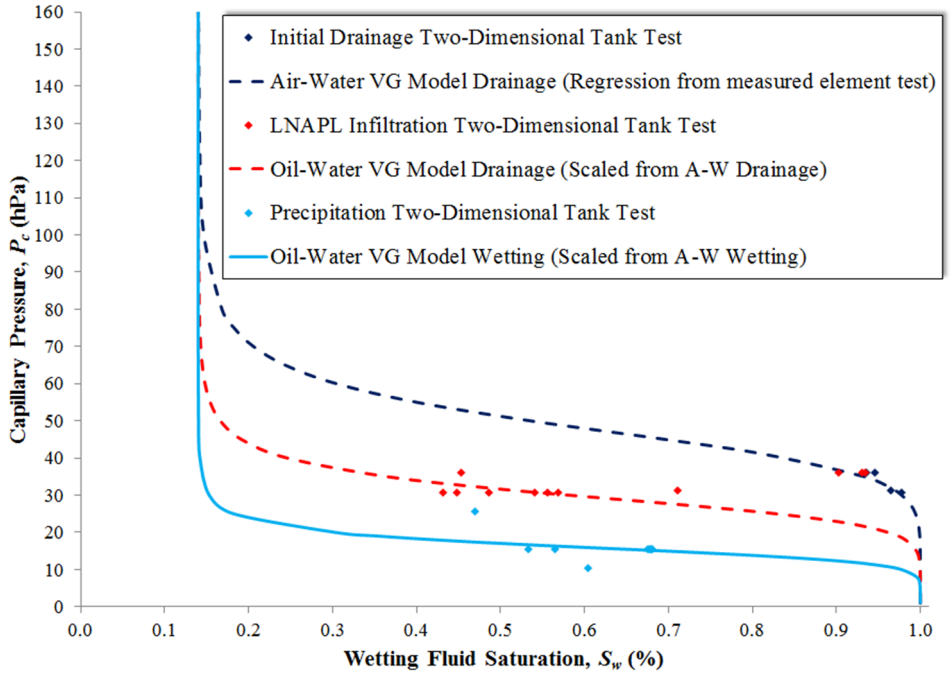

Figure 5.13 *S-p* relations for tank test during precipitation stage.

As soon as the sand was subjected to the precipitation, the saturation and capillary pressure was still at the LNAPL-water system drainage curve, continuing from the previous stage. Since the top layer of the sand was already contaminated with LNAPL, the infiltrated water had to overcome the layer of LNAPL in the soil pores as it infiltrated downward. After 10 minutes of precipitation, a small change in water saturation (about a 3% change) that started to appear could be shown in the first measured point in this stage (Figure 5.13). This change could be corresponded to the small volume of water that was drained from the layer slightly above the tensiometer elevation. This volume of water would probably drain because of increasing liquid saturation in the upper layer due to the infiltration of water, which caused movement of moisture in this layer towards water level. This initial small increase of water saturation also caused reduction of capillary pressure, as the local capillary system tried to adapt to the increase of moisture.

After 15 minutes of precipitation, a significant volume of water had already infiltrated the soil pores at the tensiometer elevation. This significant change of water saturation also initiated the migration of the LNAPL, which will be discussed in detail in Section 5.5.4. The water saturation at this point was about 53%, which means that is the wetting-fluid saturation had already increased about 10% in 15 minutes. This significant increase of water saturation

was one of the main mechanisms that initiated migration of LNAPL. This is because the migration of LNAPL can be said to be due to the infiltration water pushing the encountered LNAPL during its infiltration downward.

Besides the fact that the increase of water saturation can be corresponded to the migration of LNAPL, the changes of capillary pressure would be another or most important mechanism that initiates the migration of the LNAPL. In Figure 5.13, it can be seen that the capillary-pressure value had already changed its location from near to the LNAPL-water VG model drainage curve to the LNAPL-water VG model wetting curve. As precipitation proceeded and infiltration water progressively increased, the water saturation of the sand increased progressively. At the end of precipitation, the water saturation had already increased as much as 25% with the wetting fluid saturation at about 68%. This increasing volume of water has helped LNAPL to migrate deeper into the saturated capillary-fringe zone.

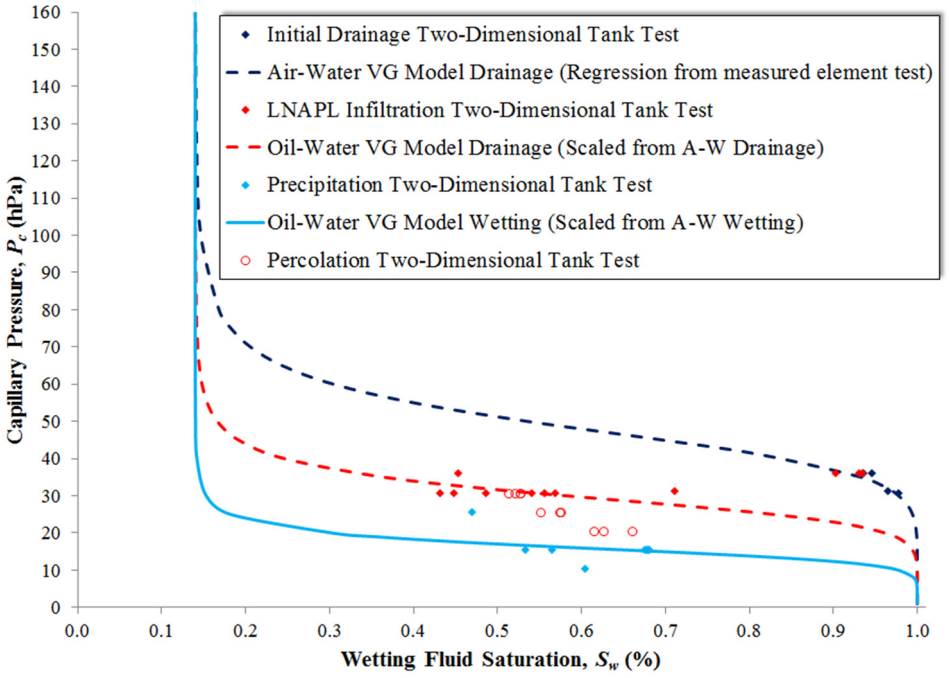

Figure 5.14 *S-p* relations for tank test during percolation stage.

Once the precipitation ceased, there wasn`t any more water supply from the top that could increase the water saturation. Therefore, during the percolation stage, the water saturation was again reduced due to the drainage of infiltration water downward towards the water level. Therefore, the *S-p* relations during this stage can be corresponded to the generated LNAPL-water VG model drainage curve shown in Figure 5.14. The reduction of water saturation as well as the increase of capillary pressure happened according to the reduced wetting-fluid saturation direction with respect to the LNAPL-water VG model drainage curve. At the end of the experiment, the measured capillary pressure was similar to the reference LNAPL-water drainage curve. The value of capillary pressure at this point was about 30 hPa, with a wetting-fluid saturation of 50%. At the end of the experiment, the water saturation had changed by about 10% since the end of precipitation and by almost 10% compared to after the LNAPL infiltration stage.

5.5.3 Saturation-Capillary Pressure Relation Comparisons between One-Dimensional Column Test and Two-Dimensional Tank Test

As shown in section 5.5.2, the *S-p* relation is able to describe changes in each stage of the two-dimensional experiment. In this section, the comparison between the one-dimensional column and two-dimensional tank tests was discussed. Based on the fluid saturation data obtained using SIAM, it was proven that precipitation helps LNAPL migrate deeper into the saturated capillary zone. In the one-dimensional column and two-dimensional tank tests, it was shown that LNAPL ceased to further infiltrate the capillary fringe when it reached equilibrium at interfacial tension. However, once the contaminated sand was subjected to precipitation, the LNAPL was able to migrate deeper into the saturated capillary fringe zone.

Throughout the experiment, as the SIAM showed similar behavior between the one-dimensional column and two-dimensional tank tests, the *S-p* relations also showed similar behavior in both experiments. Figure 5.15 shows the *S-p* relations for both one-dimensional column and two-dimensional tank tests. In the column test, the final water saturation was around 80% when the sand was still uncontaminated. This value was similar to the air-water VG model drainage curve when the capillary pressure was around 41 hPa and the wetting

saturation was 81%. Both one-dimensional and two-dimensional tests can be compared to the air-water VG model.

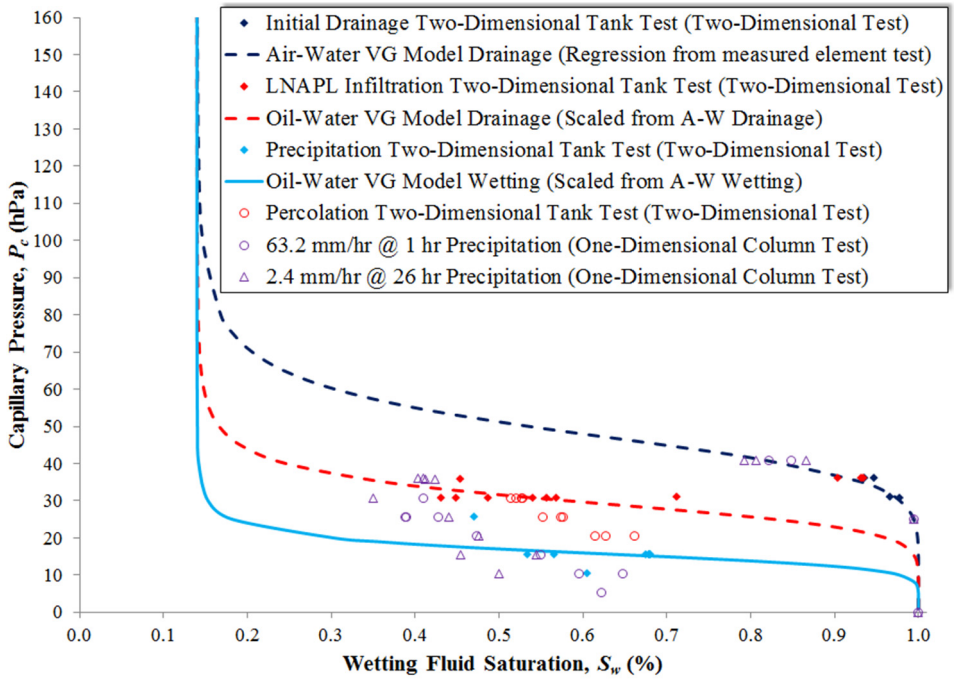

Figure 5.15 *S-p* relations for the one-dimensional column and two-dimensional tank tests.

When LNAPL was spilled into the sand, capillary pressure also decreased for both one-dimensional and two-dimensional tests due to low LNAPL interfacial tension. The capillary pressure was further reduced when the contaminated sand was subjected to the precipitation. This reduction was due to the increase of wetting saturation supplied by the precipitation. As the precipitation stopped, there was no more supply of infiltrating water, and more water started to percolate to the water level in the percolation stage. Therefore, this drainage condition caused a reduction in wetting saturation. The similarities in the *S-p* relations behavior changes in both one-dimensional and two-dimensional tests were seen from the initial drainage to the percolation stage during the experiment.

5.5.4 Controlling Parameter that Caused LNAPL Migration due to Precipitation

Chapter 4 explained the mechanism that caused the migration of LNAPL in the subsurface due to precipitation. Once precipitation water infiltrates the contaminated sand, it may encounter pores filling with LNAPL. Since both liquids are immiscible, the infiltrated water will push the LNAPL down until the migrated LNAPL becomes entrapped in deeper soil pores, or stops due to capillarity. A high amount of infiltrating water during precipitation provided a high wetting front propagation force that pushed down any LNAPL within its flow path. This mechanism helped LNAPL migrate easily into the saturated zone.

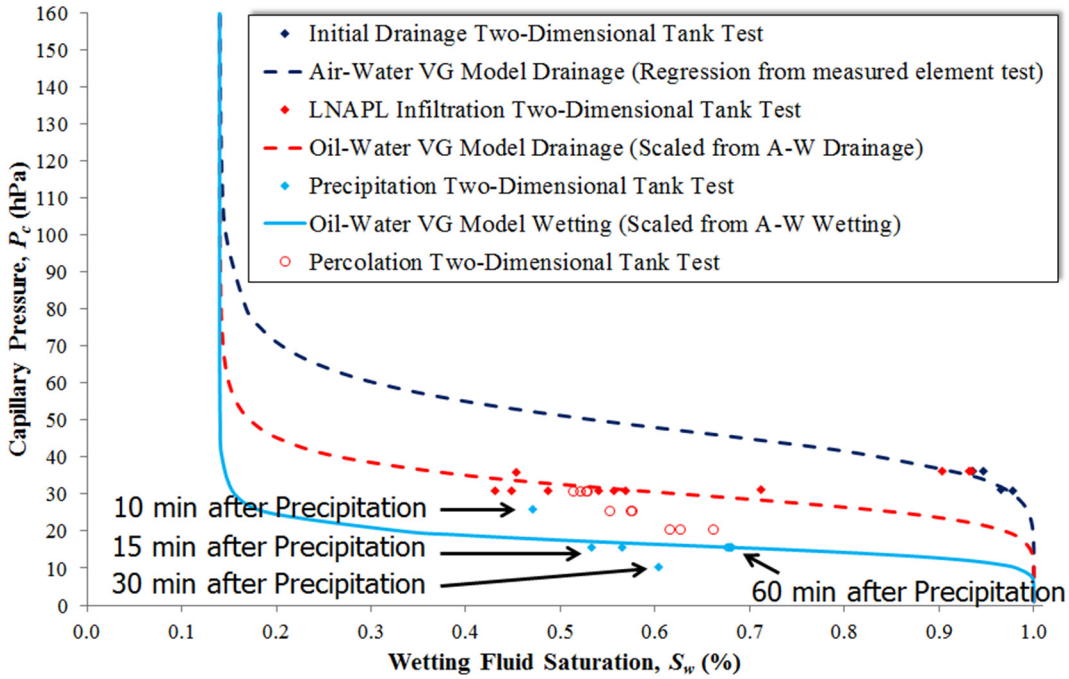

Figure 5.16 LNAPL starts to migrate as capillary pressure gets lower.

In section 5.5.2, it has been demonstrated that the LNAPL migration in the subsurface can be described using the *S-p* relations with the help of a VG model. Moreover, the controlling parameter can be seen more clearly in the *S-p* relations. It can be seen in the *S-p* relations in Figure 5.16 that the measured *S-p* was between LNAPL–water VG model drainage and wetting curves 10 minutes after the precipitation. Based on the SIAM output, there was no sign of LNAPL migration at the tensiometer elevation (450 mm) during this time. The tensiometer was actually installed about vertically in line with the LNAPL release point (40 mm offset to the left of the tank center line). The time when the LNAPL started to

migrate can be seen by examining the saturation data at time intervals during the precipitation. This was done by comparing the LNAPL and water saturation before and during the precipitation. The fluid saturation value used for this comparison was an average value to ensure that the saturation change represented the downward migration (or infiltration) and not horizontal flow movement. The fluid saturation values were based on average saturation at 50 mm width at the tensiometer area. The changes of saturation in LNAPL are shown in Figure 5.17, and that of water is shown in Figure 5.18. Both graphs show the percentage of fluid saturation changes for every elevation from the top to the bottom of the tank at the section near the tensiometer area.

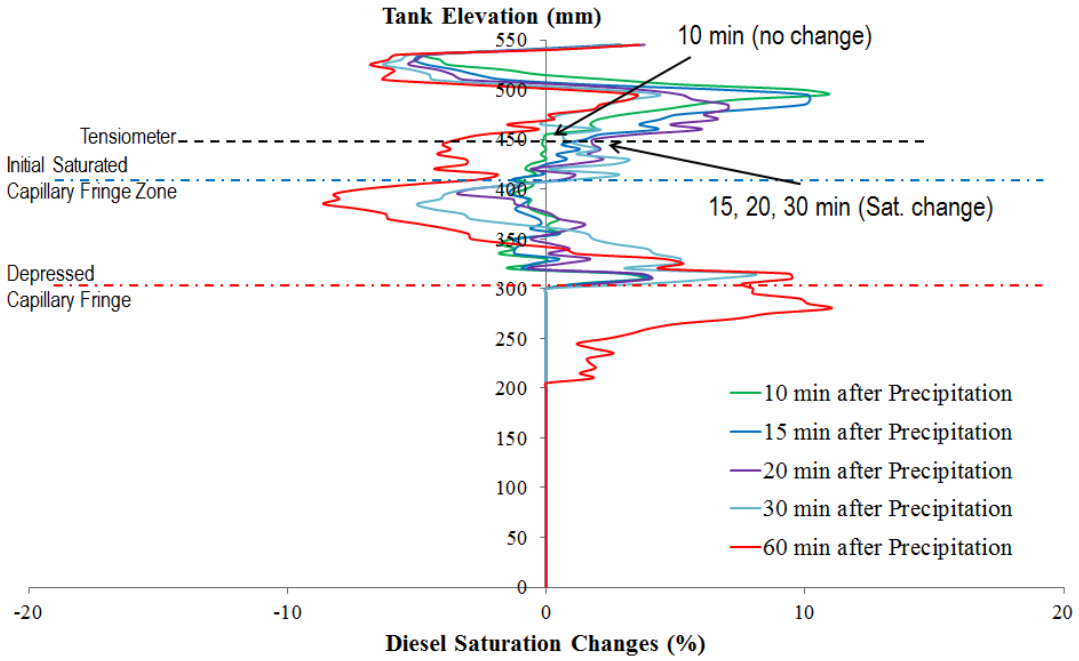

Figure 5.17 LNAPL saturation changes during precipitation.

It can be seen that after 10 minutes of precipitation, there was no significant change in water saturation (Figure 5.18), just about a 2% change. Therefore, the volume of infiltrating water is not enough to initiate the migration of LNAPL. This fact can be compared to Figure 5.17, where there is no change in LNAPL saturation 10 minutes after the precipitation at the tensiometer elevation and slightly below it. However, 5 minutes later, a relatively large change in the water saturation (about 10%) can be seen in Figure 5.18. A high amount of infiltrating water after 15 minutes of precipitation provided a high wetting front propagation force that pushed down any LNAPL within its flow path. In Figure 5.17, it can be seen that

15 minutes after the precipitation and thereafter, the LNAPL saturation started to change at the tensiometer elevation and slightly below it. This indicates that the LNAPL had already started to migrate downward.

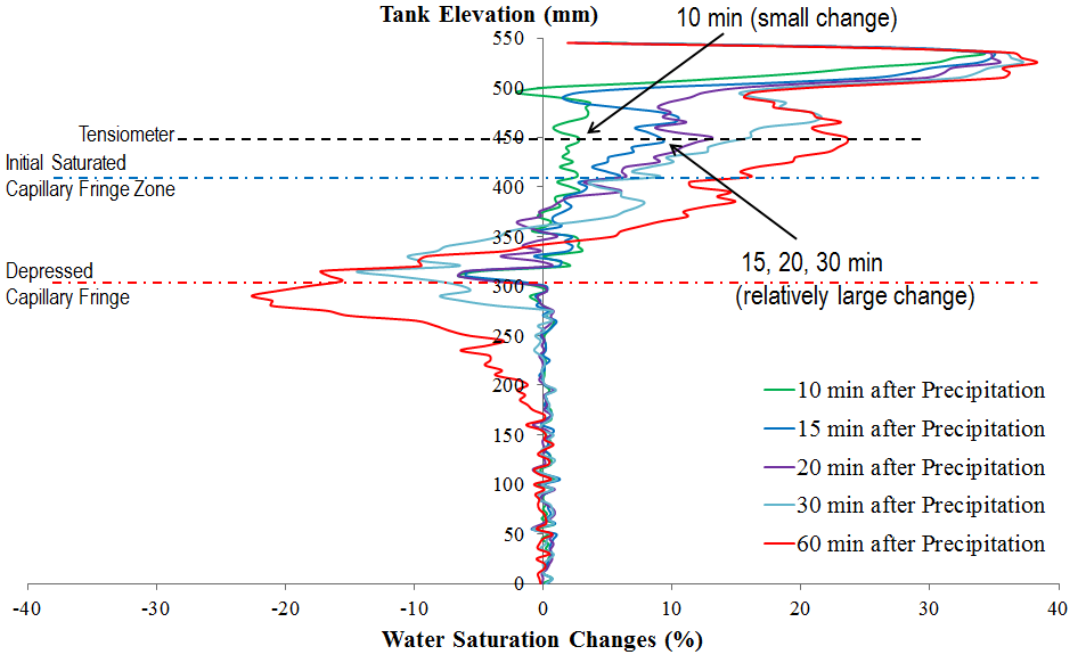

Figure 5.18 Water saturation changes during precipitation.

When referring to the *S-p* relations 15 minutes after the precipitation, it can be seen that the measured *S-p* value was below the LNAPL–water VG model wetting curves. As this curve represents the wetting condition in the LNAPL–water phase system, it corresponds with the mentioned condition, which was an increase in water saturation in LNAPL-contaminated sand due to precipitation. From the *S-p* relations, it can be said that capillary pressure plays an important role or that it is a controlling parameter that causes the migration of LNAPL due to precipitation.

If we look into the wetting saturation parameter, it can be the same depending on the drainage and wetting conditions for the same saturation value. But it is the capillary pressure parameter that helps describe the current physical condition of the phase system: either drainage or wetting. Furthermore, if we consider the physical meaning of capillary pressure in the soil system, it is the pressure that holds the LNAPL or serves as a barrier that stops the LNAPL from migrating deeper into the saturated capillary zone. In studies by Amiaz et al.

(2011) and Khaled et al. (2011), it was found that the pressure potential in the capillary fringe changed from negative to positive during precipitation. Therefore, as the capillary pressure drops to a low value due to precipitation water infiltration, it is now considered as a normal fluid flow, as is the water infiltrating downward. Consequently, since LNAPL and water are immiscible, the infiltrated water will push the LNAPL down until the migrated LNAPL becomes entrapped in deeper soil pores, or stops due to capillarity.

Once the measured *S-p* value was below the LNAPL–water VG model wetting curves after 15 minutes of precipitation, it showed a consistent trend until the precipitation ceased. Figure 5.16 shows that after 30 minutes, the capillary pressure went to the lowest capillary pressure value during the precipitation period. It is suggested that the low value is due to the available of mobile LNAPL that flows together with the infiltrated water that flows downward through the channels between the soil pores. This is because of the fact that capillary pressure is the difference between the internal pressures across the interfaces of the two immiscible fluids. The pore pressure difference between the non-wetting phase (LNAPL), P_n, and wetting phase (water), P_w, has a direct relation to interfacial tension. As the interfacial tension of LNAPL is lower than water, when it exists in the phase system with water, it reduces the capillary pressure.

5.6 Practical Implications

5.6.1 Oil Spillage on Land

Rapid economic development around the world has caused the demand for petroleum products to increase annually. More than 89 million barrels of oil per day were extracted worldwide in 2012 (USEIA 2013), a 54% increase of extraction rate compared to 30 years ago. Even with the rising volume of petroleum that needs to be managed, old equipment and facilities such as pipelines and storage tanks are still being used. As most of these old pipelines and storage tanks are made of corrodible materials, exposure to environmental elements such as precipitation and groundwater fluctuation definitely increases the possibility of leakage. Out of 2,629 ruptured onshore hazardous liquids pipelines that were classified as significant pipeline incident cases between 1993 and 2012 by USPHMSA (2013), 24% of cases were due to corrosion, and 26% were due to equipment failure. In March 2013, a near-

65-year-old pipeline that ruptured in a residential area in Arkansas, United States (Parker and Hays 2013), released an estimated 5,000 barrels of crude oil (USPHMSA 2013), proving that serious attention has to be paid to these old pipelines and storage tanks to prevent such incidents from happening. Table 5.1 shows an example of on land oil spill cases in recent years in United States and Canada.

Table 5.1 List of on land oil spill cases in United States and Canada.

Spill	**Location**	**Dates**	**Released (tonne)**
North Dakota pipeline spill	Tioga, North Dakota, United States	25 September 2013	2,810
Lac-Mégantic derailment	Lac-Mégantic, Québec, Canada	6 July 2013	4,830
Arthur Kill storage tank spill	Sewaren, New Jersey, United States	29 October 2012	1,090
Sundre, Alberta	Sundre, Canada	8 June 2012	410

The volume of an oil spill is even greater if it is caused by a natural disaster, such as the recent events of the 2011 Tohoku earthquake and tsunami (Bird and Grossman 2011) and the 2012 Hurricane Sandy (Leff 2012; USDHS 2012). In oil spills during hurricanes Katrina and Rita in 2005, an estimated 215,000 barrels (9 million gallons) of oil were released, and this did not include the additional 5,000 cases that were considered minor spills (USDHS 2006). In oil spills caused by either natural disasters or accidents and mismanagement, remediation work must be undertaken as soon as possible to ensure oil will not contaminate the groundwater.

In this study, it has been demonstrated and discussed that precipitation can cause further migration of LNAPL into the saturated zone. Consequently, the degree of groundwater contamination will increase due to the increased volume of LNAPL migrated

into the saturated zone initiated by the precipitation. In terms of practical implications, the application of this study was discussed in detail before and after the spill of LNAPL. The LNAPL spill monitoring system was discussed regarding how an LNAPL spill could be detected effectively so that further migration of LNAPL due to precipitation could be hindered. A post-spill management strategy was also discussed so that a better management strategy could be considered in order to prevent further groundwater contamination before remediation work can take place.

5.6.2 Implications of LNAPL Spill Monitoring System

In principle, the nearly symmetrical "*S*"-shaped curve of *S*-*p* relations (van Genuchten 1980) is actually similar to the curve shape for any type of soil (Holtz et al. 2011). Therefore, LNAPL migration behavior due to precipitation can be compared to other types of soil using the *S*-*p* relations. In chapter 5, it was demonstrated that LNAPL migration in the subsurface due to precipitation can be described using *S*-*p* relations with the help of a van Genuchten (1980) model (VG model). Further analysis of the *S*-*p* relations found that capillary pressure is the controlling parameter that causes the migration of LNAPL due to precipitation. These are very important findings that can be applied at a site prone to or affected by an LNAPL spill.

In order to apply the *S*-*p* relations to an LNAPL spill monitoring tool on site, saturation and capillary pressure measurements are required. The soil saturation changes can be measured using an electrical conductivity probe, whereas for capillary pressure data, a pair of tensiometers is required, which are hydrophilic to measure water pressure and hydrophobic to measure LNAPL pressure if a spill occurs. Once the electrical conductivity probe and tensiometer are placed in the subsurface near the expected LNAPL migration path (if a spill has occurred), the recorded saturation and capillary pressure data can be analyzed for monitoring of any possible LNAPL spill. The electrical conductivity probe and tensiometer measurements can be recorded using a data logger that is placed at ground level. It is recommended that at least two pairs of electrical conductivity probes and tensiometers are installed at different elevations, preferably vertically aligned for comparison and assessment of LNAPL migration in the event of a spill.

The recorded saturation and capillary pressure data can be used as an LNAPL spill monitoring tool if the fluid phases and conditions are defined accordingly in the *S-p* relations. It has already been discussed in section 5.5 that different fluid phases (air-water or LNAPL-water) and fluid conditions (drainage or wetting) result in different *S-p* relations curves, which have a significant range of capillary pressure value. The *S-p* relations can be generated by a regression curve using the VG model. Three *S-p* relation pairs are recommended for the purpose of monitoring on site, as shown in Figure 5.19, which are air-water in drainage conditions and LNAPL-water in drainage and wetting conditions. The *S-p* relation for air-water in drainage conditions is the initial condition before any contamination by LNAPL occurs. This will be considered as the baseline or reference curve that represents the uncontaminated soil condition. The *S-p* relations for LNAPL-water in drainage conditions will be used to monitor LNAPL migration when a spill occurs. Finally, the *S-p* relations for LNAPL-water in wetting conditions will be used to monitor LNAPL migration due to precipitation.

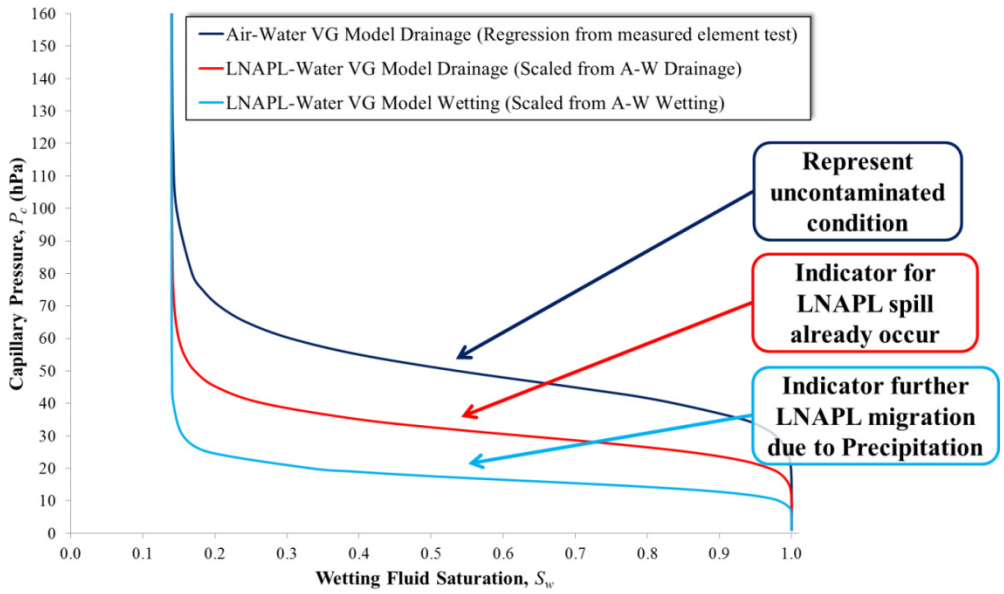

Figure 5.19 *S-p* relations as LNAPL spill monitoring tool.

In order to use the *S-p* relation for air-water in drainage conditions as a reference curve of an uncontaminated condition, the *S-p* relation must be based on the same type of soil at the installed electrical conductivity probe and tensiometer elevation. The saturation and capillary pressure data of this *S-p* relation can be obtained by the element test for *S-p* relations as discussion in section 5.4.1. Through curve fitting, the saturation and capillary-

pressure data points were fit to the VG model. Data were fitted using Equation (5.11) for drainage and Equation (5.12) for the wetting condition, where S_e is the saturation and P is the capillary pressure, to generate an *S-p* relation curve for the air-water phase. The α^d and α^i are the curve shape parameters of the VG model for drainage and wetting, respectively. The van Genuchten parameter of n, α^d and α^i obtained through fitting of the VG model based on data from the element test is important, as it can be used to obtain *S-p* relations for LNAPL-water in drainage and wetting conditions.

$$S_e = [1 + (\alpha^d P)^n]^{-m} \tag{5.11}$$

$$S_e = \left[1 + \left(\alpha^i P\right)^n\right]^{-m} \tag{5.12}$$

There are several methods of obtaining saturation and capillary pressure data for the element test for *S-p* relations. The test method developed by Van Geel and Roy (2002) as described in section 5.4.1 is recommended because the drainage and wetting data can be obtained continuously for the same sample at a relatively faster rate: less than a week, depending on soil type. The method by Thomson et al. (1992) is also suitable if there is no time constraint to obtain this value, as it could take at least three weeks for the *S-p* relation, depending on soil type. There is also a method of obtaining this value using a commercially available equipment setup such as a Tempe cell or Fredlund SWCC Device. This setup varies widely in price, however. The equipment capability, such as of the Tempe cell, can obtain data relatively quickly compared to Van Geel and Roy (2002) method, but it is only able to obtain data for drainage. If a Tempe cell is used for this purpose, the α^i value needed in the VG model for the wetting curve, as explained in sections 5.4.2 and 5.4.3, can be estimated using the expression $\alpha^i = 2\alpha^d$ as suggested by Kool and Parker (1987). In this research, it is found for Toyoura sand that the $\alpha^i = 1.86\alpha^d$.

The drainage curve of the air-water phase would probably best describe the soil moisture movement in the uncontaminated soil condition. When LNAPL contaminates the subsurface, the LNAPL-water *S-p* relations would probably best describe moisture movement in the subsurface. Based on the van Genuchten parameters, the value obtained from the air-water phase *S-p* relations together with the scaling factor as discussed in section 5.4.3, the *S-p* relations for LNAPL-water, can be estimated. When employing an adaptation of the scaling

factor to the van Genuchten expression, the scaled *S-p* relations according to Parker and Lenhard (1987) are shown for drainage in Equation (5.13) and for wetting in Equation (5.14).

$$S_e^d = [1 + (\beta_{OW}\alpha^d P_{OW})^n]^{-m} \tag{5.13}$$

$$S_e^i = \left[1 + \left(\beta_{OW}\alpha^i P_{OW}\right)^n\right]^{-m} \tag{5.14}$$

Once the required *S-p* relation as shown in Figure 5.19 has already been obtained for the same type of soil as at the installed monitoring probe elevation, it can be used as an LNAPL spill monitoring tool. When no LNAPL spill has occurred, the *S-p* relations plotting point should be around the air-water VG model drainage curve, considered on a non-rainy day. During a rainy day, the *S-p* relations point should be below the air-water VG model drainage curve due to the low capillary pressure value during wetting process in the soil pores. The downward movement of the *S-p* relation point during a rainy day may not contribute confusion to the LNAPL spill indication as two types of tensiometer have been used. In the case of an LNAPL spill occurring, the hydrophobic tensiometer should show some reading of non-wetting (LNAPL) pressure increases. Furthermore, the downward movement of uncontaminated soil should be in a direction of increasing saturation during a rainy day and decreasing saturation during a drainage period, as shown in Figure 5.20.

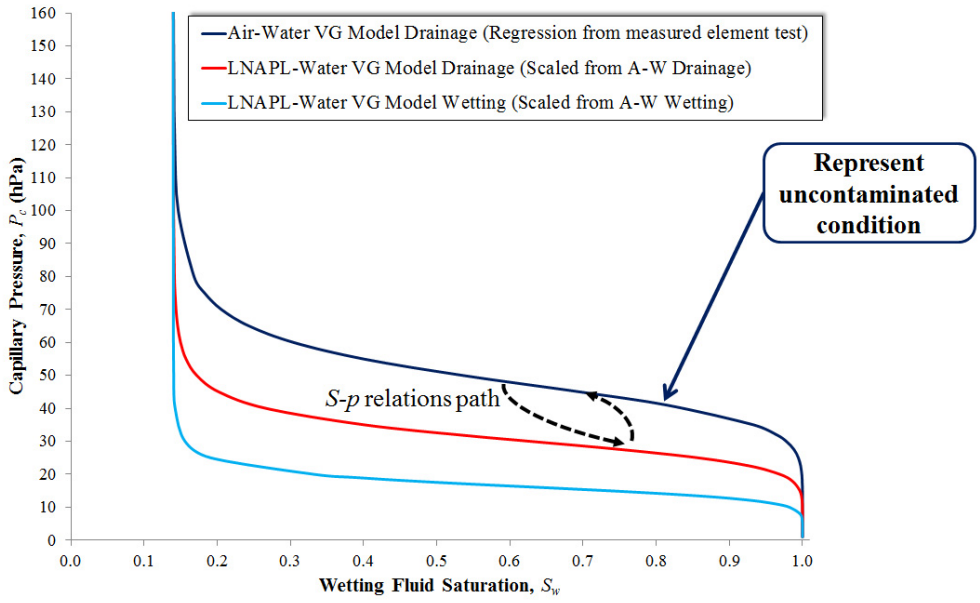

Figure 5.20 *S-p* relations path when there is no LNAPL spill.

When an LNAPL spill occurs, the *S-p* relations path due to temporal saturation changes would definitely switch from an air-water VG model of drainage to an LNAPL-water VG model of drainage, as shown in Figure 5.21. This is due to the low LNAPL-water interfacial tension compared to air-water interfacial tension that causes a significant reduction in capillary pressure. The utilization of *S-p* relations allows storage facility management to respond in the event of an LNAPL spill, especially when the leakage is unnoticed, such as from a small crack in the structure or underground leakage. Management should afterward consider preventing any water infiltration from the ground level, such as precipitation, that could cause LNAPL to migrate deeper and consequently cause complex remediation work that could take a longer duration to complete. It is recommended that the effect of water balance such as from runoff and evaporation from the soil is considered in measures taken to prevent the effect of precipitation on LNAPL migration. The consideration of other factors can be as complex as necessary to suit the surrounding and current conditions of the spill site. However, most importantly, it is necessary to monitor them to ensure the *S-p* relations path is not less than LNAPL-water VG model wetting, as it was found in this study that initiate LNAPL migration even if it is already in an equilibrium condition before precipitation occurs.

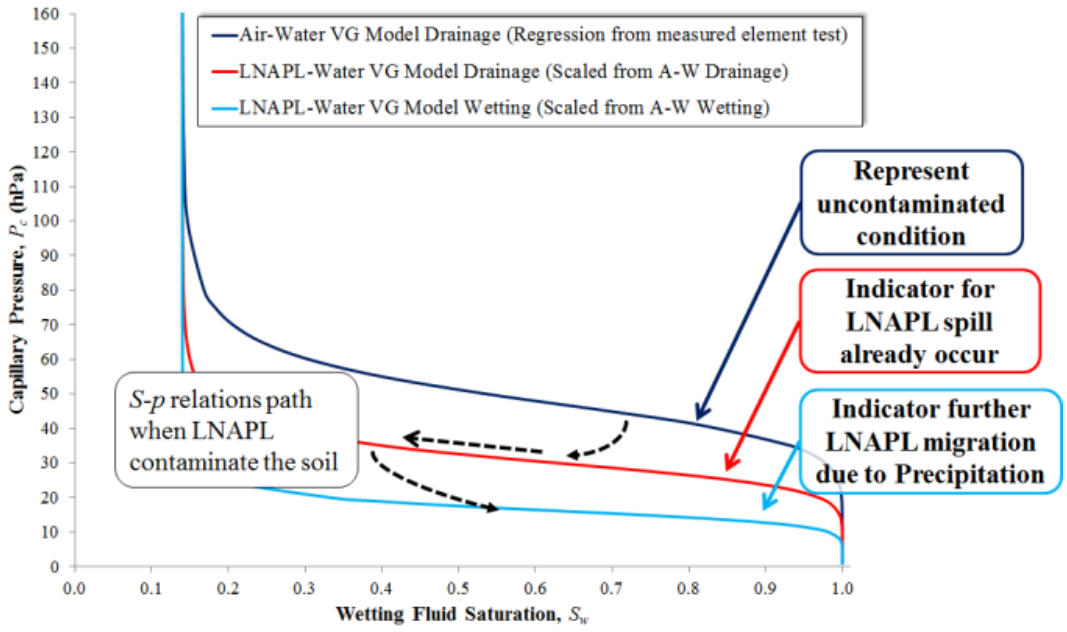

Figure 5.21 *S-p* relations path when LNAPL spill occurs and further migration due to precipitation.

5.6.3 Implications of Post-spill Management Strategy

Ideally, whenever an LNAPL spill occurs, remediation work should took place as soon as possible to clean up the entire spill in order to restore the environment to the previous condition: clean and uncontaminated. In general, there are two stages of LNAPL spill cleanup work; the first is cleanup at the surface level, and the second is cleanup of the contaminated soil to remediate the subsurface level. While the cleanup work takes place at the surface level, the available LNAPL will infiltrate downward and contaminate the subsurface. The first stage is important to ensure a clean surrounding condition and minimize the threat to human and other living organisms due to direct exposure to LNAPL. It also enables the cleanup response team to minimize the affected area as the liquid may spread to the surrounding area depending on the properties of the LNAPL and the surface conditions. Although cleanup at the surface level provides a cleaner surrounding area, it doesn't mean that all of the spilled oil is already recovered. Despite the effort to minimize the spreading at the surface level, in the subsurface, it is beyond human control as the LNAPL will infiltrate down further until it reaches the groundwater level or stops due to capillarity. Based on this study, if the contaminated land is subjected to precipitation, the LNAPL will migrate even further into the saturated zone.

The duration of the cleanup work at the surface level basically depends on the volume and spreading of the spill, the surrounding area condition, and the capability of the responsible party. The duration could be a day or even a few weeks. Then, while waiting for the spill cleanup response team to propose and execute the remediation plan will take more time. This involves consideration of the site soil investigation work, laboratory chemical analysis, proposal of the remediation plan, and approval from the regulatory agencies as well as a tendering process to the remediation company before the remediation work starts. Throughout this period, the LNAPL migration may stop at some point due to capillarity, but as the spill site is not covered and is exposed to precipitation, the infiltrated water will cause the LNAPL to migrate deeper. Therefore, it is recommended to cover the spill site and ensure that there is no possible water infiltration from above the soil surface. This is to ensure that the pushing mechanism, as explained in chapter 3 and 4, does not apply to the LNAPL and cause it migrate deeper.

The application of *S-p* relations for a monitoring system on site using an electrical conductivity probe and tensiometer has already been discussed in section 5.6.2. The same concept has also been suggested to be applied at the spill site in order to monitor further LNAPL downward migration due to precipitation so that proper action can be taken. However, as the soil at the site is already contaminated with LNAPL, it is suggested that similar soil near the spill site that is uncontaminated should be used for an element test for *S-p* relation. This soil should be similar to the soil at the installed monitoring probe elevation at the spill area. A comparison of soil profile taken from the bore log between a contaminated area and an uncontaminated area could help in selecting a suitable soil layer.

Besides preventing the spill site from the precipitation effect, the containment approach of the spill site also can be taken. Figure 5.22 shows an example of a common LNAPL remediation method, soil flushing. In this method it can be seen that a sheet pile barrier is installed around the perimeter of the cleanup area. This is to ensure LNAPL does not migrate beyond the target cleanup area while the remediation work is being performed. This barrier however, is normally installed by the remediation contractor when the remediation work begins. While waiting for the installation of this barrier, precipitation will affect the downward migration of LNAPL in the vadose zone and increase LNAPL saturation in the saturated zone. Even further, this condition also causes more LNAPL to spread farther from the source due to groundwater flow as there is additional volume of LNAPL migrating from the vadose zone into the saturated zone. Therefore, if the barrier can be installed as soon as possible or just after surface cleanup work is finished, the increase volume of LNAPL due to precipitation being spread farther from the source can be prevented. Furthermore, it is believed that more LNAPL would be trapped at the groundwater level downstream as the additional volume of LNAPL in the vadose zone migrates downward due to precipitation, then flows downstream following the groundwater direction flow. When remediation work starts, more LNAPL can be recovered at the recovery well.

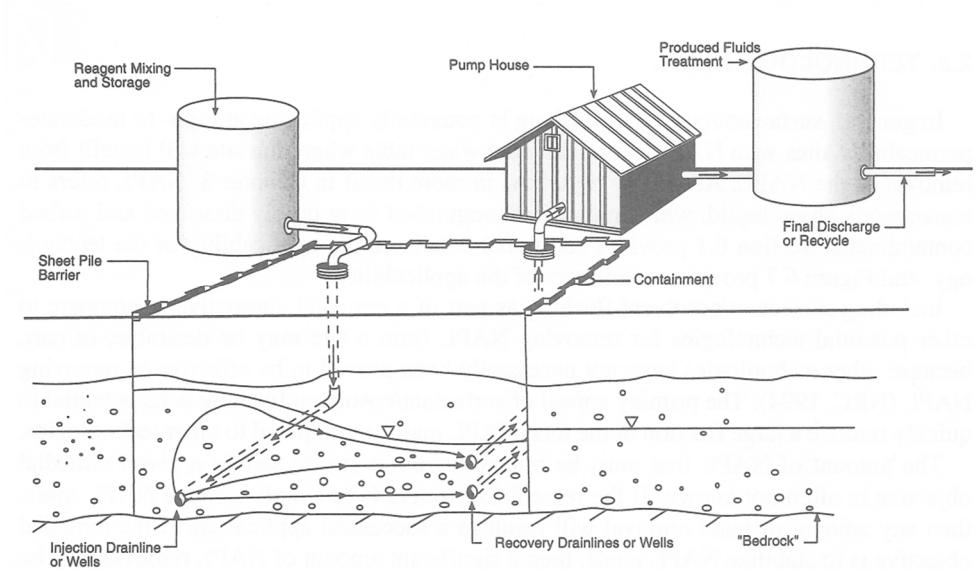

Figure 5.22 Conceptualization of soil flushing remediation work (Lowe et al. 1999).

During the remediation work, if the soil flushing system is applied for the spill site, the same tensiometer can also be utilized as a monitoring system. Remediation work can be as simple as a pump-and-treat system or as complex as bioremediation. Most of the time, soil flushing is selected because of the simplicity of the system and procedure. Compared to pump and treat, which only pumps out the contaminated groundwater and treats it, the recovery rate may be low and slow. Thus, soil flushing provides the increase of groundwater flow to hasten the process. It is however, the injection well is in the saturated zone, then the contaminated soil at the vadose zone will be treated by another method such as soil washing; by excavating the soil and washing it. However, safe excavation depth is always a limitation of soil washing method. Since this study has demonstrated that the pushing mechanism by the infiltrated precipitation water can cause LNAPL to migrate into the saturated zone, this concept can be applied to the remediation system. The main concept is actually that water from above pushes LNAPL down into the saturated zone. Therefore, water can be applied from the surface level and infiltrated downward to push the LNAPL from the vadose zone into the saturated zone. Later the LNAPL will flow toward the recovery well and be treated at treatment facilities. As discussed in chapter 4, the higher the precipitation intensity, the deeper and faster the LNAPL will migrate, thus applying a high volume of water will increase the LNAPL recovery rate. The proper tensiometer installed at the spill site, as mentioned before, can be useful in monitoring the required volume of water applied in order to initiate the LNAPL migration.

5.7 Conclusions for this Chapter

In this chapter, a two-dimensional tank test as well as saturation-capillary pressure relation from one-dimensional column and two-dimensional tank tests was presented. Even in two-dimensional condition, it is proven despite the low density of LNAPL, the infiltration of precipitation water was able to push the mobile LNAPL deeper into saturated zone. Throughout the experiment, as the saturation profile showed similar behavior between the one-dimensional column and two-dimensional tank tests, the S-p relations also showed similar behavior in both experiments. Both one-dimensional and two-dimensional tests can be compared to the air-water van Genuchten model (VG model). When LNAPL was spilled into the sand, capillary pressure also decreased for both one-dimensional and two-dimensional tests due to low LNAPL interfacial tension. The capillary pressure was further reduced when the contaminated sand was subjected to the precipitation. This reduction was due to the increase of wetting saturation supplied by the precipitation. As the precipitation stopped, there was no more supply of infiltrating water, and more water started to percolate to the water level in the percolation stage. Therefore, this drainage condition caused a reduction in wetting saturation. The similarities in the S-p relations behavior changes in both one-dimensional and two-dimensional tests were seen from the initial drainage to the percolation stage during the experiment.

It has been demonstrated that the LNAPL migration in the subsurface can be described using the S-p relations with the help of a VG model. Moreover, the controlling parameter can be seen more clearly in the S-p relations. The time when the LNAPL started to migrate can be seen by examining the saturation data at time intervals during the precipitation. Before contaminated sand was subjected to the precipitation, the measured S-p value was around LNAPL–water VG model drainage curves. Once LNAPL start to migrate, it can be seen that the measured S-p value was below the LNAPL–water VG model wetting curves. As this curve represents the wetting condition in the LNAPL–water phase system, it corresponds with the mentioned condition, which was an increase in water saturation in LNAPL-contaminated sand due to precipitation. From the S-p relations, it can be said that capillary pressure plays an important role or that it is a controlling parameter that causes the migration of LNAPL due to precipitation.

If we look into the wetting saturation parameter, it can be the same depending on the drainage and wetting conditions for the same saturation value. But it is the capillary pressure parameter that helps describe the current physical condition of the phase system: either drainage or wetting. Furthermore, if we consider the physical meaning of capillary pressure in the soil system, it is the pressure that holds the LNAPL or serves as a barrier that stops the LNAPL from migrating deeper into the saturated capillary zone. Therefore, as the capillary pressure drops to a low value due to precipitation water infiltration, it is now considered as a normal fluid flow, as is the water infiltrating downward. Consequently, since LNAPL and water are immiscible, the infiltrated water will push the LNAPL down until the migrated LNAPL becomes entrapped in deeper soil pores, or stops due to capillarity.

Based on the findings from this study, practical implications of the LNAPL spill monitoring system and post-spill management strategy was proposed. In the monitoring system, the van Genuchten model in *S-p* relations can be used to monitor possible spills of LNAPL and its migration as affected by precipitation. For practical application at site, an electrical conductivity probe can be used to obtain soil saturation, whereas tensiometer can be used for capillary pressure measurement. Once the spill occurred, action should be taken such as covering the spill site or a containment approach to minimize or prevent further migration of LNAPL deeper into saturated layers due to precipitation-infiltrated water.

CHAPTER 6: CONCLUSIONS AND FURTHER RESEARCH

6.1 Conclusions

This dissertation presents an environmental geotechnical study on the LNAPL migration behavior in subsurface due to precipitation. This study evaluates the LNAPL migration behavior based on the one-dimensional column and two-dimensional tank laboratory experimental results. The main results of this study are summarized as follows:

In Chapter 3, one-dimensional column test were conducted in order to understand the effect of LNAPL spill volume once the contaminated sand were subjected to the precipitation. As the flow and migration of LNAPL is closely related to soil saturation, the variation of high and low in LNAPL spill volume was studied. The contaminated sand was subjected to the light precipitation intensity and very heavy precipitation intensity in one-dimensional column test.

When the LNAPL spilled from the top of the column, it migrated downward due to the gravitational force. Therefore, the high LNAPL spill volume case caused deeper LNAPL migration at faster rate compared to the low LNAPL spill volume case because it has sufficient pressure to overcome the capillary forces in order to advance into the finer pores filled with water. This is mainly because the 4.08 mL/cm^2 had a higher volume and weight, which provided more pressure to push the LNAPL wetting front at a faster rate. While LNAPL infiltrated and migrated deeper, it had to overcome the capillary force; LNAPL ceases to migrate when it reaches equilibrium at interfacial tension. Although LNAPL density is lighter than water, due to the aforementioned mechanism, capillary depression occurred before equilibrium is reached.

When the infiltrated LNAPL reached a stable depth, it no longer migrated deeper, because the two immiscible liquids, LNAPL and groundwater, had reached its interfacial tension equilibrium. This condition changes as soon as precipitation infiltrates the contaminated sand layer. The infiltrating water is subjected to gravitational force; as it tries to flow towards groundwater level, it will push down any LNAPL that it encounters, and caused entrapment of LNAPL in the saturated zone. In general, it can be said that the more LNAPL

contaminated the sand, the more LNAPL migrated deeper due to precipitation. Comparing the low and high LNAPL spilled volume, more mobile LNAPL was spread through the contamination plume when subjected to precipitation in low LNAPL infiltration cases. In high LNAPL infiltration cases, LNAPL migrated downward and concentrated near the LNAPL wetting front region. Consequently, deeper high LNAPL saturation regions were created.

There are two possible mechanisms that affected LNAPL migration in these low and high LNAPL volumes. In the first mechanism, the availability of a contamination interconnecting bridge within soil pores affects how the precipitation water causes contamination migration. The interconnecting bridge of non-wetting (LNAPL) liquid is more likely to develop when the available liquid is sufficient. In other words, the greater the volume of LNAPL, the more it will occupy the void within soil pores. When more void is filled with LNAPL, the more likely it will be connected. This created a bridge within the water surface inside the pores, since water and LNAPL are immiscible, and soil is not in a dry state. In the second suggested mechanism, the initial distribution of contamination saturation affects how the precipitation water causes contamination migration. When the spilled LNAPL volume is high, LNAPL saturation will be gradually reduced from medium saturation concentrated in the wetting front region to low saturation near the top surface. For a low volume of spilled LNAPL, the LNAPL infiltration will be shallow. Therefore, the LNAPL saturation will be spread almost evenly within the height of the contamination plume. The high LNAPL spilled volume case has more available pores near the top surface since the LNAPL saturation in this region is low compared to the low volume case. Therefore, when the contaminated sand is subjected to precipitation, it is much easier for infiltration water to accumulate when the available pores are high. Later, this accumulation of water will push the LNAPL when water infiltrates downward.

The intensity and volume of precipitation are the two parameters that govern the applied water volume during precipitation. Therefore, in order to understand the mechanism that cause the migration of LNAPL due to precipitation, two series of one-dimensional column test that focused on the precipitation intensity and volume were conducted in Chapter 4. The experimental programs in the precipitation intensity study's focus were concentrated upon the migration of the LNAPL due to various precipitation intensities on a

high LNAPL spilled volume condition. Since precipitation intensity is directly related to precipitation volume, the effects of both parameters on LNAPL migration remain unknown. Therefore, an equal precipitation volume study was conducted by using the light precipitation intensity for a longer period of precipitation to achieve the same precipitation volume as very heavy precipitation intensity.

In general, the higher the precipitation intensity, the deeper LNAPL will migrate due to precipitation. This is because more pressure and force was applied to the LNAPL by infiltrating water in the higher precipitation intensity cases. In all high precipitation intensity cases, once precipitation started, a high volume of water supplied from high precipitation intensity infiltrated the sand and flowed downward due to gravitational force. This high amount of infiltrating water provided a high wetting front propagation force that pushed down any LNAPL within its flow path. This mechanism helped LNAPL migrate easily into the saturated zone. In case H2.4 (i = 2.4 mm/hr), due to the low volume of supplied water during precipitation, the infiltration of precipitation water was not able to cause LNAPL migration into the saturated zone. The water saturation profile shows that it only able to cause small increases in the water saturation. At this intensity, it was only able to wet the soil, but was not able to initiate the migration of LNAPL.

In the equal precipitation volume study's focus, it was found that there was similarity in the LNAPL migration behavior between both precipitation intensity cases; the very heavy intensity and light intensity. Although the amount of water infiltrated per time was almost 10 times lower in the light precipitation intensity cases, the constant water infiltration from the 10 hours of precipitation consequently gave a similar effect as in very heavy precipitation intensity cases. This is due to the increasing amount of supplied water from continuous long precipitation, which caused an increase in as well as an accumulation of infiltrated water. This accumulation of water consequently pushed the mobile LNAPL deeper into the saturated zone, similarly to very heavy precipitation intensity cases. Besides the LNAPL migration behavior similarity due to the pushing mechanism, it was also found that the total precipitation volume plays an important role in determining the depth of migrated LNAPL. It can be seen that whether the contaminated sand is subjected to either low or high precipitation intensity, if the precipitation total is the same, then the total depth of LNAPL migration will also be the same. Based on this study, the infiltrating water is the main

mechanisms pushing the LNAPL to migrate deeper into the saturated zone. If subjected to high precipitation, the high wetting front force will help LNAPL migrate at a faster rate.

In both experimental programs, a sharp triangle profile developed in both LNAPL and water saturation profile due to the downward movement of liquid within increased time during the experiment in the precipitation stage. These triangle patterns reflect the displacement of mobile LNAPL in the soil pores due to the infiltration of precipitation water. Since the additional water came from above and both liquids are immiscible, the precipitation water pushed any LNAPL that it overcomes as it infiltrated downward due to gravitational force. Based on both intensity and volume of precipitation study focus, it is found that the pushing mechanism by the precipitation infiltrated water is the main mechanism that caused the migration of LNAPL due to precipitation.

In Chapter 5, a two-dimensional tank test as well as saturation-capillary pressure relation from one-dimensional column and two-dimensional tank tests was presented. Even in two-dimensional condition, it is proven despite the low density of LNAPL, the infiltration of precipitation water was able to push the mobile LNAPL deeper into saturated zone. Throughout the experiment, as the saturation profile showed similar behavior between the one-dimensional column and two-dimensional tank tests, the *S-p* relations also showed similar behavior in both experiments. Both one-dimensional and two-dimensional tests can be compared to the air-water van Genuchten model (VG model). When LNAPL was spilled into the sand, capillary pressure also decreased for both one-dimensional and two-dimensional tests due to low LNAPL interfacial tension. The capillary pressure was further reduced when the contaminated sand was subjected to the precipitation. This reduction was due to the increase of wetting saturation supplied by the precipitation. As the precipitation stopped, there was no more supply of infiltrating water, and more water started to percolate to the water level in the percolation stage. Therefore, this drainage condition caused a reduction in wetting saturation. The similarities in the *S-p* relations behavior changes in both one-dimensional and two-dimensional tests were seen from the initial drainage to the percolation stage during the experiment.

It has been demonstrated that the LNAPL migration in the subsurface can be described using the *S-p* relations with the help of a VG model. Moreover, the controlling parameter can be seen more clearly in the *S-p* relations. The time when the LNAPL started to migrate can be seen by examining the saturation data at time intervals during the precipitation. Before contaminated sand was subjected to the precipitation, the measured *S-p* value was around LNAPL–water VG model drainage curves. Once LNAPL start to migrate, it can be seen that the measured *S-p* value was below the LNAPL–water VG model wetting curves. As this curve represents the wetting condition in the LNAPL–water phase system, it corresponds with the mentioned condition, which was an increase in water saturation in LNAPL-contaminated sand due to precipitation. From the *S-p* relations, it can be said that capillary pressure plays an important role or that it is a controlling parameter that causes the migration of LNAPL due to precipitation.

If we look into the wetting saturation parameter, it can be the same depending on the drainage and wetting conditions for the same saturation value. But it is the capillary pressure parameter that helps describe the current physical condition of the phase system: either drainage or wetting. Furthermore, if we consider the physical meaning of capillary pressure in the soil system, it is the pressure that holds the LNAPL or serves as a barrier that stops the LNAPL from migrating deeper into the saturated capillary zone. Therefore, as the capillary pressure drops to a low value due to precipitation water infiltration, it is now considered as a normal fluid flow, as is the water infiltrating downward. Consequently, since LNAPL and water are immiscible, the infiltrated water will push the LNAPL down until the migrated LNAPL becomes entrapped in deeper soil pores, or stops due to capillarity.

Based on the findings from this study, practical implications of the LNAPL spill monitoring system and post-spill management strategy was proposed. In the monitoring system, the van Genuchten model in *S-p* relations can be used to monitor possible spills of LNAPL and its migration as affected by precipitation. For practical application at site, an electrical conductivity probe can be used to obtain soil saturation, whereas tensiometer can be used for capillary pressure measurement. Once the spill occurred, action should be taken such as covering the spill site or a containment approach to minimize or prevent further migration of LNAPL deeper into saturated layers due to precipitation-infiltrated water.

6.2 Further Research

Evaluation of LNAPL migration in dynamic conditions is a very complex topic. Using the *Simplified Image Analysis Method*, the mechanism of LNAPL migration behavior in the dynamic condition due to precipitation was successfully proposed. Moreover, analyzing *S-p* relations using the van Genuchten model and the saturation profile, the controlling parameter that caused migration of LNAPL due to precipitation was also identified. This finding is considered the first step to deeper understanding of LNAPL migration at actual spill sites.

For further research on this topic, it is suggested to study LNAPL migration considering the effects of both groundwater fluctuation and precipitation. Although it has been found that the main mechanism that pushes LNAPL to migrate deeper into the saturation zone is due to precipitation water from above, it is suggested that the soil water balance effect is studied, especially considering the effects of precipitation on long-term experiments. In order to further assess the impact of environmental degradation due to the migration of LNAPL into saturated zones caused by precipitation, it is suggested to conduct long-term experiments and quantify the BTEX concentration in the contaminated groundwater due to the migration of LNAPL into the saturated zone caused by precipitation.

REFERENCES

Amiaz, Y., Sorek, S., Enzel, Y., and Dahan, O. (2011). Solute transport in the vadose zone and groundwater during flash floods. *Water Resources Research* ***47***(10): 1–10.

Anderson, W. G. (1986). Wettability literature survey-part 1: rock/oil/brine interactions and the effects of core handling on wettability. *Journal of Petroleum Technology* ***38***(10): 1125–1144.

Arafat, H. a., Bakel, A. J., Dilger, A. K., Nash, K. L., Rickert, P. G., and Vandegrift, G. F. (2013). Reclamation of contaminated groundwater using cooking oils in a novel, eco-friendly and high-efficiency solvent extraction process. *Desalination* ***321***: 9–21.

Archie, G. E. (1942). The electrical resistivity log as an aid in determining some reservoir characteristics. *Trans. AIMe* ***146***(1): 54–62.

Archie, G. E. (1947). Electrical resistivity an aid in core-analysis interpretation. *AAPG Bulletin* ***31***(2): 350–366.

ASTM. (1987). D2216-80: Standard Test Method for Laboratory Determination of Water (Moisture) Content of Soil, Rock and Soi-Aggregate Mixtures. *Annual Book of Standards* 355–358.

Bear, J. (1972). *Dynamics of fluids in porous media*. New York: Dover Publications, Inc.

Bear, J. (2000). Modeling Flow in the Unsaturated Zone. *Modeling Groundwater Flow and Contaminant Transport*. Retrieved from

Bear, J., and Cheng, A. H. D. (2010). *Modeling Groundwater Flow and Contaminant Transport*. New York: Springer.

Bird, W. W. A., and Grossman, E. (2011). Chemical Aftermath: Contamination and Cleanup Following the Tohoku Earthquake and Tsunami. *Environmental Health Perspective* ***119***(7): a290–a301.

Blanchard, D. C., and Spencer, A. T. (1970). Experiments on the Generation of Raindrop-Size Distributions by Drop Breakup. *Journal of the Atmospheric Sciences* ***27***(1): 101–108.

Bocheva, L., Marinova, T., Simeonov, P., and Gospodinov, I. (2009). Variability and trends of extreme precipitation events over Bulgaria (1961–2005). *Atmospheric Research* ***93***(1-3): 490–497.

Brown, A. M. (2001). A step-by-step guide to non-linear regression analysis of experimental data using a Microsoft Excel spreadsheet. *Computer methods and programs in biomedicine* ***65***(3): 191–200.

Buckingham, E. (1907). *Studies on the movement of soil moisture*. (M. Whitney, Ed.)*Bulletin (United States. Division of Agricultural Soils)* (Vol. 38, pp. 9–60). Washington: Government Printing Office.

Busby, R. D., Lenhard, R. J., and Rolston, D. E. (1995). An Investigation of Saturation-Capillary Pressure Relations in Two- and Three-Fluid Systems for Several NAPLS in Different Porous Media. *Ground Water* ***33***(4): 570–578.

Canale, R. P., and Chapra, S. C. (1998). *Numerical methods for engineers*. New York: McGraw-Hill.

Causapé, J., Quílez, D., and Aragüés, R. (2006). Groundwater quality in CR-V irrigation district (Bardenas I, Spain): Alternative scenarios to reduce off-site salt and nitrate contamination. *Agricultural Water Management* ***84***(3): 281–289.

Chang, J. I., and Lin, C.-C. (2006). A study of storage tank accidents. *Journal of Loss Prevention in the Process Industries* ***19***(1): 51–59.

Chen, D., and Chen, H. W. (2013). Using the Köppen classification to quantify climate variation and change: An example for 1901 – 2010. *Environmental Development* ***6***: 69–79.

Dai, A., Fung, I. Y., and Del Genio, A. D. (1997). Surface Observed Global Land Precipitation Variations during 1900–88. *Journal of Climate* ***10***(11): 2943–2962.

David, H. F. L., and Bela, G. L. (Eds.). (2000). *Groundwater and Surface Water Pollution* (p. 48). Florida: Lewis Publishers.

Department for Environment Food Rural Affairs. Environmental Protection Act 1990 : Part 2A Contaminated Land Statutory Guidance (2012). United Kingdom. Retrieved from https://www.gov.uk/government/uploads/system/uploads/attachment_data/file/223705/pb13735cont-land-guidance.pdf

Deshpande, N. R., Kulkarni, a., and Krishna Kumar, K. (2012). Characteristic features of hourly rainfall in India. *International Journal of Climatology* ***32***(11): 1730–1744.

Dullien, F. A. L. (1992). *Porous media : fluid transport and pore structure*. San Diego: Academic Press.

Easterling, D. R., Meehl, G. A., Parmesan, C., Changnon, S. A., Karl, T. R., and Mearns, L. O. (2000). Climate Extremes: Observations, Modeling, and Impacts. *Science* ***289***(5487): 2068–2074.

Endo, K. (2002). *Characteristics of DNAPL Distribution in a Contaminated Subsurface*. Kyoto University.

Farias, C. O., Hamacher, C., Wagener, A. D. L. R., and Scofield, A. D. L. (2008). Origin and degradation of hydrocarbons in mangrove sediments (Rio de Janeiro, Brazil) contaminated by an oil spill. *Organic Geochemistry* ***39***(3): 289–307.

Flores, G., Katsumi, T., Inui, T., and Kamon, M. (2011). A Simplified Image Analysis Method to Study LNAPL Migration in Porous Media. *Soils and Foundations* ***51***(5): 835–847.

Foster, S. S. D., and Chilton, P. J. (2003). Groundwater: the processes and global significance of aquifer degradation. *Philosophical transactions of the Royal Society of London. Series B, Biological sciences* ***358***(1440): 1957–72.

Franco, Z., and Nguyen, Q. D. (2011). Flow properties of vegetable oil–diesel fuel blends. *Fuel* ***90***(2): 838–843.

Helland, J. O., and Skjæveland, S. M. (2007). Relationship between capillary pressure , saturation, and interfacial area from a model of mixed-wet triangular tubes. *Water Resources Research* ***43***: 1–15.

Hill Iii, E. H., Kupper, L. L., and Miller, C. T. (2002). Evaluation of path-length estimators for characterizing multiphase systems using polyenergetic X-ray absorptiometry. *Soil science* ***167***(11): 703–719.

Holdridge, L. R. (1967). *Life zone ecology*. *Life zone ecology*. San José, Costa Rica: Tropical Science Center.

Holtz, R. D., Kovacs, W. D., and Sheahan, T. C. (2011). *An introduction to geotechnical engineering* (2nd ed.). New Jersey: Prentice Hall.

Høst-Madsen, J., and Høgh Jensen, K. (1992). Laboratory and numerical investigations of immiscible multiphase flow in soil. *Journal of Hydrology* ***135***(1-4): 13–52.

Illingworth, A. J. (1988). The formation of rain in convective clouds. *Nature* ***336***(6201): 754–756.

Jenamani, R. K., Bhan, S. C., and Kalsi, S. R. (2006). Observational/forecasting aspects of the meteorological event that caused a record highest rainfall in Mumbai. *Current Science* ***90***(10): 1344–1362.

Kamon, M., Endo, K., and Katsumi, T. (2003). Measuring the k–S–p relations on DNAPLs migration. *Engineering Geology* ***70***(3-4): 351–363.

Kamon, M., Endo, K., Kawabata, J., Inui, T., and Katsumi, T. (2004). Two-dimensional DNAPL migration affected by groundwater flow in unconfined aquifer. *Journal of hazardous materials* ***110***(1-3): 1–12.

Kechavarzi, C., Soga, K., and Illangasekare, T. H. (2005). Two-dimensional laboratory simulation of LNAPL infiltration and redistribution in the vadose zone. *Journal of contaminant hydrology* ***76***(3-4): 211–33.

Kechavarzi, C., Soga, K., and Wiart, P. (2000). Multispectral image analysis method to determine dynamic fluid saturation distribution in two-dimensional three-fluid phase flow laboratory experiments. *Journal of Contaminant Hydrology* ***46***(3-4): 265–293.

Khaled, I. M., Tsuyoshi, M., Kohei, N., Taku, N., and Hiromi, I. (2011). Experimental and Modeling Investigation of Shallow Water Table Fluctuations in Relation to Reverse Wieringermeer Effect. *Open Journal of Soil Science* ***01***(02): 17–24.

Kool, J. B., and Parker, J. C. (1987). Development and evaluation of closed-form expressions for hysteretic soil hydraulic properties. *Water Resources Research* ***23***(1): 105–114.

Lang, R. (1920). *Verwitterung und Bodenbildung als Einführung in die Bodenkunde*. E. Schweizerbart'sche verlagsbuchhandlung (E. Nagele).

Leff, J. (2012, November). CORRECTED-UPDATE 2-Fuel spill reported at NJ refinery after Sandy. *Reuters*. Retrieved from http://www.reuters.com/article/2012/11/05/storm-sandy-energy-spill-idUSL1E8M56R020121105

Lenhard, R J, and Parker, J. C. (1988). Experimental validation of the theory of extending two-phase saturation-pressure relations to three-fluid phase systems for monotonic drainage paths. *Water Resources Research* ***24***(3): 373–380.

Lenhard, R.J., and Parker, J. C. (1987). Measurement and prediction of saturation-pressure relationships in three-phase porous media systems. *Journal of Contaminant Hydrology* ***1***(4): 407–424.

Leverett, M. C. (1941). Capillary behavior in porous solids. *Transactions of the AIME* ***142***(1): 152–169.

Li, Y. (2005). *Mechanism of LNAPL Migration in Conjuntion with Groundwater Fluctuation*. Kyoto University.

Liu, Y. ., Hopmans, J. ., Grismer, M. ., and Chen, J. . (1998). Direct estimation of air–oil and oil–water capillary pressure and permeability relations from multi-step outflow experiments. *Journal of Contaminant Hydrology* ***32***(3-4): 223–245.

Llasat, M.-C. (2001). An objective classification of rainfall events on the basis of their convective features: application to rainfall intensity in the northeast of spain. *International Journal of Climatology* ***21***(11): 1385–1400.

Lohman, F. H. (1955). The mathematical combination of Lambert's law and Beer's law. *Journal of Chemical Education* ***32***(3): 155.

Low, T. B., and List, R. (1982). Collision, Coalescence and Breakup of Raindrops. Part I: Experimentally Established Coalescence Efficiencies and Fragment Size Distributions in Breakup. *Journal of the Atmospheric Sciences* ***39***(7): 1591–1606.

Lowe, D. F., Oubre, C. L., and Ward, C. H. (Eds.). (1999). *Surfactans and Cosolvents for NAPL Remedation: A Technology Practices Manual*. Florida: Lewis Publishers.

Lu, N., and Likos, W. J. (2004). *Unsaturated Soil Mechanics*. New Jersey: John Wiley & Sons, Ltd.

Margat, J. F., and Van Der Gun, J. (2013). *Groundwater Around the World: A Geographic Synopsis* (p. 303). Leiden, Netherlands: CRC Press/Balkema.

Mason, B. B. J., and Andrews, J. B. (1960). Drop-size distributions from various types of rain. *Quarterly Journal of the Royal Meteorological Society* ***86***(369): 346–353.

McCleneghan, K., Reiter, G. a., Hardwick, J. E., and McGovern, P. T. (2002). Management of Oil Spill Response and Cleanup in a River Under Severe Winter Conditions. *Spill Science & Technology Bulletin* ***7***(3-4): 163–172.

McTaggart-Cowan, J. D., and List, R. (1975). Collision and Breakup of Water Drops at Terminal Velocity. *Journal of the Atmospheric Sciences* ***32***(7): 1401–1411.

Ministry of Environment Japan. (1993). Environmental Basic Act in 1993. *Law No.91 of 1993*.

Nadim, F., Zack, P., Hoag, G. E., Liu, S., and Carley, R. J. (2001). Non-Uniform Regulations of Underground Storage Tanks in the United States Calls for a National-Scale Revision. *Spill Science & Technology Bulletin* ***6***(5): 341–348.

Oostrom, M., Hofstee, C., Dane, H., and Lenhard, R. J. (1998). Single-source gamma radiation procedures for improved calibration and measurements in porous media. *Soil Science* ***163***(8): 646–656.

Parker, J C, and Lenhard, R. J. (1987). A model for hysteretic constitutive relations governing multiphase flow: 1. Saturation-pressure relations. *Water Resources Research* ***23***(12): 2187–2196.

Parker, J C, Lenhard, R. J., and Kuppusamy, T. (1987). A parametric model for constitutive properties governing multiphase flow in porous media. *Water Resources Research* ***23***(4): 618–624.

Parker, J.C., and Lenhard, R. J. (1990). Determining three-phase permeability-saturation-pressure relations from two-phase system measurements. *Journal of Petroleum Science and Engineering* ***4***(1): 57–65.

Parker, S., and Hays, K. (2013, April). Exxon oil spill cleanup ongoing in Arkansas, pipeline shut. *Reuters*. New York. Retrieved from http://www.reuters.com/article/2013/04/01/us-exxon-pipeline-spill-idUSBRE92U00220130401

Porter, M. L., Schaap, M. G., and Wildenschild, D. (2009). Advances in Water Resources Lattice-Boltzmann simulations of the capillary pressure – saturation – interfacial area relationship for porous media. *Advances in Water Resources* ***32***(11): 1632–1640.

Pruppacher, H. R., and Klett, J. D. (1978). *Microphysics of Clouds and Precipitation*. Dordrecht: Springer Netherlands.

Raeesi, B., and Piri, M. (2009). The effects of wettability and trapping on relationships between interfacial area, capillary pressure and saturation in porous media : A pore-scale network modeling approach. *Journal of Hydrology* ***376***(3-4): 337–352.

Rimmer, A., DiCarlo, D. a., Steenhuis, T. S., Bierck, B., Durnford, D., and Parlange, J.-Y. (1998). Rapid fluid content measurement method for fingered flow in an oil–water–sand system using synchrotron X-rays. *Journal of Contaminant Hydrology* ***31***(3-4): 315–335.

Schubert, M., Paschke, A., Lau, S., Geyer, W., and Knöller, K. (2007). Radon as a naturally occurring tracer for the assessment of residual NAPL contamination of aquifers. *Environmental pollution (Barking, Essex : 1987)* ***145***(3): 920–7.

Sharma, R. S., and Mohamed, M. H. . (2003). An experimental investigation of LNAPL migration in an unsaturated/saturated sand. *Engineering Geology* ***70***(3-4): 305–313.

Stone, H. L. (1970). Probability model for estimating three-phase relative permeability. *Journal of Petroleum Technology* ***22***(2): 214–218.

Takahashi, T. (1978). Riming Electrification as a Charge Generation Mechanism in Thunderstorms. *Journal of the Atmospheric Sciences* ***35***(8): 1536–1548.

Thomson, N. R., Graham, D. N., and Farquhar, G. J. (1992). One-dimensional immiscible displacement experiments. *Journal of Contaminant Hydrology* ***10***(3): 197–223.

U.S. Department of Homeland Security. (2006). *Report to Congress : Oil Spill Liability Trust Fund Hurricane Impact* (p. 1). Washington, DC.

U.S. Department of Homeland Security. (2012). *Daily Open Source Infrastructure Report* (p. 2). Washington, DC.

U.S. Energy Information Administration. (2013). International Energy Statistics (online). Retrieved from http://www.eia.gov/cfapps/ipdbproject/IEDIndex3.cfm?tid=5&pid=53&aid=1

U.S. Pipeline & Hazardous Materials Safety Administration. (2013). Significant Incident Cause Breakdown. *PHMSA Significant Incidents Files, Dec 31, 2013*. Retrieved from http://phmsa.dot.gov/pipeline/library/data-stats

United States Environmental Protection Agency. (2005). *2005 Remediation General Permit Fact Sheet Excerpts* (p. 14). United States of America.

Van Geel, P J, and Roy, S. D. (2002). A proposed model to include a residual NAPL saturation in a hysteretic capillary pressure-saturation relationship. *Journal of contaminant hydrology* ***58***(1-2): 79–110.

Van Geel, P. J., and Sykes, J. F. (1994a). Laboratory and model simulations of a LNAPL spill in a variably-saturated sand, 1. Laboratory experiment and image analysis techniques. *Journal of Contaminant Hydrology* ***17***(1): 1–25.

Van Geel, P. J., and Sykes, J. F. (1994b). Laboratory and model simulations of a LNAPL spill in a variably-saturated sand, 2. Comparison of laboratory and model results. *Journal of Contaminant Hydrology* ***17***: 27–53.

Van Geel, P.J., and Sykes, J. F. (1997). The importance of fluid entrapment, saturation hysteresis and residual saturations on the distribution of a lighter-than-water non-aqueous phase liquid in a variably saturated sand medium. *Journal of Contaminant Hydrology* ***25***(3-4): 249–270.

Van Genuchten, M. T. (1980). A closed-form equation for predicting the hydraulic conductivity of unsaturated soils. *Soil Science Society of America Journal* ***44***(5): 892–898.

Vargaftik, N. B., Volkov, B. N., and Voljak, L. D. (1983). *International tables of the surface tension of water*. Washington, DC: American Chemical Society and the American Institute of Physics for the National Bureau of Standards.

Waldvogel, A. (1974). The N 0 Jump of Raindrop Spectra. *Journal of the Atmospheric Sciences* ***31***(4): 1067–1078.

Wilcock, A. A. (1968). Köppen after Fifty Years. *Annals of the Association of American Geographers* ***58***(1): 12–28.

Willis, P. T., and Hallett, J. (1991). Microphysical Measurements from an Aircraft Ascending with a Growing Isolated Maritime Cumulus Tower. *Journal of the Atmospheric Sciences* ***48***(2): 283–299.

Wraith, J. M., and Or, D. (1998). Nonlinear parameter estimation using spreadsheet software. *Journal of Natural Resources and Life Sciences Education* ***27***: 13–19.

Yu, C., Yao, Y., Hayes, G., Zhang, B., and Zheng, C. (2010). Quantitative assessment of groundwater vulnerability using index system and transport simulation, Huangshuihe catchment, China. *The Science of the total environment* ***408***(24): 6108–16.

Zanon, F., Borga, M., Zoccatelli, D., Marchi, L., Gaume, E., Bonnifait, L., and Delrieu, G. (2010). Hydrological analysis of a flash flood across a climatic and geologic gradient: The September 18, 2007 event in Western Slovenia. *Journal of Hydrology* ***394***(1-2): 182–197.

Zawadzki, I., and Antonio, M. D. A. (1988). Equilibrium Raindrop Size Distributions in Tropical Rain. *Journal of the Atmospheric Sciences* ***45***(22): 3452–3459.

Zhou, Y., and Ran, L. (2012). Torrential rainfall responses to vertical wind shear, radiation and ice clouds: A rainfall partitioning analysis based on surface rainfall budget. *Atmospheric Research* ***108***(July 2007): 1–8.